THE ROLE OF SEROTONIN IN ATHEROSCLEROSIS

Dissertation

Zur Erlangung des akademischen Grades
Doctor rerum naturalium
(Dr. rer. nat.)

Im Fach Biologie

eingereicht an der

Lebenswissenschaftlichen Fakultät
der Humboldt-Universität zu Berlin

von

M.Sc. YASMINE JENNIFER SEIBEL (geb. GRAF)

Präsidentin der Humboldt-Universität zu Berlin
Prof. Dr.-Ing. Dr. Sabine Kunst

Dekan der Lebenswissenschaftlichen Fakultät
Prof. Dr. Bernhard Grimm

Gutachter/innen: 1. Prof. Dr. Michael Bader

2. Prof. Dr. Martina Seifert

3. Prof. Dr. Thomas Sommer

Tag der mündlichen Prüfung: 28. Februar 2020

https://doi.org/10.18452/21818

Für Elly

Abstract

Atherosclerosis and its possible consequences, infarction events in various arteries, are very common diseases in industrialized countries and the mechanisms of their pathogenesis are only poorly understood. It's known that external (diet, exercise, stress) as well as internal (genetic predispositions, physiological changes, sex) factors play a role, but the exact processes need to be investigated more intensively to develop novel therapy approaches.

As an all-round talent in the mammalian body, the monoamine serotonin (5-HT) might be a promising candidate to play a crucial role in the pathogenesis of atherosclerosis. If and how this hormone affects atherosclerotic plaque formation, macrophage invasion, calcification and fibrotic changes in vessels and heart was the focus of this study.

This study is the first of its kind using the novel approach of transgenic double knockout mice lacking the apolipoprotein E (ApoE, atherosclerosis model) and additionally either the key enzyme in peripheral 5-HT synthesis, tryptophan hydroxylase 1 (Tph1) or the major 5-HT transporter in cells, SERT. Physiology, metabolic parameters and atherogenic processes in *ApoE/Tph1*$^{-/-}$ and *ApoE/Sert*$^{-/-}$ animals were examined using a very broad spectrum of biological, biochemical, molecular and histological methods and resulted in an extensive overview of how 5-HT might influence the pathogenesis of atherosclerosis.

The most striking results of this study are the following:

5-HT receptor distribution is altered in vessels of different mouse strains, such as C57Bl/6 (B6) and FVB/N, and also in *Tph1* deficient animals generated in these background strains. This phenomenon partly explains why atherosclerosis-related processes, such as vascular calcification or blood pressure regulation are differently exhibited in mice of these strains. Further, the examination of *ApoE/Tph1*$^{-/-}$ and *ApoE/Sert*$^{-/-}$ mice elucidated that both double knockouts exhibit by far not the same phenotypes: While *Tph1* deficiency resulted in significantly decreased bodyweight, plasma cholesterol and liver damage parameter levels and significantly increased relative liver weight, *Sert* deficiency caused significant increases in blood glucose, plasma cholesterol, atherosclerotic plaque size in aortas and collagen amounts in atherosclerotic plaques. Long term Western Diet applied to *ApoE/Tph1*$^{-/-}$ and *ApoE*$^{-/-}$ control animals (acute atherosclerosis induction) confirmed that *Tph1* deficiency decreases bodyweight gain and has protective effects on lipid metabolism, but a clear effect on atherogenesis could not be reported.

Concluding, this study highlights the complex relationship between many factors acting on atherosclerotic pathogenesis. 5-HT plays a role in many of those factors, but seems to have only minor but protective effects on atherogenesis itself.

Zusammenfassung

Atherosklerose und als mögliche Folge auch diverse Infarktereignisse in verschiedenen Gefäßen, sind in Industrieländern weit verbreitete Krankheiten, und die Mechanismen ihrer Pathogenese sind nur unzureichend bekannt. Sehr wohl bekannt ist jedoch, dass sowohl externe (Ernährung, Bewegung, Stress) als auch interne (genetische Veranlagung, physiologische Veränderungen, Geschlecht) Faktoren eine Rolle spielen. Die zugrunde liegenden Prozesse müssen jedoch genauer untersucht werden, um neue Therapieansätze zu entwickeln.

Als Allroundtalent im Säugetierkörper könnte das Monoamin Serotonin (5-HT) ein vielversprechender Kandidat sein, der eine entscheidende Rolle bei der atherosklerotischen Pathogenese spielt. Ob und wie dieses Hormon die Bildung atherosklerotischer Plaques, die Makrophageninvasion in die Gefäßwände, die Verkalkung und die fibrotischen Veränderungen in den Gefäßen und im Herzen beeinflusst, war Gegenstand dieser Studie.

Die vorliegende Studie ist die erste ihrer Art, die den neuartigen Ansatz von transgenen Doppel-Knockout-Mäusen verwendet, denen das Apolipoprotein E (ApoE, ein Atherosklerosemodell) fehlt und, die zusätzlich entweder das Schlüsselenzym für die periphere 5-HT-Synthese, Tryptophanhydroxylase 1 (Tph1), oder den primären Transporter für 5-HT in Zellen (SERT) nicht bilden können. Physiologie, Stoffwechselparameter und atherogene Prozesse wurden in *ApoE/Tph1*$^{-/-}$ und *ApoE/Sert*$^{-/-}$ Tieren mithilfe eines sehr breiten Spektrums an biologischen, biochemischen, molekularen und histologischen Methoden untersucht und resultierten in einem umfassenden Überblick über die möglichen Wirkungsweisen von 5-HT auf die atherosklerotische Pathogenese.

Die bedeutendsten Ergebnisse dieser Studie sind die folgenden:

Die 5-HT-Rezeptorverteilung ist unterschiedlich in Gefäßen von verschiedenen Mauslinien, wie C57Bl/6 (B6) und FVB/N und ebenfalls in denen von Tieren mit *Tph1*-Defizienz, die in diesen Hintergrundstämmen erzeugt wurden. Dieses Phänomen erklärt zum Teil, warum atheroskleroseverwandte Prozesse wie Gefäßverkalkung oder Blutdruckregulation bei Mäusen dieser Stämme unterschiedlich ausgeprägt sind. Ferner ergab die Untersuchung von *ApoE/Tph1*$^{-/-}$ und *ApoE/Sert*$^{-/-}$ Mäusen, dass beide Doppel-Knockouts bei weitem nicht dieselben Phänotypen aufweisen: Während die *Tph1*-Defizienz im Atherosklerosemodell zu einer signifikant verminderten Zunahme des Körpergewichts, niedrigeren Plasmacholesterinwerten und Leberschadensparametern und einem erhöhten relativen Lebergewicht führte, verursachte eine *Sert*-Defizienz signifikante Erhöhungen des Blutzuckers, des Plasmacholesterins und die Ausbildung größerer atherosklerotischer Plaques in der Aorta und eine vermehrte Kollagenakkumulation innerhalb dieser atherosklerotischen Plaques. Die Langzeitgabe einer sogenannten Western-Diät, die bei den getesteten *ApoE/Tph1*$^{-/-}$ und *ApoE*$^{-/-}$ Kontrolltieren zu akuter Atherogenese führte, bestätigte, dass eine *Tph1*-Defizienz die Zunahme von Körpergewicht vermindert und schützende Auswirkungen auf den Lipidstoffwechsel hat, ein klarer Effekt auf die Atherogenese konnte jedoch nicht ermittelt werden.

Zusammenfassend hebt diese Studie die komplexen Beziehungen zwischen vielen Faktoren, die auf die atherosklerotische Pathogenese einwirken, hervor. 5-HT spielt bei vielen dieser

Faktoren eine Rolle, scheint jedoch nur eine schwache aber protektive Wirkung auf Atherogenese selbst zu haben.

Table of Content

1 Introduction

1.1 Serotonin – The Story begins

In the years around 1950 two independent research groups identified a molecular substance isolated from gastrointestinal enterochromaffin cells (EC) (Erspamer & Asero, 1952) and in bovine blood-serum (Rapport et al., 1948a, b, c). While one group found that the substance had the ability to induce smooth-muscle cell contraction the other showed that it caused vasoconstriction after being released from blood platelets. Only in 1952, after some years of research on the chemical structure of the pretended two matters it could be proven that they were identical and the substance finally got named after its major function: being located in the **serum** and influencing the vaso-**tonus**: "serotonin". Since then it could be shown that serotonin is present in many taxa throughout the whole animal kingdom from insects (e.g. *Drosophila melanogaster*, *Apis mellifera* and *Periplaneta americana*) (Bishop & O'Shea, 1983; Schürmann & Klemm, 1984; Vallés & White, 1988) to mammals and it is located not just in several peripheral organs, but also in the central and peripheral nervous system (CNS and PNS) (Twarog & Page, 1953).

1.2 The Structure of the Mammalian Serotonergic System

1.2.1 Two households, both alike in dignity[1]

As well as many other animal species mammals feature a barrier between the CNS and peripheral system, a thin layer of brain capillary endothelial cells connected to each other by complex tight-junctions (Ohtsuki, 2004), namely the blood brain barrier (BBB). Serotonin can be found on both sides of this barrier, unable to cross it (Hardebo & Owman, 1980) due to its hydrophilic structure (see Fig. 1). It was assumed for many years that the mammalian serotonin system is located at two different sites but its synthesis and distribution processes are identically structured and controlled by the same mediators: Serotonin is synthesized by a two-step process (see Fig. 2) which is primarily mediated by the enzyme tryptophan hydroxylase (TPH), determining the rate-limiting step, and the aromatic amino acid decarboxylase (AADC).

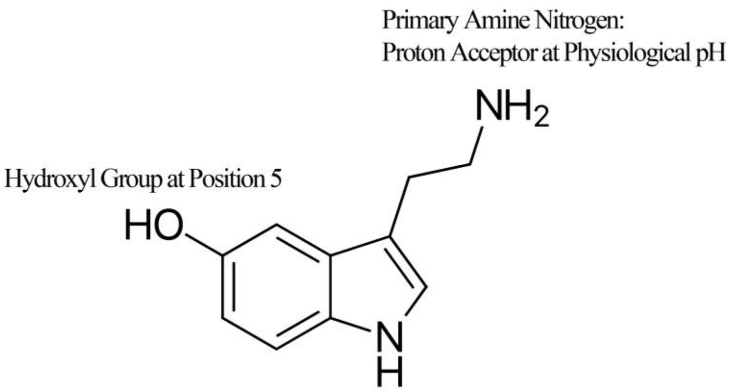

Fig. 1 – Structural Formula of 5-HT
Chemical structural formula of the monoamine 5-HT. 5-HT is an indolamine with a hydroxylation of the fifth position (hydroxyl group) and a primary amine nitrogen which serves as a proton acceptor at physiological pH. This combination makes 5-HT a hydrophic substance.

However, this concept was challenged in 2003 when Walther and colleagues generated a classical knock-out mouse model for TPH, originally to investigate the role of serotonin in cardiovascular regulation (Walther & Bader, 2003; Walther et al., 2003a). After confirming the loss of serotonin-production in several peripheral organs, the

[1] From William Shakespeare's 'Romeo & Juliet', Act 1, Prologue

authors surprisingly found unaltered levels of serotonin in the CNS. Following genetic screens indicated another *tph*-gene that codes a second TPH isoform in the CNS. Since then, the paradigm changed to the idea that at least mammals have two separate serotonin systems based on two separate genes and enzymes.

While the novel CNS-specific TPH isoform was named TPH2, the initially examined isoform in the peripheral system was renamed TPH1. The two TPH isoforms show a homology of 71% (Walther & Bader, 2003) and of about 50% to other members of the aromatic amino acid hydroxylase family, such as the tyrosine hydroxylase (TH) and phenylalanine hydroxylase (PAH) (reviewed in Beis, 2014). As the major enzyme controlling serotonin synthesis in the periphery, TPH1 could be shown to be present in structures like EC, thymus, immune cells, heart and chromaffine cells of the suprarenal gland medulla and additionally in the pineal gland in the CNS (Ahern, 2011; Côté et al., 2003; Watts et al., 2012). Contrasting, TPH2 is the major enzyme isoform in the adult mammalian CNS and could be detected in the murine raphe nuclei (RN) and human pons, cortex, striatum, hippocampus and other brain regions (Côté et al., 2003; Gutknecht et al., 2009; Liu et al., 2008; Patel et al., 2004; Walther & Bader, 2003; Yadav et al., 2009). TPH2 cannot be found in peripheral organs (Gutknecht et al., 2009; Patel et al., 2004; Walther et al., 2003a; Yadav et al., 2009; Zill et al., 2007), except in the gut enteric nervous system where it acts as a neuroprotector and activates neurogenesis (Gershon, 2012).

In conclusion, the major amount of serotonin in the mammalian body is stored in the gastrointestinal tract (70-90%). The here located serotonin comes from both synthesis systems (e.g. TPH1 in the EC and TPH2 in the myenteric plexus neurons) and helps controlling gut activity and, in case of disturbances or inflammations, correlates with "irritable bowel-syndrome" (reviewed in Fujimiya & Inui, 2000; Gershon, 2012).

1.2.2 Serotonin – Who are you, where do you come from and where do you go?

Chemically, serotonin belongs to the family of tryptamines and, as mentioned above, it appears to have a hydrophilic structure. This trait is caused by the hydroxyl-group at fifth-position within the heterocyclic indole-structure and the primary amine nitrogen which acts as a proton acceptor at physiological pH (see **Fig. 1**). Congruously, the chemically correct name of serotonin is 5-hydroxytryptamine (5-HT).

The biochemical story of 5-HT starts with L-Tryptophan (Trp), an essential amino acid for humans that is encoded genetically by the codon UGG and can naturally be found in nutrients as milk and some seeds (e.g. sunflower). Commonly, the L-stereoisomer of Trp is used as biogenic amino acid for enzymes and structural proteins and is produced by plants and microorganisms (Radwanski & Last, 1995), in contrast the R-stereoisomer is only occasionally found in nature (Pallaghy et al., 1999).

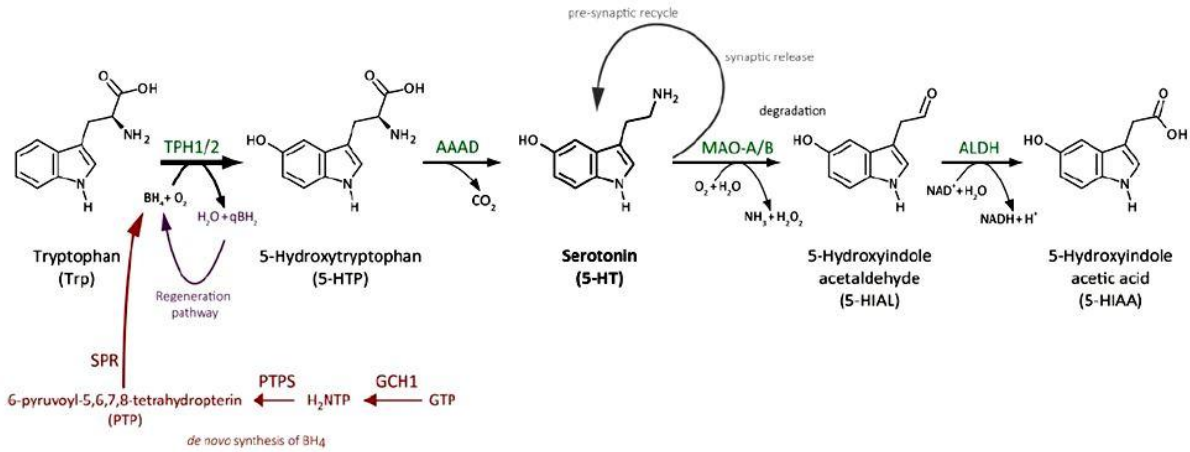

Fig. 2 – Synthesis and Degradation of 5-HT

This figure shows the pathway of 5-HT synthesis and degradation with the key-enzymes and cofactors. Highlighted in green are the sequential enzymes of the 5-HT metabolism, in purple the regeneration pathway of tetrahydrobiopterin (BH_4) and in red the *de novo* synthesis pathway for BH_4. AADC: aromatic amino acid decarboxylase; ALDH: aldehyde dehydrogenase; MAO-A/-B: monoamine oxidase A and B; GCH1: cyclohydrolase 1; PTPS: 6-pyruvoyl-5,6,7,8-tetrahydropterin; qBH2: quinoid dihydrobiopterin.

The first step in 5-HT synthesis is the TPH mediated hydroxylation of Trp to 5-hydroxytryptophan (5-HTP); however calculations estimate that only 5-10% of total bioavailable Trp is used for 5-HTP synthesis in humans (Salter et al., 1995; Stone & Darlington, 2002; Watts et al., 2012). Trp is mainly used for other biochemical pathways and for protein synthesis. There are even studies suggesting that about 99% of all ingested Trp is used for other pathways than 5-HT synthesis, such as metabolization by indoleamine dioxygenase 1 and 2 (IDO 1 and 2) (Ball et al., 2009; Duleu et al., 2010; Kwidzinski & Bechmann, 2007; Kwidzinski et al., 2003; Stone & Darlington, 2002).

This first anabolic step is mediated by either TPH1 or TPH2 in a rate-limiting manner and chemically identical. The reaction requires Fe^{2+}-ions, oxygen (O_2) and tetrabiopterin (BH_4) as cofactors (Lovenberg et al., 1967) (see Fig. 2). The here generated 5-HTP gets decarboxylated by an aromatic amino acid decarboxylase (AADC) to 5-HT in the second step. AADC is broadly distributed throughout the whole mammalian body with highest activity levels in pineal gland, liver, and adrenal glands (Rahman et al., 1981). It can also decarboxylate Trp directly to tryptamine.

In the end, 5-HT is degraded by monoamine oxidases (MAO) to 5-hydroxyindole acetaldehyde (5-HIAL) (see Fig. 2). The flavoproteins MAO can be found throughout the mammalian body, are located at the outer mitochondria membrane of cells and arise in two isoforms, coded by two different genes: MAO-A and MAO-B. Both isoforms are able to metabolize numerous biogenic amines in the body with different specificities (Shih & Chen, 2004). 5-HT, dopamine and norepinephrine are mainly degraded by MAO-A, while trace amines (tyramines, benzylamine, or beta-phenylethylamines) are degraded by MAO-B (Beis, 2014; Luo et al., 2003). Finally, 5-HIAL is degraded to 5-hydroxyindole acetic acid (5-HIAA) via aldehyde dehydrogenase (ALDH). 5-HIAA is the last catabolic substrate of this pathway and gets secreted in the urine (Brady et al., 2012). Elevated urinary levels of 5-HIAA can be found in patients with malignant carcinoid tumors, especially with liver metastases, which synthesize massive amounts of 5-HT.

1.3 From Serotonin Transporters and Receptors and other Signaling Mechanisms

The cytoplasmatically synthesized pool of 5-HT (e.g. in EC in the gut or RN in the brain) can be used for either serotonylation of some proteins (Paulmann et al., 2009; Walther et al., 2003b) or needs to leave the cells to act as an ubiquitous hormone throughout the periphery or as a neurotransmitter in the CNS. For that 5-HT has to switch cellular compartments and needs a transporter. Consistently, released 5-HT needs molecular receivers on target cells that respond to signaling (reviewed in Beis, 2014).

1.3.1 Large neutral amino acid transporter (LNAAT)

Not directly a 5-HT transporter but still important to mention is the large neutral amino acid transporter (LNAAT) that is located (luminal and abluminal) in endothelial cells and translocates Trp from the plasma into the brain tissue to supply the 5-HT synthesis via TPH2 here. This carrier is able to transport large neutral amino acids (LNAA[2]) like Trp through the BBB in a sodium-dependent manner (O'Kane et al., 2004).

1.3.2 Vesicular monoamine transporter (VMAT)

If the 5-HT content in the cytoplasm is not used for serotonylation of proteins via transglutaminases (TG) (Hummerich & Schloss, 2010; Paulmann et al., 2009), it must be transferred into vesicles for the further transport. For this purpose there is a transport system controlled by the vesicular monoamine transporters (VMAT). VMAT are integrated in the lipid bilayer of secretory vesicles for intracellular storage and release of biogenic amines. There are two isoforms of VMAT existing: VMAT1, that is expressed in the peripheral system (e.g. in chromaffine cells and EC) but also in neuronal cells of the PNS, and VMAT2, that is mainly expressed in monoaminergic cells of the CNS, but also in some cells of the uterus and the oxyntic mucosa of the stomach (Bottalico et al., 2004; Erickson et al., 1996) and in the biggest storage site for peripheral 5-HT: the blood platelets (Cesura et al., 1990; Zucker et al., 2001).

1.3.3 Serotonin transporter (SERT)

After 5-HT has been released into the extracellular space or, in case of the CNS, into the synaptic cleft, its activity is terminated by the re-uptake into the releasing cell or into another cell (e.g. blood platelets or glia cells) (Höltje et al., 2003; Rudnick, 2006a). This transport is mediated by a serotonin transporter (SERT or 5-HTT), which is a 12-membrane spanning transporter encoded by a single gene (*Slc6a4*) and it is expressed in many different cell types, as blood platelets, liver cells, cells of the intestine and 5-HT positive neurons in the CNS (Hensler, 2012; Lesch et al., 1993; Mercado & Kilic, 2010; Rudnick, 2006). As an anti-porter SERT exchanges extracellular 5-HT against intracellular K^+ at physiological conditions (physiological gradient of Na^+ and Cl^- is needed (Rudnick, 2006b)).

[2] Large neutral amino acids (LNAA) are: Leucine, isoleucine, valine, tryptophan, tyrosine, phenylalanine, methionine, alanine, histidine, threonine and gycine.

1.3.4 Serotonin receptors (5-HT receptors)

Generally, each neurotransmitter needs a proper recipient structure on a target cell to transmit a signal or activate cellular processes. According to the latest statement of the International Union of Basic and Clinical Pharmacology (IUPHAR) there are at least 14 different receptor types in the mammalian serotonergic system which are encoded by at least 18 different genes. These receptors can be classified into seven groups due to their pharmacological properties, molecular structure and downstream second messenger signaling. Most of the 5-HT receptors are G-protein coupled seven transmembrane receptors (GPCR). Only one group appears to be an unselective ligand gated ion channel (LGIC) namely 5-HT_3 (5-HT receptor type 3 and subtypes) that mediates post-synaptic depolarization and rapid desensitization (Niesler et al., 2003; van Hooft & Yakel, 2003).

Besides the numerous inter- and intracellular effects throughout the CNS which were subject of equally numerous studies (see for example Barnes & Sharp, 1999; Lesch & Waider, 2012; Millan et al., 2008; Nichols & Nichols, 2008) GPCR 5-HT receptors are broadly involved in activation and signaling in the mammalian peripheral system:

In the **gut** the major 5-HT receptor is 5-HT_4 which, activated by 5-HT, enhance the release of transmitters from submucosal intrinsic afferent neurons and hence controls peristaltic and secretory reflexes. Another receptor which is discussed to be involved in this area is the 5-HT_{1P} type (unofficial name) (Frazer & Hensler, 1999; Gershon, 2004).

In **liver** it is known that 5-HT_{2A} and 5-HT_{2B} are the key players in tissue regeneration and cell proliferation as well as in controlling of the hepatic blood flow (Clavien, 2008; Ruddell, Mann, & Ramm, 2008; Ruddell et al., 2006).

In **kidney** it could not clearly be shown which receptor type is dominantly active, but is was validated that 5-HT_{2A} and 5-HT_{2B} are expressed (Watts & Thompson, 2004) as well as 5-HT_{1A} (Raymond et al., 1993). What seems to be quite certain as well is that 5-HT receptors mediate the salt and water transport in the mammalian kidney and hence regulate blood volume and pressure.

In the mammalian **heart** the story becomes even more complicated: It is well-known that 5-HT_4 is expressed in cardiomyocytes and at the heart valves and it is mainly involved in increasing atrial function and arrhythmias as well as positive inotropic[3], lusitropic[4], and arrhythmic effects in the ventricles (Kaumann & Levy, 2006). HT_{2B} was shown to be crucial for normal heart development and function (Nebigil & Maroteaux, 2001). 5-HT can also act as a sympatholytic through activation of 5-HT_1 receptors on sympathetic nerve terminals, inhibiting norepinephrine release. Even though they are not GPCR 5-HT receptors, it needs to be mentioned here, that 5-HT_3 receptors also play a critical role in the heart due to their distribution in the vagus nerve (*nervus vagus, n. vagus*) and their ability to activate the Bezold-Jarisch[5] reflex (Saxena & Villalón, 1990). Other 5-HT receptors can be found in the heart or

[3] Positive inotropic effect: Increase of the strength of muscular contraction.
[4] Lusitropic effect: Rate of myocardial relaxation
[5] Bezold-Jarisch reflex: Variety of cardiovascular and neurological processes which cause hypopnea (excessively shallow breathing or an abnormally low respiratory rate) and bradycardia (abnormally low resting heart rate).

related structures and all are handled as modulators for heart rate, blood pressure and cell proliferation (Watts et al., 2012).

The last peripheral organ that will be introduced here is, to be correct, an organ network, namely the **blood vessels**: As described above, 5-HT was discovered, in part, as a vasoconstrictor and for this property 5-HT is known best in the cardiovascular and maybe even in the whole peripheral system. As reviewed in Watts et al., 2012 it can be summarized that 'virtually every blood vessel, when mounted in a tissue bath, responds to 5-HT with contraction from baseline. By contrast, not all blood vessels can relax to 5-HT.'. To elucidate this general statement a bit, here are the major 5-HT receptor types and their function in the human and/or murine vasculature: Mouse **aorta** (contraction by 5-HT_{2B}); human **coronary artery**, *arteria coronaria* (contraction by 5-HT_2); human **femoral artery**, *arteria femoralis* (contraction by 5-HT_2); human **saphenous vein**, *vena saphena magna* (contraction by 5-HT_{1B}, 5-HT_{2A}); human **cerebral artery**, *arteria cerebri* (contraction by 5-HT_{1B}, 5-HT_{2A}; relaxation by unknown receptor type). There are several more 5-HT receptors acting on the vessels of different mammalian species (see **Fig. 3**) and the exact detailed structure and distribution of 5-HT receptors in the mammalian vasculature stays unclear.

1.3.5 Serotonylation

In addition to all above described modes of action, 5-HT has been shown to play the key role in another critical intracellular process: the serotonylation. Serotonylation is a receptor independent signaling mechanism in which 5-HT is covalently bound to small GTPases by transglutaminase 2 (Walther et al., 2003b). It could be demonstrated that serotonylation of those small GTPases leads to α-granule release. α-granules are known to carry a broad variety of molecules, such as adhesion molecules, inflammatory molecules, pro- and anticoagulation factors, chemokines and membrane proteins (Barthels, 2012). Hence, 5-HT is able to trigger processes like platelet aggregation, cell proliferation and inflammation but also insulin secretion (Hummerich & Schloss, 2010; Paulmann et al., 2009; Walther et al., 2003b). Furthermore, it could been shown that serotonylation of the small GTPase Ras homolog gene family, member A (RhoA) is involved in the development of pulmonary hypertension (PH) in mice (Guilluy et al., 2009) and that serotonylation of cell skeleton proteins can cause contraction of blood vessels (e.g. aorta) in rat (Watts, Priestley, & Thompson, 2009). Latest findings even identified a direct role of 5-HT, independent from its contributions to neurotransmission and cellular signaling, in the mediation of permissive gene expression (Farrelly et al., 2019).

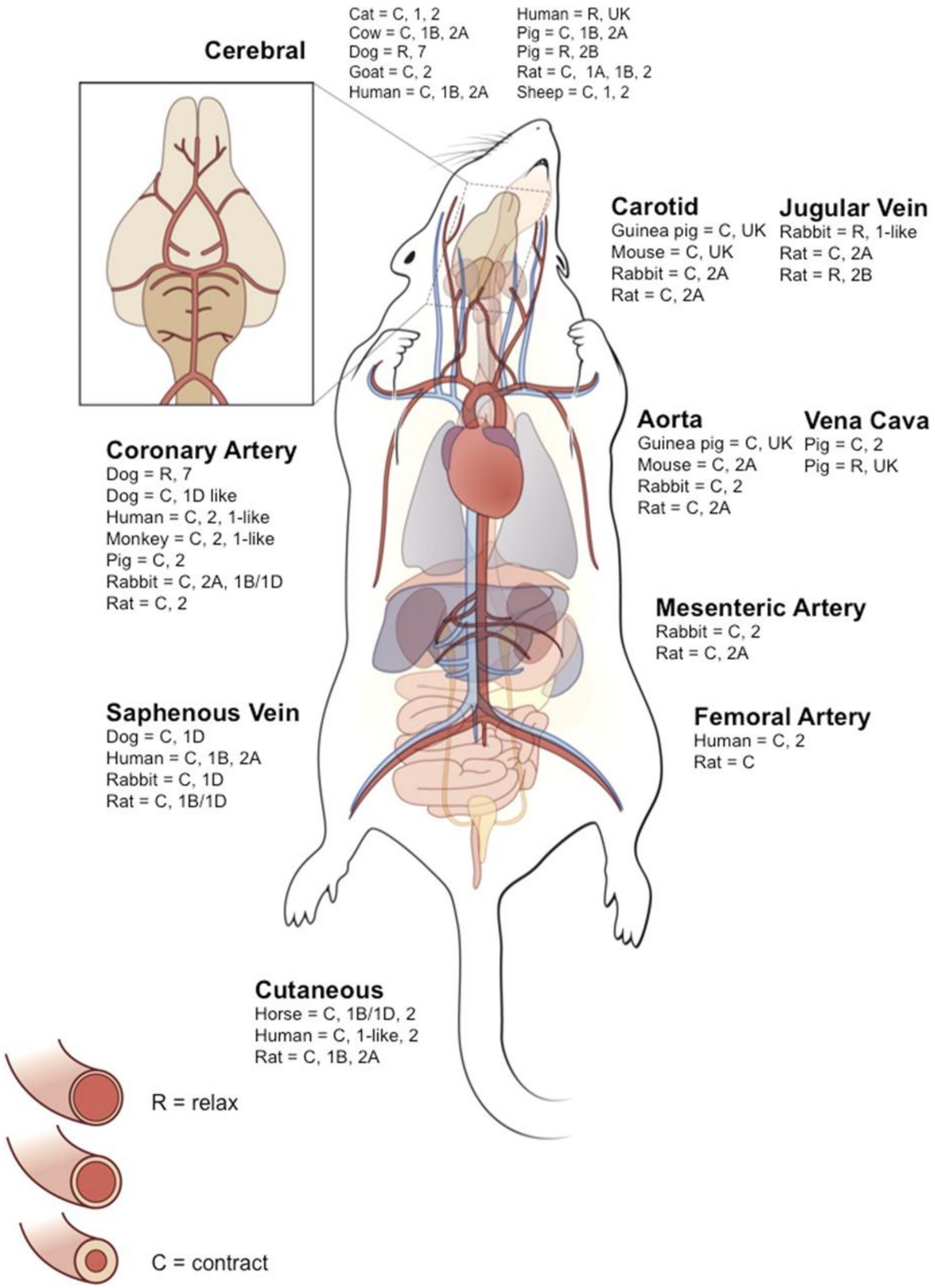

Fig. 3 – Response of the Mammalian Vasculature to 5-HT
A scheme of the mammalian vasculature, as depicted by using the rat vasculature as a model. Both constriction (C) and relaxation (R) may be listed for the same species if both responses were observed. Species name is listed, and the subtype of the receptor mediating the response is listed second (1B, 2A). UK, unknown receptor mechanism. Picture taken from Watts et al., 2012.

Tab. 1 - 5-HT Receptors Overview
Overview of 5-HT receptors, their tissue distribution and a selection of possible agonists and antagonists. All specifications are reviewed from Watts et al., 2012, and currentness of data was confirmed by the 'Guide to Pharmacology – 5-HT receptors' (https://www.guidetopharmacology.org/GRAC/FamilyDisplayForward?familyId=1). Some of the agonists and antagonists could not be confirmed by both of the mentioned authorities; in these cases the substances got labeled with either *(only from Watts et al., 2012), #(CP-809101: Strong et al., 2009; CPBG: Kondaurova et al., 2012), °(receptor type not described in the 'Guide to Pharmacology'. SMC: Smooth muscle cells.

5-HT Receptor Name	Location and Function (selection)	Agonists (selection)	Antagonists (selection)
5-HT_{1A}	CNS; lower, raise blood pressure **Kidney** Coronary arteries (poorly expressed)	8-OH-DPAT U92016A NLX-112	WAY100635 NAN 190 Robalzotan
5-HT_{1B}	SMC; contraction CNS + PNS; lower, raise blood pressure Coronary arteries, Heart	Eletriptan (partial) Sumatriptan (partial) 8-OH-DPAT	GR 127935 GR-55562 SB236057 (inverse)
5-HT_{1D}	SMC; contraction Coronary artery, Heart (poorly expressed)	PNU109291 Alniditan Eletriptan	SB 272183 Zotepine Metergoline
5-HT_{1E}	CNS (partly)	BRL-54443	Methylergonovine
5-HT_{1F}	SMC; contraction CNS	LY334370	Methysergide
5-HT_{2A}	Platelets; aggregation, 5-HT release SMC; contraction Heart; contraction CNS **Liver** **Kidney**	TCB-2* DOB DOI	Fananserin Ketanserin LY86057 Sarpogrelate
5-HT_{2B}	Endothelium; relaxation SMC; contraction **Cardiac valves; proliferation** **Liver** **Kidney**	BW723C86 LSD Methylergonovine	RS-127445 BF-1 EGIS-7625
5-HT_{2C}	CNS Resting lymphocytes	CP-809101# WAY-163909	RS-102221 SB 242084
5-$HT_{3A,B,C,D,E}$[6]	**N. vagus**; Bezold-Jarisch reflex	CPBG#°	Ondansetron*°
5-HT_4	**Cardiomyocytes; contraction** Intestine CNS	RS67506	GR 113808
5-HT_{5A}	CNS	LSD	methiothepin
5-HT_6	CNS Thymus	WAY-181187	SB399885
5-HT_7	SMC; relaxation Cardiomyocytes, contraction Aorta CNS	AS-19 LP-12 LP-44	SB269970 SB 258719 Lurasidone

[6] Only genes are described for 5-HT receptors 3D and 3E (Beis, 2014).

1.4 The Omnipresence of Serotonin in the Periphery

Based on all of its previously described chemical properties, biological abilities and physiological interactions one could really call 5-HT a 'fantastic beast'.

As mentioned before 5-HT receptors can be widely found in the CNS and organs of the periphery, such as gut, liver, kidney, adrenal gland, smooth muscle cells (SMCs), heart and blood vessels. The same is naturally true for 5-HT which was shown to influence hepatic regeneration (Lesurtel & Clavien, 2012 and 2012a; Lesurtel & Clavien, 2014; López et al., 2014; Starlinger et al., 2014) , modulation of the immune system (Cadirci et al., 2013; Medina-Martel et al., 2013; Regmi et al., 2014) and indirectly influence peristaltic processes via stimulation of the enteric nervous system (ENS-stimulation) (Ahern, 2011; Gershon, 2012). It was even discussed whether plasma 5-HT has an effect on osteoblast proliferation and hence influences bone mass (Cui et al., 2011; Lee et al., 2014; Yadav et al., 2009). Other studies could prove that 5-HT is present in testis and breast cells, endothelial cells, pancreatic Langerhans cells, some renal cell types, and more (reviewed in Grohmann, 2009). Consequently, peripheral serotonin plays a role in multiple processes, such as embryonic development (Buznikov et al., 2001; Nebigil et al., 2000), cardiac development and function (Côté et al., 2003), pulmonary hypertrophy (Morecroft et al., 2007), insulin-release from beta-cells (Paulmann et al., 2009), and many more.

In general, 5-HT acts at manifold target sites para-, auto-, and endocrine as hormone or growth factor ("autacoid") (Gershon, 2012). The endocrine pool of 5-HT in the periphery is mainly taken up by platelets (thrombocytes) that express SERT and then stored in small dense vesicles (Ormsbee & Fondacaro, 1985). This 5-HT pool has a major impact on primary homeostasis and liver regeneration (Lesurtel et al., 2006).

Regarding all the different tissues and cell types where 5-HT can be found and all the different processes in which it is involved it becomes obvious that targeting the 5-HT system with any kind of systemically applied medication or genetic modulation may cause several physiological effects in between it might become difficult to differentiate.

1.5 Serotonin and Atherosclerosis

As described, 5-HT, 5-HT receptors as well as TPH and SERT can be found throughout the mammalian peripheral system. Same is true for **macrophages** (Nocito et al., 2008; Sternberg et al., 1986; Suguro et al., 2006), **smooth muscle cells** (SMCs) (Höltje et al., 2003; Liu et al., 2008), **endothelial cells** (Pakala et al., 1994; Vanhoutte, 1991; Vikenes et al., 1999), **mast cells** (Kushnir-Sukhov et al., 2007) and **platelets** (Clavien, 2008; Dees et al., 2011; Walther & Bader, 2003). All of these cell types are involved in the pathogenesis of atherosclerosis and atherosclerotic plaque (AP) formation (Hansson et al., 2006; Ross, 1994) (see Fig. 4). Hence, it is reasonable to suppose that 5-HT is involved in atherosclerotic processes.

1.5.1 A short Introduction to Atherosclerosis

According to the World Health Organization (WHO) cardiovascular diseases (CVD) are the number one cause of death globally: more people die annually from CVDs than from any other cause. An estimated 17.9 million people died from CVDs in 2016, representing 31% of all global deaths. Of these deaths, 85% are due to heart attack and stroke (World Health

Organization (WHO), 2017). And these facts are true for people all over the world, independent from income or other social factors. The major mechanism involved in many types of CVDs is atherosclerosis which can be promoted by risk factors, such as high blood pressure, smoking, diabetes mellitus, lack of exercise, obesity, high blood cholesterol, poor diet, and excessive alcohol consumption (Mendis et al., 2011).

Atherosclerosis is a chronic disease of arterial blood vessels that causes their narrowing by the accumulation of atherosclerotic plaques (APs) at the vascular wall (see **Fig. 4, Overview**). AP formation is a multistep process that initiates by a damage of endothelial cells of the blood vessel. This leads to endothelial dysfunction which is characterized by a decreased production of nitric oxide (NO) and reduced vasodilation (Endemann & Schiffrin, 2004). Low-density lipoproteins (LDL) from the blood stream invade the arterial intima and oxidize. In the following, leukocytes, such as monocytes and neutrophils, were shown to attach to the damaged endothelial cells followed by rolling, adhesion and transendothelial migration (von Hundelshausen et al., 2009) (see **Fig. 4A**). This step was shown to be supported by intra-intimal mast cells which secret pro-inflammatory cytokines (Kelley et al., 2000; Sun et al., 2007). Monocytes which get in contact with the oxidized LDL differentiate to macrophages (see **Fig. 4B**) These monocyte-derived macrophages inside of the intima bind the oxidized LDL via a family of receptors known as scavenger receptors, which recognize LDL exclusively in an oxidized state (Goldstein et al., 1979; Ross, 1994). Uptake of oxidized LDL makes the macrophages less mobile, thereby promoting the accumulation of these lipid-laden cells in the intima, where they form foam cells (Gerrity, 1981; Yu et al., 2013). At this stage of the AP formation the accumulation of cells and debris in the arterial intima is called a 'fatty streak' (see **Fig. 4B,C**). Another important cell type in this early stage of AP formation is the neutrophil. It was documented that neutrophils produce and excrete chemokines, which determine whether macrophages differentiate towards pro- or anti-inflammatory cells (van Leeuwen et al., 2008) (see **Fig. 4C**), and they could be detected in ruptured APs what suggests a role in AP stability (Sasaki et al., 2006).

Vascular smooth muscle cells (VSMC) are also involved in the AP formation process. They migrate from the arterial media through openings in the internal elastic lamina to the intima responding to cytokines and growth factors secreted by activated platelets (e.g. platelet-derived growth factor B (PDGF-B)), monocytes and endothelial cells in arterial lesions (Ross, 1993) (see **Fig. 4D**). In the intima they form thickenings by proliferation and secretion of extracellular matrix (ECM) components. They lose their contractile phenotype by reduction of their actin and myosin filaments and become secretory, by an increased formation of endoplasmic reticulum and Golgi apparatus (Thyberg et al., 1995). In the AP, VSMC form a fibrous cap which covers the fatty streak and provides the plaques with more stability. Furthermore, the secreted growth factors inside of the intima induce collagen accumulation. Collagen can constitute up to 60% of the complete AP protein (Smith, 1965). The fragile balance between collagen synthesis and breakdown inside of the AP can be crucial for the fibrous cap stability (Amento et al., 1991; Rekhter, 1999) (see **Fig. 4D**).

At a late stage of atherogenesis it can come to the process of vascular calcification; more precisely, intimal and medial calcification. Vascular calcification is the pathological deposition of mineral in the vascular system that leads to vascular stiffness and reduced vascular flexibility (Wu et al., 2013). It could be demonstrated that in human patients the amount of e.g. coronary calcium correlates with hypertension and that it can be used as a reliable predictor for future cardiovascular events, such as myocardial infarction. Vascular (here coronary) calcium amounts represent an additional and independent risk factor for CVD (Mayer et al., 2007; Shaw et al., 2003).

The final phase of atherogenesis is the severe narrowing of the affected blood vessel (see **Fig. 4E**) what can result in a decreased blood flow in the following tissues (e.g. extremities) (Derrick et al., 1959). If the AP is big enough the shear stress of the bypassing blood, plus instability of the AP fibrous cap will lead to an AP rupture. This results in a release of the necrotic core material from the AP into the blood stream where platelets immediately attach to the debris and form blood clots (thrombosis) (see **Fig. 4F**). Those clots or AP compartments can also detach and get into the blood stream where they get transported through the vascular system and have a high risk to block the following smaller arteries. Blocked arteries cause embolic events, such as myocardial infarction or stroke (Falk, 1992; Fuster et al., 1990).

One, at the first glance, maybe a bit underestimated cell type involved in AP formation (also: atherogenesis), is the blood platelet. The role of the blood platelets in atherogenesis goes way beyond its obvious functions in haemostasis and thrombosis: It was shown that platelets are a crucial player in pro-inflammatory processes (e.g. atherogenesis) and act on all involved cell types, from endothelial cells to VSMC, triggering for example chemokine secretion and proliferation (Huo et al., 2003; Lievens & van Hundelshausen, 2011; Weber, 2005). And since platelets are the major 5-HT storage in the mammalian blood (Becker, 2008), the story of blood platelets in atherosclerosis can be told as a story of 5-HT in atherosclerosis…

1.5.2 The Role of Serotonin in Atherosclerosis

It could be shown that patients with atherosclerosis exhibit higher concentrations of plasma 5-HT (ratio of plasma 5-HT to whole blood 5-HT) than healthy controls (Hara et al., 2004). On the other hand patients with hypercholesterolemia were documented to exhibit decreased platelet 5-HT levels than controls (Smith & Betteridge, 1997) (see also **Tab. 2**). These findings taken together with the fact that in mice oxidized LDL stimulates platelets to release 5-HT from dense granules into the plasma (Zhao et al., 1995) support the image of 5-HT release from platelets into the plasma is a crucial part of atherogenesis and can be used as a biomarker for the disease.

In 2008, van Leeuwen and colleagues showed that a long-term high-fat diet, which was described previously to induce atherogenetic processes in mice (Nishina et al., 1990), activates neutrophils which subsequently tend to accumulate at the lesion sites and secret drastically increased levels of myeloperoxidase (MPO). As described above, in this situation 5-HT is released from activated platelets, serves as a physiological substrate for MPO and reacts to the cytotoxic compound tryptamine-4.5-dione. MPO was shown to be able to injure the endothelium (Ximenes et al., 2009). Furthermore, 5-HT stimulates endothelial cells to produce a neutrophil chemoattractants (Charles et al., 1991) which may increase the amount of neutrophils in atherosclerotic plaques further and boost their local toxicity. In contrast, 5-HT could also be shown to have a mitogenic effect on arterial endothelial cells which is mediated by 5-HT_2 receptor type (Pakala et al., 1994) (see also **Tab. 2**).

The next step in the AP formation process 5-HT actively influences, is the macrophage-derived foam cell formation in the arterial intima: 5-HT was demonstrated to up-regulate the expression of acyl-coenzyme A:cholesterol acyltransferase-1 (ACAT-1) inside of monocyte-derived macrophages via 5-HT_{2A} receptor pathway which results in an increased intracellular transformation of free cholesterol (FC) to cholesterol esters (CE) (Suguro et al., 2006). CE can be used for intracellular storage in lipid droplets which is an important step in foam cell formation (see also **Tab. 2**).

Cultured VSMC express TPH1, are able to synthesize 5-HT and take it up by SERT. In VSMC, 5-HT is not stored in vesicles but located in a scattered manner in the cytoplasm (Ni et al., 2008). Various studies have shown the potential of 5-HT to induce proliferation and migration of VSMC (Guilluy et al., 2009; Lee et al., 1998; Liu et al., 2011; Nemecek et al., 1986; Tull et al., 2006) (see also **Tab. 2**). These processes can be blocked by 5-HT_{2A} receptor antagonist application (e.g. sarpogrelate) (Sharma et al., 1999).

Mast cells, that store and release 5-HT, could also be detected in AP. Mice lacking mast cells showed smaller lesion size with less fatty streaks, and with a decreased number of T-cells and macrophages in the plaques (Sun et al., 2007) (see also **Tab. 2**).

As there is some evidence that 5-HT affects bone mass (Cui et al., 2011; Lee et al., 2014; Yadav et al., 2009) it appears plausible that 5-HT might as well act on vascular calcification. It was highlighted recently that calcification is a response to the injury that is caused by the primary event of atherogenesis (Aherrahrou & Schunkert, 2013) and latest data support the hypothesis that a lack of peripheral 5-HT increases cardiac and aortic calcification (Aherrahrou & Alenina, unpublished data) (see **Tab. 2**).

Lastly, the role of 5-HT in the ECM synthesis needs to be mentioned. It could be demonstrated that mice lacking peripheral 5-HT ($Tph1^{-/-}$) are protected from bleomycin induced dermal fibrosis. The same is true for $5\text{-}HT_{2B}^{-/-}$ which are lacking the 5-HT_{2B} receptor (Dees et al., 2011) (see also **Tab. 2**). Since the accumulation of collagen, which is one of the main compounds of the ECM, is important for AP stability, 5-HT could be crucial for AP composition, the prevention of AP rupture and, subsequently, of embolic events.

In conclusion, there are many possible target sites for 5-HT in the atherogenetic process. However, there is no systematic study of the importance of 5-HT in the parthenogenesis of atherosclerosis in an animal model. The possible modes of action for 5-HT in atherosclerosis are manifold (see **Tab. 2**) and this study is going to offer a novel approach in this field based on a peripherally 5-HT lacking mouse model which may open up new avenue for future scientific questions.

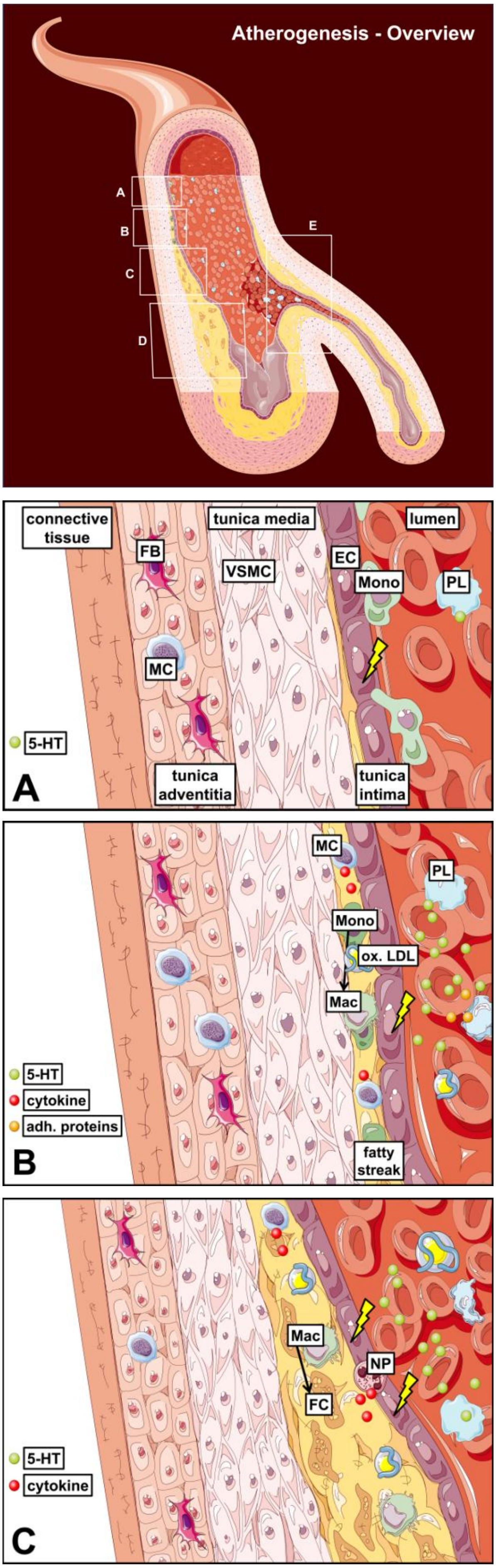

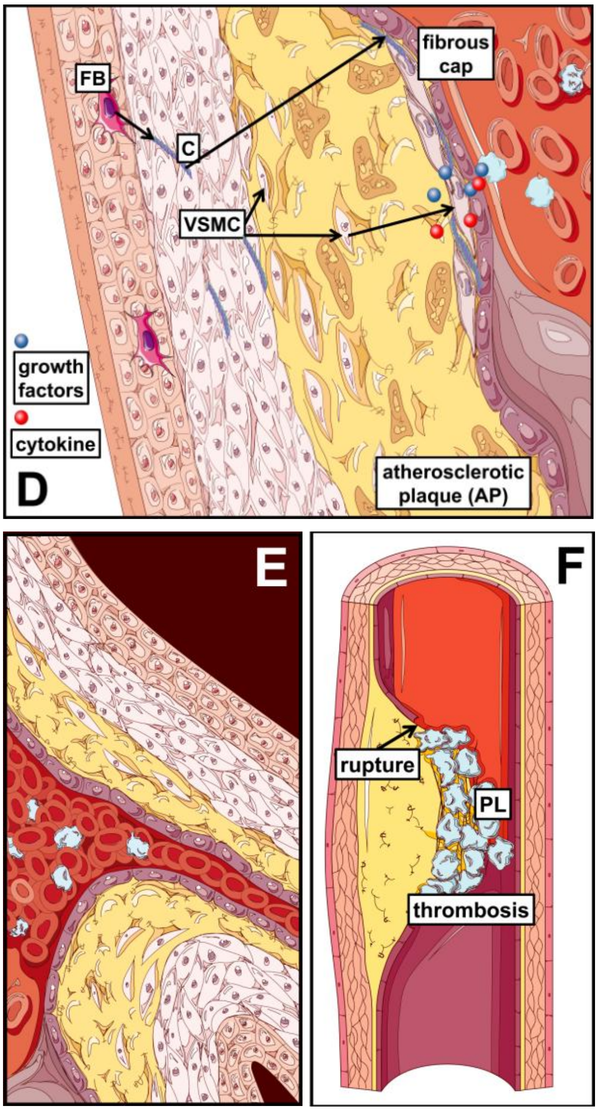

5-HT: Serotonin; **FB:** Fibroblast; **MC:** Mast Cell; **VCMS:** Vascular Smooth Muscle Cell; **EC:** Endothelial Cell; **Mono:** Monocyte; **PL:** Platelet; **ox.LDL:** oxidized Low-density Lipoprotein; **Mac:** Macrophage; **FC:** Foam Cell; **NP:** Neutrophil; **C:** Collagen

Fig. 4 – Atherogenesis
Summary of processes during atherogenesis. Overview sketch illustrates all phases of atherogenesis in one arterial blood vessel. **A** depicts different cell layers of the artery and the onset of atherogenesis including endothelial damage (yellow lightning) which leads to endothelial dysfunction. **B** highlights formation of fatty streaks including the intra-intimal differentiation of monocyte-derived macrophages and the luminal secretion of 5-HT from platelets. **C** shows formation of macrophage-derived foam cells, while **D** depicts late phase including development of fibrous cap via migrating VSMC and Collagen. **E** illustrates severe vessel narrowing, whereas **F** shows AP rupture and thrombosis formation.

Tab. 2 – 5-HT effects in Atherogenesis
Overview of 5-HT modes of action and their effect during atherogenesis. ↑ indicate an increase; ↓ indicate a decrease. Data reviewed from text references.

Involved Tissue/Cell Type	5-HT Mode of Action	Effect
Platelets	• Atherosclerotic lesions/presence of oxidized LDL cause 5-HT secretion from platelets into plasma • 5-HT triggers secretion of chemokines, adhesive proteins and growth factors from platelets	Plasma 5-HT ↑ Chemokines ↑ Adhesive Proteins ↑ Growth Factors ↑
Neutrophils	• 5-HT stimulates endothelial cells to produce neutrophil chemoattractants • 5-HT reacts with neutrophil-derived MPO to tryptamine-4.5-dione	Neutrophils at Lesion ↑ Chemokines ↑
Endothelial cells	• 5-HT stimulates endothelial cells to produce neutrophil chemoattractants • 5-HT has a mitogenic effect on endothelial cells	Neutrophils at Lesion ↑ Endothelial damage ↓
Macrophages/ Foam cells	• 5-HT up-regulates ACAT-1 which increases FC transformation to CE, this supports foam cell formation	Foam Cell Formation ↑
VSMC	• 5-HT induces VSMC proliferation and migration	Fibrous Cap ↑
Mast cells	• Mast cell-derived 5-HT and pro-inflammatory cytokines exacerbate atherogenetic processes	Pro-inflammatory Cytokines ↑
Fibroblasts/ECM	• 5-HT appears to be important for ECM synthesis	Fibrous Cap ↑ Fibrous Cap Stability↑
Calcification	• unknown	Calcification ↓

1.6 Studying Atherosclerosis in a Mouse Model

The mouse has been used in medical research for decades. Well-known genetic background, easy to breed and low cost of maintenance are among advantages of this model. However, small size and some physiological characteristics may be considered as limiting factors. For example, the plasma lipoprotein profile in mice is very different from that in humans. The circulating cholesterol is mainly in high-density lipoprotein (HDL) particles in the mouse, while it is in LDL particles in humans. This is probably the main reason that wild-type mice do not develop atherosclerosis, but humans do (Kapourchali et al., 2014).

Today, there are numerous genetically modified mouse models available for basic cardiovascular research and, to be more precise, for the research on atherosclerosis. Among them, LDL receptor-knockout (KO), hepatic lipase-KO, human apo B_{100} expression and human cholesterylester transfer protein (CETP) expression can be named (Kapourchali et al., 2014). A probably similarly high number of mouse models is accessible for research in the field of 5-HT and related targets of interest: A broad variety of classical and conditional 5-HT receptor knockout, knock-down or knock-in mouse models is provided as well as genetic models possessing dysfunction in 5-HT production (TPH1, TPH2 or BH_4 deficiency), intracellular transport (VMAT), re-uptake (SERT) or degradation (MAO) are at hand.

In the light of this huge spectrum of options, it is very important to choose the right animal model for the present scientific question. In case of this study it was important to choose a reliable animal model for all phases of atherosclerosis (e.g. the ApoE-deficient mouse) and a mouse model which consistently lacks 5-HT at the peripheral system (e.g. the Tph1-deficient mouse). Well planned breeding strategies enabled us to combine the properties of interest in double KO animals. During the course of the study it became more and more important to additionally investigate a mouse model for a depleted re-uptake of 5-HT into the cells (e.g. the SERT-deficient mouse).

1.6.1 The *ApoE*$^{-/-}$ Mouse

The *ApoE*$^{-/-}$ mouse was firstly bred in 1992 by Zhang and colleagues, who successfully deleted the apolipoprotein (Apo) E gene from the mouse genome. The hence generated KO mouse exhibits five times normal plasma cholesterol compared to controls (more than 10-times when fed high-fat Western-type diet (Plump et al., 1992)) and develops foam-cell rich depositions in their proximal aortas by the age of three months. These spontaneous lesions were reported to progress and cause severe occlusions of the coronary ostium by an age of eight months (Zhang et al., 1992). Later studies confirmed the initial results and demonstrated that the *ApoE*$^{-/-}$ exhibits all phases of atherogenesis throughout the arterial tree and serves as a promising model system to study atherosclerosis (Nakashima et al. 1994).

1.6.2 The *Tph1*$^{-/-}$ Mouse

As described above, it was in 2003 when Walther and colleagues established a classical KO mouse model for TPH1 depletion which resulted in a complete lack of 5-HT in the periphery, except for the duodenum which contained approx. 4-10% of the control 5-HT levels. This was discussed to be either due to the serotonergic neurons innervating this tissue (Walther et al., 2003a) or to an alternative 5-HT synthesis pathway via phenylalanine hydroxylase (Matthes & Bader, 2018). In *Tph1*$^{-/-}$ mice the levels of brain 5-HT (e.g. hippocampus and frontal cortex) stay unaltered compared to control. This is of importance since it was shown that brain 5-HT has a direct influence on cardiovascular parameters, such as heart rate, respiration rate and the mean arterial blood pressure (Beis, 2014; Kellett et al., 2005; McCall, 1990) which play an important role in atherosclerosis as well.

1.6.3 The *Sert*$^{-/-}$ Mouse

Originally generated via homologous recombination the *Sert*$^{-/-}$ mouse (*Slc6a4*$^{-/-}$) lacks the full length SERT protein and exhibits an absence of 5-HT reuptake, leading to a decreased rate of synaptic 5-HT clearance and a 4-fold to 6-fold increase in basal levels of forebrain extracellular 5-HT (Bengel et al., 1998; Holmes et al., 2003). In *Sert*$^{-/-}$ animals the blood 5-HT was shown to be zero (Chen et al., 2001). Those absent or decreased intracellular levels of 5-HT in platelets may lead to an inhibition of platelet aggregation at atherosclerotic lesion sites and inhibited platelet activity in general. That is one possible reason why selective serotonin reuptake inhibitors (short SSRIs[7]) are widely discussed to be beneficial for CVD patients and can lower the risk for infarction events (reviewed in Wozniak et al., 2011). Interestingly, it could be shown that *Sert*$^{-/-}$ mice exhibit increased levels of cardiac fibrosis and valvulopathy (Mekontso-Dessap et al., 2006) which underlines the close relationship between 5-HT and ECM synthesis.

1.6.4 The Double Knockouts

Within the framework of this project we generated double KO mice for both, *ApoE* deficiency and *Tph1* deficiency, and for *ApoE* deficiency and *Sert* deficiency via planned breeding strategy. With these *ApoE/Tph1*$^{-/-}$, respectively *ApoE/Sert*$^{-/-}$, animals I had great animal models available for the elucidation of the complex systemic connections between all phases of atherosclerosis and either the complete lack of peripheral 5-HT or the extensive lack of intracellular 5-HT combined with an increased baseline level of 5-HT in the extracellular space. The latter was especially of interest in the case of blood platelets and their function on atherogenesis.

1.6.5 The Trouble with Background Strains…

A short comment needs to be made on background strains for biomedical research: It cannot be over-emphasized how important it is to consider the appropriate genetic background strain for the planned experiment.

Background strains are supposed to come along with a largely standardized and natural genome which widely lacks genetic variation in between individuals due to inbreeding over numerous generations. This is important to obtain comparable results for investigated groups of animals and for getting stable genetic mutations and phenotypes. However, it was shown that in part there are huge differences in treatment effects (e.g. drug effects) between mouse background strains (Sato et al., 2006) and, that genetic mutations sometimes lead to completely different phenotypes when applied to different genetic background strains (reviewed in The Jackson Laboratory, 2006).

For the present study there was evidence that distribution of 5-HT receptors might be different in C57Bl/6 (B6) and Friend virus B (FVB/N) mice (Todiras & Bader, unpublished data). Hence, to investigate expression and distribution of 5-HT receptors in vascularisation, I decided to use both background strains and their respective *Tph1* knockout lines. For all other experiments on atherosclerotic processes I opted for genetically modified animals in the B6 background since the majority of studies was performed similarly and the B6 mouse is known to only barely develop atherosclerotic lesions spontaneously (and only under modified diet) (reviewed in Whitman, 2004), and is genetically very susceptive for the applied mutations (*ApoE*$^{-/-}$, *Tph1*$^{-/-}$, *Sert*$^{-/-}$).

[7] Selective serotonin reuptake inhibitors (short SSRIs) are a class of drugs that are typically used as antidepressants in the treatment of major depressive disorder and anxiety disorders. Classical SSRIs are citalopram, escitalopram, fluoxetine (Prozac™), fluvoxamine, paroxetine and sertraline.

2 Materials

2.1 Chemicals

Chemical Name	Abbreviation	Company / Supplier
100bp DNA Ladder	100 bp	New England Biolabs GmbH (Germany)
2-amino-2-methyl-1-propanol		Randox Laboratories Ltd (United Kingdom)
4',6-Diamidino-2-phenylindole	DAPI	Sigma-Aldrich (Germany)
5-Hydroxytryptamine	5-HT	Sigma-Aldrich (Germany)
5-Hydroxytryptophan	5-HTP	Sigma-Aldrich (Germany)
8-Hydroxyquinoline		Randox Laboratories Ltd (United Kingdom)
Acetic acid	CH3COOH	Sigma-Aldrich (Germany)
Acetone	C3H6O	Roth (Germany)
Agarose		Biozym Scientific GmbH (Germany)
Aniline blue solution		Sigma-Aldrich (Germany)
Biebrich scarlet-acid fuchsin solution		Sigma-Aldrich (Germany)
Bouin solution		Sigma-Aldrich (Germany)
Bromphenol blue		Roth (Germany)
Butylated hydroxytoluene	BHT	Sigma-Aldrich (Germany)
Calcein (Fluorexon)		Sigma-Aldrich (Germany)
Calcium standard solution		Randox Laboratories Ltd (United Kingdom)
Carbon dioxide (Dry ice)	CO2	MDC Berlin (Germany)
carboxy-X-rhodamine	CRX	Promega GmbH (Germany)
Chloroform	CHCl3	Merck KGaA (Germany)
Citric acid	C6H8O7	Merck KGaA (Germany)
Deoxyribonucleotide	dNTP	Bioline (Germany)
Diethylpyrocarbonat	DEPC	Sigma-Aldrich (Germany)
DNase I		New England Biolabs GmbH (Germany)
DNase I reaction buffer (10x)		New England Biolabs GmbH (Germany)
DNAzol® reagent		Invitrogen (Germany)
Ethanol	C2H5OH	BERKEL AHK GmbH & Co.KG (Germany)
Ethidium bromide	EtBr	SERVA Electrophoresis GmbH (Germany)
Ethylenediaminetetraacetic acid	EDTA	Sigma-Aldrich (Germany)
Formaldehyde (37%)		Merck KGaA (Germany)
Glucose	Glc	Merck KGaA (Germany)
Glycerol		Roth (Germany)
Glycerol Gelatin (Mounting medium)		Sigma-Aldrich (Germany)
Hematoxylin		Sigma-Aldrich (Germany)
Heparine		Roth (Germany)
Hydrochloric acid	HCl	Roth (Germany)
Isoflurane		Abbott (Germany)
Isopropanol	C3H7OH	BERKEL AHK GmbH & Co.KG (Germany)
Ketamidor®		WDT eG (Germany)
Magnesium chloride	MgCl2	Merck KGaA (Germany)
Neo-Mount®		Merck KGaA (Germany)
Normal Donkey Serum	NDS	DIANOVA GmbH (Germany)
O-Cresolphthalein complexone		Randox Laboratories Ltd (United Kingdom)
Oil Red O	ORO	Sigma-Aldrich (Germany)
Paraformaldehyde (4%)	PFA	Merck KGaA (Germany)

Phosphate buffered saline	PBS	Life Technologies (USA)
Phosphomolybdic acid solution		Sigma-Aldrich (Germany)
Phosphotungstic acid solution		Sigma-Aldrich (Germany)
Proteinase K		Roth (Germany)
Random Hexamer Primer	RHP	Roche AG (Switzerland)
REDTaq® DNA Polymerase	RedTaq	Sigma-Aldrich (Germany)
RNAlater		Sigma-Aldrich (Germany)
RNase A		Promega GmbH (Germany)
Rnase inhibitor	Rnasin	ROBOKLON GMBH (Germany)
Rompun® (Xylazine)		Bayer AG (Germany)
Sodium chloride	NaCl	Roth (Germany)
Sodium chloride solution (0.9%)	Saline	MDC Pharmacy – PZN: 02737756 (Germany)
Sodium dodecylsulfate	SDS	SERVA Electrophoresis GmbH (Germany)
Sodium hydroxide	NaOH	Roth (Germany)
Sucrose		Merck KGaA (Germany)
SYBR Green		Promega GmbH (Germany)
Taq polymerase	TaqPol	New England Biolabs GmbH (Germany)
ThermoPol® reaction buffer	Pol-Buffer	New England Biolabs GmbH (Germany)
Tissue-Plus OCT™ Compound	OCT	Newcomer Supply Inc. (USA)
tris(hydroxymethyl)aminomethane	Tris, (HOCH2)3CNH2	Roth (Germany)
Tri-sodium citrate (dehydrate)		Sigma-Aldrich (Germany)
Triton X-100		Merck KGaA (Germany)
Trizol®		Life Technologies (USA)
Tween-20		Sigma-Aldrich (Germany)
Vectashield Mounting Medium with DAPI		Vector Laboratories Inc. (USA)
Weigert's haematoxylin solution		Sigma-Aldrich (Germany)
Xylol		Roth (Germany)

2.2 Antibodies

Marker	Host	Reactivity (Species)	Company / Supplier
Mac2 (Galectin-3)	rat	mouse	ORIGENE Technologies, Inc. (USA)

2.3 Oligonucleotides…

2.3.1 …for Polymerase Chain Reaction (PCR)

Gene of Interest	Primer Name	Oligonucleotide Sequence	Sequence Source
Mouse *ApoE*	ApoE_3	5'- CGAAGCCAGCTTGAGTTACAG	BioTeZ (Germany)
Mouse *ApoE*	ApoE_WT5	5' - TATCTAAACAGACTCCACAGC	BioTeZ (Germany)
Mouse *ApoE*	ApoE_KO5	5'- GACTGGGCACAACAGACAATC	BioTeZ (Germany)
Mouse *Tph1*	GTPH3	5'-CAGCTCTGTGATGGACGGTA	BioTeZ (Germany)
Mouse *Tph1*	GTPH5	5'-GCTTGCAGGAGTTGGTTCTC	BioTeZ (Germany)
Mouse *Tph1*	Neo3	5'-CTGCGCTGACAGCCGGAACAC	BioTeZ (Germany)
Mouse *Slc6a4*	IMR8899	5'-AATGGTGAGGAGTGGTGGAG	BioTeZ (Germany)
Mouse *Slc6a4*	IMR7415	5'-GCCAGAGGCCACTTGTGTAG	BioTeZ (Germany)
Mouse *Slc6a4*	IMR8890	5'-CCTAGATACCAGGCCCACAA	BioTeZ (Germany)

2.3.2 … for Quantitative Polymerase Chain Reaction (qPCR)

Gene of Interest	Primer Name	Oligonucleotide Sequence	Sequence Source
Mouse *HTr1a*	mHtr1a_FW	5'-CCGATCTCATGGTGTCAGTG	IIEG Lübeck
Mouse *HTr1a*	mHtr1a_REV	5'-GGTGATTGCCCAGTACCTGT	IIEG Lübeck
Mouse *HTr1b*	mHtr1b_FW	5'-ATGCGGTGGAGTATTCTGCT	IIEG Lübeck
Mouse *HTr1b*	mHtr1b_REV	5'-TCACAAAGCAGTCCAGCATC	IIEG Lübeck
Mouse *HTr1d*	mHtr1d_FW	5'-CACGGACCTCCTGGTTTCTA	IIEG Lübeck
Mouse *HTr1d*	mHtr1d_REV	5'-GCCCAGTATCTGTCCAGAGC	IIEG Lübeck
Mouse *HTr2a*	mHtr2a_FW	5'-TCATCATGGCAGTGTCCCTA	IIEG Lübeck
Mouse *HTr2a*	mHtr2a_REV	5'-AGGTAAATCCAGACGGCACA	IIEG Lübeck
Mouse *HTr2b*	mHtr2b_FW	5'-GCAGATTTGCTGGTTGGATT	IIEG Lübeck
Mouse *HTr2b*	mHtr2b_REV	5'-AGGGAAATGGCACAGAGATG	IIEG Lübeck
Mouse *HTr2c*	mHtr2c_FW	5'-CCATTGCTGATATGCTGGTG	IIEG Lübeck
Mouse *HTr2c*	mHtr2c_REV	5'-CATGATGGACGCAGTTGAAA	IIEG Lübeck
Mouse *HTr3a*	mHtr3a_FW	5'-CGGCAGTACTGGACTGATGA	IIEG Lübeck
Mouse *HTr3a*	mHtr3a_REV	5'-TCACCTCGATGATGCACGTA	IIEG Lübeck
Mouse *HTr3b*	mHtr3b_FW	5'-ATCCAGAACTGCAGCCTCAC	IIEG Lübeck
Mouse *HTr3b*	mHtr3b_REV	5'-GCTGCCACTCACTGTCATTC	IIEG Lübeck
Mouse *HTr4*	mHtr4_FW	5'-TCGATCTTTCACCTGTGCTG	IIEG Lübeck
Mouse *HTr4*	mHtr4_REV	5'-CCTTGCATTATGGGGAGAAA	IIEG Lübeck
Mouse *HTr5a*	mHtr5a_FW	5'-CAGGAAGACCAACAGCGTCT	IIEG Lübeck
Mouse *HTr5a*	mHtr5a_REV	5'-CGTATCCCCTTCTGTCTGGA	IIEG Lübeck
Mouse *HTr6*	mHtr6_FW	5'-GGTGCCATCTGCTTCACCTA	IIEG Lübeck
Mouse *HTr6*	mHtr6_REV	5'-GGTGGTCAGACGCCTACTGT	IIEG Lübeck
Mouse *HTr7*	mHtr7_FW	5'-CTTCTGCAACGTCTTCATCG	IIEG Lübeck
Mouse *HTr7*	mHtr7_REV	5'-TTGGCCATACATTTCCCATT	IIEG Lübeck
Mouse *MAO-A*	mMaoa _FW	5'-TGTGAGGCAGTGTGGAGGTA	IIEG Lübeck
Mouse *MAO-A*	mMaoa _REV	5'-TTATCCCCAAGGAGGACCAT	IIEG Lübeck
Mouse *Slc6a4*	mSlc6a4_FW	5'-CTGGACCAGCTGCAAGAACT	IIEG Lübeck
Mouse *Slc6a4*	mSlc6a4_REV	5'-CCTGGAGTCCCTTTGACTGA	IIEG Lübeck
Mouse *Tph1*	mTph1_FW	5'-GTGGCTATCGGGAAGACAAC	IIEG Lübeck
Mouse *Tph1*	mTph1_REV	5'-GGGGATCTGAACTGTGTCTCA	IIEG Lübeck
Mouse *Tph2*	mTph2_FW	5'-CGGGAGCTCTCCAAACTCTA	IIEG Lübeck
Mouse *Tph2*	mTph2_REV	5'-AGGTAGCCAGCCACTGGTC	IIEG Lübeck

2.4 Enzymes

2.4.1 DNA Polymerases

DNA Polymerase	Abbreviation	Company / Supplier
Moloney Murine Leukemia Virus Reverse Transcriptase	M-MLV RT	Promega GmbH (Germany)
REDTaq® DNA Polymerase	RedTaq	Sigma-Aldrich (Germany)
Taq polymerase	TaqPol	New England Biolabs GmbH (Germany)

2.4.2 Other Enzymes

Enzyme	Company / Supplier
DNase I	Roche AG (Switzerland)
Proteinase K	Roth (Germany)
RNAse A	Promega GmbH (Germany)

2.5 Kits

Kit	Company/Supplier
Calcium assay	Randox Laboratories Ltd (United Kingdom)
Cholesterol (Colorimetric) assay	Sede Industrial da Labtest (Brazil)
NEFA ASC-ACOD assay	FUJIFILM Wako Chemicals Europe GmbH (Germany)
Triglycerides (Enzymatic) assay	Sede Industrial da Labtest (Brazil)

2.6 Laboratory Instruments

Instrument	Company / Supplier
1/4" Ceramic Sphere Banded Satellite	MP Biomedicals Inc. (USA)
384-well optical plate MicroAmp®	Biozym (USA)
96-well clear microplate F-bottom	Sarstedt AG & Co.KG (Germany)
96-well clear microplate U-bottom	Sarstedt AG & Co.KG (Germany)
Accu-Chek® blood glucose meter	Roche Diabetes Care GmbH (Germany)
Agarose gel electrophoresis chamber	Biometra (Germany)
AU480 Chemistry Analyzer	Beckman Coulter Inc. (USA)
Beebee Bone Scissors (15mm cutting edge; Straight; Stainless Steel)	Fine Science Tools GmbH (Germany)
Binocular Leica MZ 9_5	Leica Microsystems (Germany)
Binocular MZFLIII	Leica Microsystems (Germany)
C1000 Thermal Cycler	Bio-Rad Laboratories Inc. (USA)
Centrifuge 5415C	Eppendorf AG (Germany)
Ceramic beads for homogenizer (2.8mm)	VWR International (USA)
Cooling centrifuge 5804R	Eppendorf AG (Germany)
Cooling centrifuge Megafuge 1.0R	Heraeus Intruments GmbH/Thermo Fisher Scientific Inc. (USA)
Cryostat CM3050 S	Leica Microsystems (Germany)
Disposable pipettes Cellstar®	Greiner bio-one (Germany)
DRY-CHEM NX500i Analyzer	Fujifilm (Japan)
Dumont #5 Forceps (0.05mm x 0.02mm; Titanium)	Fine Science Tools GmbH (Germany)
Dumont Forceps - Micro-Blunted Tips (Angled 45; 0.1 x 0.06mm; Inox)	Fine Science Tools GmbH (Germany)
Dumont Forceps - Micro-Blunted Tips (Curved – 12cm; 0.1 x 0.06mm; Titanium)	Fine Science Tools GmbH (Germany)
Dumont Forceps - Micro-Blunted Tips (Standard; 0.1 x 0.06mm; Inox)	Fine Science Tools GmbH (Germany)
EDTA tubes MiniCollect®	Greiner bio-one (Germany)
Falcon tubes	Greiner bio-one (Germany)
FastPrep^{TM} lysing matrix tubes	MP Biomedicals (France)
FastPrep^{TM}-24 instrument	MP Biomedicals (France)
Filter tips	Biozym (USA)
Fine balance	Kern & Sohn GmbH (Germany)
Fluorescence microscope BZ-9000	Keyence (Germany)
Mastercycler Nexus GX2	Eppendorf AG (Germany)
Microbalance	Sartorius (Germany)
Microplate reader Infinite® M200	Tecan Trading AG (Switzerland)
MiniSpec LF 90_{II}	Bruker Corporation (USA)
Minutien Pins (Tip: 0.0125mm; Stainless Steel)	Fine Science Tools GmbH (Germany)
Multipette® plus	Eppendorf AG (Germany)
NanoDrop^{TM} 1000 spectrophotometer	Peqlab (Germany)
Olympus IX70 microscope	Olympus Europa SE & CO. KG (Germany)
Pasteur pipettes	Roth (Germany)
PCR tubes	Biozym Scientific GmbH (Germany)

pH meter pH Level 1	WTW (Germany)
Pipetboy acu 2	Integra Bioscience (Switzerland)
Pipettes Gilson Disposable pipettes CellstarR 1, 2, 5, 10, 25ml	Gilson (USA)
Precision balance 440-43N	Kern & Sohn GmbH (Germany)
Real time PCR system QuantStudio™ 5	Applied Biosystems™/Thermo Fisher Scientific Inc. (USA)
Research Plus Multichannel Pipette	Eppendorf AG (Germany)
Rotable platform Polymax 1040	Heidolph Instruments (Germany)
Save-Lock tubes	Eppendorf AG (Germany)
Single channel micropipette Transferpette®	Brand GmbH & Co KG (Germany)
Single pipettes	Discovery Abimed (Germany)
Spring Scissors (8mm cutting edge; Straight; Stainless Steel)	Fine Science Tools GmbH (Germany)
Stereomicroscope Leica M205 FA	Leica Microsystems (Germany)
Student Fine Scissors (23mm cutting edge; Straight; Student Stainless Steel)	Fine Science Tools GmbH (Germany)
Student Vannas Spring Scissors (5mm cutting edge; Straight; Student Stainless Steel)	Fine Science Tools GmbH (Germany)
Super Frost Ultra Plus® object slices	Menzel Gläser (Germany)
Surgical Scissors - Sharp-Blunt (41mm cutting edge; Straight; Stainless Steel)	Fine Science Tools GmbH (Germany)
Syringe filter	Sartorius (Germany)
Thermomixer 5437	Eppendorf AG (Germany)
Thermomixer comfort	Eppendorf AG (Germany)
Ultrasound Sonopuls	Bandelin Electronic (Germany)
UV Gel Documentation System c600	Biozym Scientific GmbH (Germany)
Vannas Spring Scissors (4mm cutting edge; Curved; Stainless Steel)	Fine Science Tools GmbH (Germany)
Vortex Genie 2	Bender & Hobein AG (Switzerland)

2.7 Software and Online Programs

Software / Program	Company / Supplier / Webpage
BZII Analyzer	Keyence GmbH (Germany)
Dataquest ART system, version 2.1	Data Sciences International (USA)
GraphPad Prism5	GraphPad Software (USA)
GraphPad QuickCalcs Outlier Calculator	https://www.graphpad.com/quickcalcs/Grubbs1.cfm
Guide to Pharmacology – 5-HT receptors	https://www.guidetopharmacology.org/GRAC/FamilyDisplayForward?familyId=1
ImageJ v1.52o	National Institutes of Health (USA)
Kyoto Encyclopedia of Genes and Genomes	https://www.genome.jp/kegg/
Leica Application Suite X (LASX)	Leica Microsystems (Germany)
Leica QWin v3	Leica Microsystems (Germany)
Mendeley Reference Manager	Mendeley Ltd./Elsevier B.V. (Netherlands)
MS Office 2007 Excel	Microsoft Ireland Operations Limited (Ireland)
MS Office 2007 Power Point	Microsoft Ireland Operations Limited (Ireland)
MS Office 2007 WORD	Microsoft Ireland Operations Limited (Ireland)
PASW Statistics 18, SPSS	IBM (Germany)
Photoshop, Adobe CS5	Adobe Systems GmbH (Germany)
QuantStudio™ Design & Analysis Software 1.3.1	Applied Biosystems™/Thermo Fisher Scientific Inc. (USA)
Reactome Pathway Finder	https://reactome.org/PathwayBrowser/
Statistica 8	StatSoft (Europe) GmbH (Germany)
Tecan i-Control™ V1.40	Tecan Trading AG (Switzerland)

3 Animals

All animal experiments described in the present thesis were in accordance with the ethical principles and guidelines for safety, care and use of laboratory animals adopted by German local authorities (*Landesamt für Gesundheit und Soziales*, LAGeSo, Berlin) corresponding to the standards prescribed by the American Physiological Society.

3.1 Mice Strains

3.1.1 C57Bl/6 wildtype mice

One of the most commonly used inbred mouse line in science is the C57Bl/6 (short B6). B6 mice have been bred for almost a century, now and substrains of the B6 mouse developed. But most of the original traits of the B6 mouse stayed unaltered. The B6 mouse is associated with typical black coat which is due to a homozygously carried mutated *nonagouti* (a) allele. Beside this external trait, the B6 mouse is known to be a permissive background for maximal expression of most mutations. B6 mice could be shown to exhibit an increased corticosteroid-metabolism, age-related vulnerability for deafness, diet induced adiposity, and amyloid plaques, but not for spontaneous atherosclerotic plaque development. The B6 mouse is a commonly used animal model in cardiovascular research and the C57BL/6J (originally from The Jackson Laboratory, https://www.jax.org/) substrain was even used for the mouse genome project. For this thesis, B6 mice were obtained from an internal MDC-breeding pool that is refreshed by Charles Rivers C57BL/6N mice approximately each third year.

3.1.2 FVB/N wildtype mice

Another commonly used inbred mouse line is the albino FVB/N, which was originally generated by NIH from the N:GP (NIH general purpose) Swiss mouse strain and has been bred since 1966. It could be shown that FVB/N mice appear to behave more aggressively and are more active than other strains. The here used FVB/N mice where as well obtained from an internal MDC-breeding pool.

3.1.3 *ApoE* deficient mice

ApoE$^{-/-}$ mice lack the apolipoprotein E and develop spontaneous hypercholesterolemia and atherosclerotic lesions throughout the complete aortic tree due to an impaired transport mechanism for VLDL and LDL and reduced lipoprotein binding performance to hepatocytes and other peripheral tissues that leads to increased levels of circulating VLDL and LDL and thus, increased circulating lipids such as cholesterol. *ApoE*$^{-/-}$ mice used for this study were originally generated by Zhang et al. (1992) and obtained from The Jackson Laboratory (USA).

3.1.4 *Tph1* deficient mice

Mice lacking the first isoform of tryptophanhydroxylase (TPH1) do not synthesize 5-HT in the periphery (~4% left), but central 5-HT levels stay unaltered. *Tph1*$^{-/-}$ mice were originally generated by our research group (Walther et al., 2003a) and kept at the MDC-breeding facility. *Tph1*$^{-/-}$ mice were backcrossed for 10 generations to the C57BL/6N genetic background.

3.1.5 *Sert* deficient mice

Sert deficient mice used in this study were originally generated by Bengel et al. (1998). They are lacking the gene function for the murine *Slc6a4* gene which codes for the SERT protein.

Consequently, *Sert*$^{-/-}$ mice exhibit unaltered 5-HT synthesis, but since SERT is not present to transport 5-HT into the cells, the total blood 5-HT level in these animals is 0% (Chen et al., 2001).

3.1.6 Double Knockouts

For this study, double knockout mice with deficiencies for *ApoE* and either *Tph1* or *Sert* were generated at the MDC-breeding facility via well planned breeding strategies: Homozygous *ApoE*$^{-/-}$ mice were crossed to either homozygous *Tph1*$^{-/-}$ or *Sert*$^{-/-}$ mice to generate double heterozygotes which were subsequently intercrossed to generate homozygous double knockout animals.

3.2 Animal Husbandry and Test Materials

3.2.1 Animal Husbandry and Breeding

All mice were kept in individually ventilated cages (IVC), either group or single housed (only if aggressive behavior caused injuries) with constant temperature of 22 ± 2 °C and humidity of 65 ± 5%. Animals were exposed to a 12h/12h light/dark cycle (lights on at 7 am) with free access to standard chow and drinking water *ad libitum*, unless otherwise specified. Cage changing and regular supervision of animal health status was performed by the staff of the animal house of the MDC Berlin. If an animal showed signs of sickness, tumors or other health limitations, it was excluded from any experimental cohorts. If the health status did not normalized within a day the responsible veterinary was informed and/or the animal was terminally anaesthetized. Offspring were weaned at around post natal day PND 21 and genotyped by ear-mark biopsies. If young animals had to be genotyped tail-cut biopsies were performed before PND 6. For tail-cut biopsies pre-heated sterile scissors (60°C) were used to make the wound desolate.

All animal tests were in accordance with the ethical principles and guidelines for safety, care and use of laboratory animals adopted by German local authorities (Landesamt *für Gesundheit und Soziales,* LAGeSo, Berlin) corresponding to the standards prescribed by the American Physiological Society.

3.2.2 Food and Water

Diet	Company / Supplier
Drinking water (not acidified)	Autoclaved tap water of the animal facility (MDC-Berlin, Germany)
Normal chow (0.25% sodium)	Sniff Spezialdiäten GmbH (Germany)
Western Type Diet (2071mg/kg cholesterol)	Sniff Spezialdiäten GmbH (Germany)

3.2.3 Drugs

Drug	Active Ingredient	Company / Supplier
Isoflurane	(RS)-Difluormethoxy-1-chlor-2,2,2-trifluorethan	Abbott (Germany)
Ketamidor®	Ketamin	WDT eG (Germany)
Rompun®	Xylazinhydrochlorid	Bayer AG (Germany)
Saline 0.9%	Sodiumchloride	MDC Pharmacy – PZN: 02737756 (Germany)
Betadine 10%	Povidone-iodine (PVP-I)	Mundipharma (Germany)
Heparine	Heparine Sodium	Roth (Germany)

3.2.4 Material for Animal Tests and Husbandry

Material	Company / Supplier
200ml water bottle	Tecniplast Deutschland GmbH (Germany)
Accu-Chek® blood glucose meter	Roche Diabetes Care GmbH (Germany)
EDTA tubes MiniCollect®	Greiner bio-one (Germany)
Individually ventilated cages (IVC), 34x19x13cm	Tecniplast Deutschland GmbH (Germany)
Single housing cages (SHC), 27x21x13cm	Tecniplast Deutschland GmbH (Germany)
Ear notching tool	Fisher Scientific International Inc. (USA)
Restrainer (Bodycomposition)	MDC Workshop (Germany)

4 Methods

4.1 Methods for Genetic Modifications

As described above, the genetically modified mouse lines where either obtained from The Jackson Laboratory (USA) (*ApoE*$^{-/-}$) or generated as described in Walther et al., 2003a (*Tph1*$^{-/-}$) and Bengel et al., 1998 (*Sert*$^{-/-}$). The double KO animals that were used for this study were generated via breeding in the MDC animal facility and respective genotypes were controlled throughout the whole experiment via DNA amplification as described below (see **page 37**).

4.2 Animal Treatments

4.2.1 Western Diet

Male and female animals of the *ApoE*$^{-/-}$ and *ApoE/Tph1*$^{-/-}$genotypes were fed a high fat Western type diet (21.2% crude fat, 0.21% cholesterol; TD88137 from Sniff Spezieldiäten GmbH, Germany) over a period of 8 or 12 weeks (see **Fig. 5**) to quickly induce atherosclerotic processes. Furthermore, three experimental groups were tested in the exact same manner, only that they were not provided with high fat Western type diet, but normal chow. In these groups atherosclerosis was supposed to be induced naturally by the animals' age: animals were dissected at the ages of 45, 60 and 100 weeks (see **Fig. 5**). Diet and water were always provided *ad libitum*, only diet was removed one day before sacrifice to guarantee sober blood glucose measurements. Western diet pellets were changed latest 4 days after administration to avoid spoiling which happens quicker to diet with high fat content.

4.2.2 Anesthesia of mice

Mice were anaesthetized via intraperitoneal (i.p.) Rompun®/Ketamidor® injection and if applicable, anesthesia was deepened via isoflurane inhalation. Rompun®/Ketamidor® solution was freshly prepared right before each experiment as follows: 10% Ketamidor® (ketaminhydrochloride, 100.0 mg/ml) and 5% Rompun® (xylazinhydrochlorid, 23.3 mg/ml) were added to 0.9% saline. Each animal got an injection of 10µl Rompun®/Ketamidor® solu-

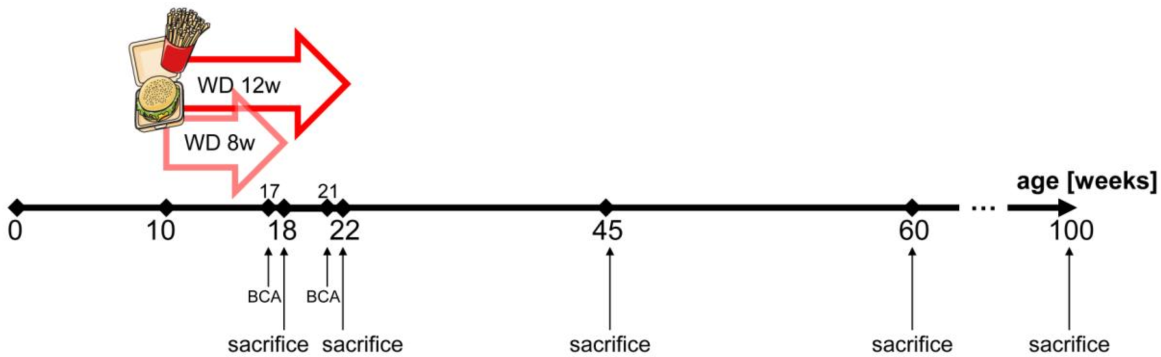

Fig. 5 – Schedule for Atherosclerosis Experiments

Overview of all experiments investigating induced atherosclerosis including time schedule. Timescale indicates age of the animals: from 0 to 100 weeks. Events are highlighted with either red arrows for time periods (8 and 12 weeks of Western diet) or black arrows for time points (BCA: body composition analysis; date of sacrifice). Five experimental groups were investigated: 2x Western diet and 45, 60 and 100 weeks naturally aged animals.

tion per 1g of bodyweight resulting in 2 – 4mg/animal (100mg/kg) Ketamidor® and 0.2 – 0.4mg/animal (11.5mg/kg) Rompun®. Before any treatment the level of anesthesia was validated by reflex tests on tail, hind and front legs. Operations or treatments were only performed if all reflex responses were totally lost. If re-anesthesia was necessary, only Ketamidor® was injected again. For terminal anesthesia, animals were left under the respective isoflurane concentration until breathing stopped and cardiovascular failure under deep anesthesia occurred.

4.2.3 Perfusion

Mice were deeply anesthetized via i.p. Rompun®/Ketamidor® injection (see above). After deep anaesthesia was visible and all reflexes disappeared, mice were fixed to an operation table under permanent isofluran inhalation. A small incision was applied right under the *sternum* and the abdominal wall was carefully opened without harming any bones. The abdominal wall was slightly lifted and an EDTA rinsed cannula was used to transperitoneally puncture the heart, precisely the ventricle. Blood was removed (see **page 27**) until the animal collapsed and breathing was no longer visible. Right after this had happened, the *thorax* was opened, so that the heart region became visible. The right *atrium* was opened minimally and another cannula was inserted into the ventricle through the lesion which was used for the blood removal before. The remaining blood was then removed by an ice cold heparinized saline (solution 1, see **Tab. 3**) exchange which was performed manually with constant pressure on the syringe. After approximately 2ml of solution 1 were applied and tissues like liver or lung were visibly loosing reddish color the second cannula was connected to the animal's circulation and a second ice cold solution, based on PBS containing the antioxidant butylated hydroxytoluene (BHT) (solution 2, see **Tab. 3**) was used to remove remaining blood compartments. Subsequent to these two blood exchanging steps all organs and tissues that were used for biochemical analysis got removed and only after that the last perfusion step was performed using ice cold paraformaldehyde (PFA) solution (solution 3, see **Tab. 3**) and thus fixating the remaining tissues, especially heart and aorta of the animals.

Tab. 3 – Perfusion Solutions
Composition of solutions used for manual perfusion. Amounts are specified in percent, but additionally in volume weight calculated for 250ml of solution. Application of the respective solution during dissection is also stated.

Perfusion Solution	Composition (%)	in 250ml	Application
Solution 1	NaCl (0.9%)..................99.995% Heparine (5000 U/ml)....0.005%	248.75ml 1.25ml	Physiological blood exchange, inhibited blood clotting
Solution 2	PBS (1x, pH 7.4)……....99.98996% EDTA (0.2M)…………0.01% BHT (0.5M)…………....0.00004%	247.49ml 2.5ml 10µl	Physiological blood exchange, inhibited blood clotting, impaired cellular oxidation
Solution 3	PFA (4%)………………94.98996% Sucrose…………………5.0% EDTA (0.2M)…………..0.01% BHT (0.5M)……………0.00004%	247.49ml 12.5g 2.5ml 10µl	Tissue fixation, cryoprotection, inhibited blood clotting, impaired cellular oxidation

4.3 Physiological Measurements

4.3.1 Monitoring of Bodyweight Gain and Food Consumption under Western Diet

Animals that were fed Western diet (WD) stayed under very close monitoring and their food intake, as well as their bodyweight gain was documented accurately. When diet administration started, all animals got weighed and marked via ear notching (if applicable) to guarantee individual documentation. WD chow was weighed before administration and reweighed after it had to be changed (latest after 4 days). Food consumption was then calculated per cage and per animal by dividing the cage consumption by the animal number per cage. Furthermore, individual bodyweight gain was calculated each week and at the end of the experiment for the complete 8 or 12 weeks of WD always using the start bodyweight as 100%.

4.3.2 Body Composition Analysis (BCA)

After 8 and/or 12 weeks of WD, animals were fasted over night (≤16 hours) and underwent a non-invasive body composition analysis (BCA) to determine the relative amount of body fat, muscle mass and water. BCA was performed in collaboration with Stefanie Schelenz and Martin Taube of the Pathophysiology core facility of the MDC Berlin. All measurements were executed with a nuclear magnetic resonance (NMR) spectrometer (MiniSpec $LF90_{II}$, Bruker Corporation, USA) and lasted about 3 minutes with the animal being completely restrained in a warm-temperate chamber rendering anesthesia unnecessary.

4.3.3 Blood Sampling

4.3.3.1 Blood Glucose Measurement

Animals were starved over night before the experiment to allow measurement of sober blood glucose levels; access to water was given *ad libitum*. For measuring the blood glucose level unchallenged animals were quickly grabbed and fixated by hand. A very small cut was applied at the tail tip using student fine scissors (Fine Science Tools GmbH, Germany) and the small amount of blood was directly transferred to a fresh test strip and analyzed via blood glucose meter (Accu-Chek®, Roche Diabetes Care GmbH, Germany). Only after the blood glucose measurement further experimental treatments (e.g. anesthesia) were applied since elevated stress levels in the animals may influence the data.

4.3.3.2 Whole Blood Sampling

Animals were deeply anaesthetized, fixated and the abdominal cavity was opened (see above). The abdominal wall was slightly lifted and an EDTA rinsed cannula was used to transperitoneally puncture the ventricle. Blood was removed to the greatest possible extend (0.5-1.5ml) with a EDTA coated syringe and sampled into EDTA MinCollect tubes (Greiner bio-one, Germany). The physiological status of the animals during blood sampling: naturally positioned (no pressure on any organs) and widely unharmed (only small incision) with stable circulation allowed an extraction of a large blood volume compared to other methods (e.g. complete thorax opening).

4.3.3.3 Generation of Plasma (and Haematocrit)

Anti-coagulated blood, sampled in EDTA MinCollect tubes (Greiner bio-one, Germany) was centrifuged at 3000 rpm for 15 minutes at 4°C. Supernatant was transferred into a fresh tube and stored at -80°C until usage. The lower phase (pellet) contained the haematocrit and was also stored at -80°C.

4.3.3.4 Liver Parameters AST and ALT

Undiluted plasma samples from 45 week old mice, as well as from mice after WD were thawed on ice and pipetted into 50µl aliquots. Measurement of the plasma liver parameters aspartate aminotransferase (AST) and alanine aminotransferase (ALT) were performed in close collaboration with Patrick Langner of the MDC Pathophysiology core facility with a DRY-CHEM NX500i Analyzer (Fujifilm, Japan). Therefore, plasma samples were applied to dry-chemical test plates and color change was measured photometrically.

4.3.3.5 Cholesterol and Triglycerides in Plasma

Undiluted plasma samples from 45 week old mice and from mice after WD were thawed on ice and pipetted into 50µl aliquots. Measurements of plasma cholesterol and triglycerides were performed in close collaboration with Patrick Langner of the MDC Pathophysiology core facility with an AU480 Chemistry Analyzer (Beckman Coulter Inc., USA). Enzymatically induced color change of cholesterol in plasma samples was measured at 540/600nm, of triglycerides at 660/800nm. In case of severe hemolysis, samples were excluded from analysis; in case of severe lipemia, samples were adequately diluted in ddH_2O and measurement was repeated; the original cholesterol and triglyceride values were then calculated for the undiluted samples.

4.4 Tissue and Organ Processing

4.4.1 Standardized Protocol for Organ Dissection

All organs and tissues for later biochemical analysis (e.g. enzyme-linked colorimetric assays, real time PCR, etc.) were dissected after the second perfusion step (see **page 26**) and in a quick and accurate manner, such that loss of physiologically unimpaired tissue was as little as possible.

The mice' abdominal cavity was opened with a cut along the entire length of the abdomen using surgical scissors (Sharp-Blunt, Fine Science Tools GmbH, Germany). Thorax was opened bilaterally using Beebee bone scissors (Fine Science Tools GmbH, Germany) and the ventral part of the mice' ribcage was removed to allow a completely unobstructed dissection of the thoracic cavity.

4.4.1.1 Liver

Liver and adhered gallbladder were removed from the abdomen entirely and without injuring the tissue. They got transferred to a dissection dish and covered slightly with solution 2 (see **Tab. 3**) to avoid drying. The gallbladder was carefully removed without harming it since leaking bile (containing bile salts and digestion enzymes) may affect liver tissue. Several liver samples were taken for histology and biochemical analysis (see **Fig. 6**).

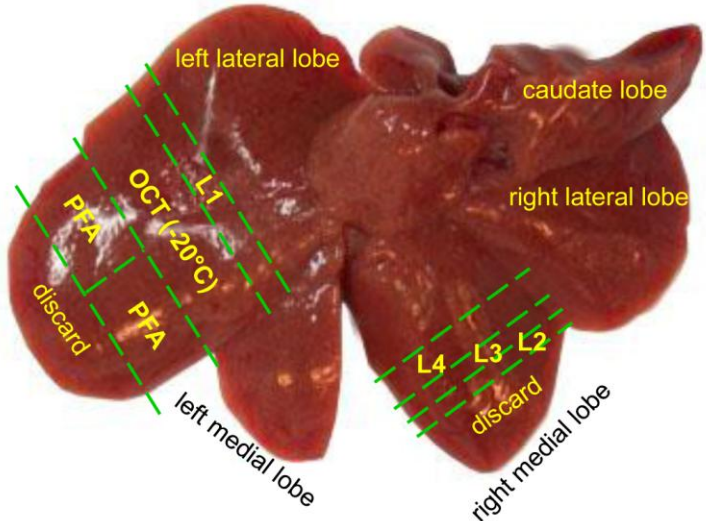

Fig. 6 – Liver Dissection
Overview of all liver samples and their sampling locations. The liver was extracted from the abdomen and transferred to a dissection dish were the gallbladder was removed. All liver lobes were spread like depicted and samples were taken from left lateral lobe and right medial lobe. Samples from left lateral lobe were transferred into 4% PFA or embedded into Tissue Tek® OCT™ Compound (Newcomer Supply Inc., USA) and immediately frozen at -20°C to use them for histology (2x PFA and OCT). Further, one sample of approximately 100µg was taken from the left lateral lobe and used for later biochemical analysis (L1). Three samples from the right medial lobe were dissected and used for biochemical analysis (L2 & L3: ~50µg; L4: ~100µg).

4.4.1.2 Spleen, Visceral Fat, Kidney & Lung

Spleen was dissected and cleaned from surrounding tissue. Visceral fat was completely extracted bilaterally, weighed and two cuts of approximately 50µg, as well as one complete half (right body part) were stored. The right kidney was taken and decapsulated. Additionally, the left lung was dissected from some animals. One half of spleen and kidney, as well as the entire right visceral fat sample and the entire lung were fixated in 4% PFA for one week, cryoprotected in 30% sucrose solution (in 1x PBS) and subsequently stored at -20°C. The remaining samples (half spleen and kidney and the visceral fat samples F1 and F2) were stored at -80°C for further biochemical analysis.

4.4.1.3 Aorta and Heart

Heart and the entire aorta for histology were dissected after the last perfusion step, hence after fixation via 4% PFA (see **Tab. 3**). The dissection was performed under a binocular (MZFLIII, Leica Micro-Systems, Germany). In a first step the surrounding fat and muscle tissue was removed using Spring Scissors (8mm cutting edge, Fine Science Tools GmbH, Germany). As soon as the aorta became visible, it was slightly lifted up (several fine forceps, Fine Science Tools GmbH, Germany) to detach it from the underlying tissue with careful and accurate cuts performed with Student Vannas spring scissors (5mm cutting edge, Fine Science Tools GmbH, Germany). Aorta was loosened over the complete length of the abdomen and thorax - from aortic bifurcation up to aortic arch – but is was not yet cut axially. In a second step the aorta was detached from *arteria brachiocephalica*, *arteria carotis communis* and *arteria subclavia*, whereat the bifurcation of *arteria brachiocephalica* was as well dissected and stored in 4% PFA. Only after that step the entire structure of heart and aorta was loosened from both *arteriae iliaca communis* and hence extracted from the body. It was stored one week in solution 3 (see **Tab. 3**) before further dissection.

Dissection of aorta and other vessels for quantitative polymerase chain reaction (qPCR) analysis is described below (see **page 31**).

4.4.2 Fixation and Cryoprotection of Organs and Tissues

Dissected organs and tissues were fixated using 4% PFA or solution 3 (see **Tab. 3**) which is based on 4% PFA. All samples were incubated in the respective fixative at 4°C for at least one week and no longer than two weeks. Cryoprotection was applied using 30% sucrose solution in 1x PBS at pH 7.4 for at least 5 days or until the sample was saturated.

4.4.3 Cryocutting of Organs (Hearts)

Cryoprotected organs were cut with help of the cryostat CM3050 S (Leica Microsystems, Germany).

Tab. 4 – Scheme of Heart Sections
Description of the sampled heart section from cryostat. 10µm thin heart sections where transferred to glass slides, forming 4 sets of 10 sections each (400µm in total). Hence, all 4 sets are maximally comparable amongst each other. **1A-2D:** Slide names; 1A1-2D5: Section names; (#1)-(…): slice number; [200µm]: total covered sample thickness.

Slide Name	**1A**	**1B**	**1C**	**1D**
Sections	1A1(#1)	1B1(#2)	1C1(#3)	1D1(#4)
	1A2(#5)	1B2(#6)	1C2(…)	1D2
	1A3	1B3	1C3	1D3
	1A4	1B4	1C4	1D4
	1A5	1B5	1C5	1D5 [200µm]
Slide Name	**2A**	**2B**	**2C**	**2D**
Sections	2A1(#21)	2B1(#22)	2C1(…)	2D1
	2A2	2B2	2C2	2D2
	2A3	2B3	2C3	2D3
	2A4	2B4	2C4	2D4
	2A5	2B5	2C5	2D5 [400µm]

For thin sections, hearts were fixed upright (with the pericardium upwards) with OCT (Tissue-Plus OCT™ Compound, Newcomer Supply Inc., USA) on a prepared OCT platform previously fixed on a metal table (briefly at -40°C, permanent -18°C) and cut inside the cryostat (chamber temperature -19°C, table temperature -19°C) to 10µm slices. The cuts were directly transferred to adhesion glass-slides.

Samples were put into 4 sets (A, B, C, D) of 10 slices with always 5 slices per glass slide, such that one glass slide carried each fourth section and at least two glass slides represented 400µm of the complete aortic root area (see **Tab. 4**). Section sampling was started at the point where all three aortic valves became visible, latest when two valves where fully distinct. If necessary, more than two glass slides were prepared per set.

4.4.4 Dissection of the Aortic Arch

Aortas that were fixated for one week in solution 3 were rinsed with 1x PBS and transferred to a Petri dish containing solid 1% agarose gel. The gel served as a flexible, translucent dissection surface to which aortas could be fixated using minutien pins (Tip: 0.0125mm, Fine Science Tools GmbH, Germany) and what allowed optimal illumination of the working area. Aortas were cut from the heart as tight as possible to avoid any loss of aortic tissue. For dissection of the aortic arch, each aorta was shortened to exact 15mm after the bifurcation of *arteria subclavia*. Aortic arch dissection was performed using 5mm Student Vannas Spring Scissors, Dumont #5 Forceps and Angled 45 Dumont Forceps (Fine Science Tools GmbH, Germany).

4.4.4.1 Situs preparation of the Aortic Arch

After shortening, the aorta was covered with 1x PBS to avoid drying and the remaining parts of *arteria brachiocephalica*, *arteria carotis communis* and *arteria subclavia* were cut to stubs ≤ 1mm. Hence, only atherosclerotic plaques located directly at a distinct part of the aorta were analyzed in subsequent histological staining and colorimetric calcium assay.

In the following, the aorta was entirely cleaned from attached tissue material by removal of the *tunica adventitia*. For this purpose, a small rip (two forceps) was applied to the *tunica adventitia* at the rostral end of the aorta, such that a gap arose between *tunica adventitia* and the rest of the aorta. With the help of two forceps this gap was opened further and by only holding the loose parts of *tunica adventitia* and carefully pulling them, it could be detached from the aorta more and more. In the end there was only a little part of the *tunica adventitia* being connected to the caudal end of the aorta which was then detached by very carefully pushing the aorta into the flexible agarose surface with one forceps and ripping the adventitia off with the second forceps. As a result, the clean, translucent aorta was ready for ORO staining, which was performed before *en face* preparation. Microscopic images were taken similarly from closed and opened (*en face*) aortas.

4.4.4.2 En face preparation of the Aortic Arch

The cleaned and ORO stained aortic arch was transferred to the 1% agarose filled Petri dish and got covered with 1x PBS to avoid drying. A longitudinal cut was set at the outer flexure of the aortic arch (crossing all three arterial bifurcations) and the aorta was completely opened. With the help of minutien pins (Tip: 0.0125mm, Fine Science Tools GmbH, Germany), the aorta was stepwise opened and fixed to the agarose gel surface, such that as few minutien pins as possible were used and without puncturing any atherosclerotic plaque area (red ORO staining) to avoid rupture and loss of plaque material. In the end, the aorta inner face was completely exposed and microscopic images were taken by Leica M205 FA (Leica Microsystems, Germany) with the following settings: 12.5 magnification, transmitted light with fully opened light shade (mirror at 20°), exposure: 20.00ms, digital gain: 2.0, saturation: 50%, color balance: red (18%), green (15%), blue (50%). White reflections must not be visible. Examined aortas where transferred to 200µl of 0.6N HCl.

4.4.5 Dissection of Blood Vessels (and *Nervus vagus*) for qPCR

Blood vessels (*arteria carotis communis, arteria femoralis, aorta* (thoracic aorta and arch)*, vena cava, vena saphena arteria mesentrica, arteria pulmonaria* and *vena porta*) and as control tissues *nervus vagus*, as well as multiple organs (spleen, liver, intestine, thymus, brain and heart) of male B6, FVB/N, *B6/Tph1*$^{-/-}$ and *FVB/N/Tph1*$^{-/-}$ mice (5-6 per group and experiment) at the age of 8-12 weeks were dissected for RNA extraction followed qPCR analysis. Therefore, mice were quickly decapitated without any anesthesia to assure a minimum stress level in the animals and avoid side effects of anesthesia on the 5-HT system. All organs were cleaned from surrounding tissue and dissected in a highly rapid manner, such that inherent RNA degradation was put to a minimum. The specimens were immediately put to FastPrep™ lysing matrix tubes (MP Biomedicals, France) containing 1ml of Trizol® (Life Technologies, USA) and 5 ceramic beads (2.8mm, VWR International, USA) or (for aortas) one 1/4" Ceramic Sphere Banded Satellite (MP Biomedicals Inc., USA) and stored at -80°C for subsequent RNA extraction. Complete dissection of one animal took no longer than 5 minutes.

4.5 Histology

4.5.1 Oil Red O Staining

Oil red O (ORO) staining in whole aortas (aortic arch and thoracic aorta) and cryo slices of the heart aortic root region was performed to visualize and analyze size and distribution of atherosclerotic plaques. ORO is a lysochrome diazo dye[8] that stains neutral triglycerides and lipids, such as mainly present in atherosclerotic plaques, in fresh and PFA fixated samples. For the staining protocol a ORO saturated stock solution was freshly prepared by dissolving 0.5g ORO powder (Sigma-Aldrich, Germany) in 100ml of 99% isopropanol. From this saturated stock solution a 60% working solution was prepared by mixing 60ml ORO stock with 40ml ddH_2O and incubating it at room temperature (RT) for 1 hour. Afterwards, the ORO working solution was filtered twice through standard filter paper to avoid pigment particle contamination. The working solution was freshly prepared for each experiment.

4.5.1.1 Oil Red O Staining of whole Aortas

4.5.1.1.1 Staining Protocol

Aortas were stained for ORO before *en face* preparation. For this purpose, the samples were dehydrated in 60% isopropanol for 10 minutes at room temperature (RT). In the second step, the aortas were transferred to 60% ORO working solution and incubated for 30-60 minutes at RT on a shaker (Rotable platform Polymax 1040, Heidolph Instruments, Germany). Afterwards, the samples underwent a 10 minute cleaning step with 60% isopropanol and were rehydrated by ddH_2O (2 minutes) at RT. The ready-stained aortas were stored in 1xPBS at 4°C and microscopic images were taken before and after *en face* preparation.

4.5.1.1.2 Image Acquisition

Microscopic images of closed and opened (*en face* preparation) aortas were taken by using the Leica M205 FA stereomicroscope (Leica Microsystems, Germany) with the following settings: 12.5 magnification, transmitted light with fully opened light shade (mirror at 20°), exposure: 20.00ms, digital gain: 2.0, saturation: 50%, color balance: red (18%), green (15%), blue (50%). White reflections must not be visible. Afterwards, examined aortas where transferred to 200µl of 0.6N HCl for subsequent colorimetric calcium assay (see **page 43**).

4.5.1.1.3 Image Analysis with *ImageJ* and Data Acquisition

Each microscopic image of aortas was acquired featuring an equal 2500µm scale bar, which allowed the unit translation from pixels to µm and µm^2. Unit translation was performed using the ImageJ (v1.52o, National Institutes of Health, USA) command ‘Analyze’ > ‘Set Scale…’ on the before defined scale bar length (‘Straight’ tool). The known distance was translated into 2500µm with a pixel aspect ratio of 1.0. The ‘Global’ box was ticked to use the scale for

[8] Azo dyes are the biggest group of synthetic dyes and contain at least one azo compound (-N=N-). Diazo dyes, such as Oil red O contain two azo compounds.

each analyzed image. In a first step, the blue background of each aorta image was knocked out using the ‘Polygon selection’ tool; at the same time each aorta was cropped to exactly $11.\bar{6}$mm length after *arteria subclavia* bifurcation and the aortic area was measured using the command ‘Analyze’ > ‘Measure’. Additionally, in images of aortic *en face* preparation, minutien pins were knocked out using the ‘Polygon selection’ tool after the measurement of the whole aortic area. In the next step, the red ORO stained area was measure by using the command ‘Image’ > ‘Adjust’ > ‘Color Threshold…’: In the RGB color space the red and green channels were accepted entirely (0-255), whereas the blue channel threshold was set to 120. Hitting ‘Select’ resulted in the complete red stained area becoming selected, what allowed the area measurement by the command ‘Analyze’ > ‘Measure’. As a result two areas were defined: ‘whole aorta’ and ‘plaque area’, and a % ratio was calculated by dividing ‘plaque area’ by ‘whole aorta’ and multiplying the result with 100.

4.5.1.2 Oil Red O Staining of Heart Sections

4.5.1.2.1 Staining Protocol

Set A of heart cryo slice was used for ORO staining which was performed at RT in 200ml glass cuvettes. In a first step, cryo slices were dehydrated by immersing them 10 times in 60% isopropanol. Subsequently, slices were incubated for 15 minutes in 60% ORO working solution and then again immersed 10 times in 60% isopropanol to remove excess ORO solution. Afterwards, slices were rinsed 5 minutes with running tap water and counterstained for 3 minutes with hematoxylin solution (Sigma-Aldrich, Germany). Bluing was obtained by 5 minute rinsing in running tap water. Wet slices were immediately embedded in 55-60°C warm glycerol-gelatin (Sigma-Aldrich, Germany) and cover slips were added. After one night storage at 4°C, cover slips were sealed with commercially available nail polish.

4.5.1.2.2 Image Acquisition

Image acquisition on cryo heart slices was performed at our partner institute in Lübeck and at the MDC in Berlin. In Lübeck, microscopic images of cryo heart slices stained for ORO and Masson’s trichrome from 100 week old animals were taken on the Olympus IX70 microscope (Olympus Europa SE & CO. KG, Germany) with a 4 fold magnification and brightfield illumination as described elsewhere (Segura-Puimedon et al., 2016). In Berlin, microscopic images of cryo heart slices stained for ORO and Masson’s trichrome from 45 week old animals were taken by using the fluorescence microscope BZ-9000 (Keyence, Germany) with a 5 fold magnification (2x ocular and 2.5x digital magnification) and brightfield illumination. For ORO staining, images of 10 consecutive slices were taken and analyzed.

4.5.1.2.3 Image Analysis with *ImageJ* and Data Acquisition

Images of 100 week old animals, which were acquired at our partner institute in Lübeck were analyzed immediately after acquisition using the Leica software QWin v3 (Leica Microsystems, Germany) with the self-made software application for plaque analysis. This application calculates the total aortic ring area, subtracts the aortic lumen and then counts the red stained zones. As a result, the total plaque area per slice was calculated in µm2. Images of 45 week old animals, acquired in Berlin, were analyzed via ImageJ. Scaling was performed via the command ‘Analyze’ > ‘Set Scale…’ as described for aorta analysis (see **page 32**). In the first step, the image background was knocked out (‘Polygon selection’ tool) remaining only the aortic ring which was then measured (‘Analyze’ > ‘Measure’). Afterwards, the ORO staining allowed an exact free hand masking of all atherosclerotic plaques which were then measured (‘Analyze’ > ‘Measure’). In both analysis procedures, the results were calculated as the mean atherosclerotic plaque size per animal by analyzing 10 consecutive slices and calculating the mean of them.

4.5.2 Masson’s Trichrome Staining

The Masson’s trichrome staining is a staining combination of multiple histological dyes which allows an optical differentiation of tissue types, such as muscles and connective tissue, in histological specimens. The methods is based on the chemical characteristics of different tissue types and was used in this study to investigate the collagen amount within atherosclerotic plaques in cryo slices of the aortic root area.

4.5.2.1 Staining Protocol

Masson’ trichrome staining was performed on sample set B in 200ml glass cuvettes at RT. Cryo slices were prepared for 15 minutes in a 56°C preheated Bouins solution what ensured an optimal fixation of the slices and promoted later staining steps. Afterwards, the samples were cooled down to 18-26°C in tap water and excess Bouins solution was removed by running tap water. In the next step, cell nuclei were stained black by 5 minute incubation in Weigert’s haematoxylin solution followed by a 5 minute blacking step under running tap water. After washing in ddH2O, samples were incubated for 5 minutes in Biebrich scarlet-acid fucsin solution, what stained muscles red and cytoplasm pink; samples got washed in ddH2O again. Subsequently, the red staining was removed from connective tissue by 5 minute incubation in a 1:1 Phosphomolybdic acid/ Phosphotungstic acid solution. Instantaneously, the collagen fibers of the connective tissue could be stained in blue by incubating the samples for 5 minutes in Aniline blue solution. Subsequent 2 minute incubation in 1% Acetic acid stabilized the blue staining and gently removed excess dyes from the samples. In the last step, cryo slices were treated with a dehydration series (30%, 50%, 70%, 80%, 90% ethanol), cleared with Xylol and embedded in NeoMount® (Merck KGaA, Germany).

4.5.2.2 Image Acquisition

Images of Masson’s trichrome stained cryo heart slices were acquired by using the fluorescence microscope BZ-9000 (Keyence, Germany) as described above (see **page 33**). For the collagen analysis, images of 5 consecutive slices were taken.

4.5.2.3 Image Analysis with ImageJ and Data Acquisition

Scaling was performed via the command ‘Analyze’ > ‘Set Scale…’ as described for aorta analysis (see **page 32**). In the first step of collagen analysis, atherosclerotic plaques were selected via ‘Polygon selection’ tool and the image background was knocked out (white matte). A reliability analysis for atherosclerotic plaque selection was performed on 10+ randomly chosen images and resulted in a reliability score of ≥99%. In the second step, the ImageJ plugin ‘Color Deconvolution’ was used with vectors for ‘Masson Trichrome’ and a threshold (‘Image’ > ‘Adjust’ > ‘Threshold…’) was set for the channel ‘Color 1’ (blue one) with the following frame: 0-140. Applying the threshold area allowed a measurement (‘Analyze’ > ‘Measure’) of the clearly blue stained parts of the previously selected plaques. As a result, a collagen per plaque percentage was calculated for 5 consecutive slices and the mean per animal was extrapolated.

4.5.3 Calcein Staining

Calcein, or Fluorexon, is a fluorescence dye which is able to cross the cell membrane and forms chelates with intracellular calcium. In this study, calcein was used to stain intraintimal calcium deposits in cryo slices of the aortic root area and hence, make calcification of atherosclerotic plaques visible. Due to very weak results, an analysis on the stained samples could not be performed, but representative images are depicted (see Fig. 16A-C).

4.5.3.1 StainingProtocol

For calcein staining, set D was used. Staining was operated in 200ml glass cuvettes at RT. Samples were incubated for 30 minutes with calcein (Sigma-Aldrich, Germany) working solution (0.1mM calcein in 50mM Trisbase TBS (pH 9.0)) in a dark chamber. Afterwards, samples were washed 3 times with TBS on a shaker and incubated with DAPI working solution (0.01% DAPI in 50mM in 50mM Trisbase TBS (pH 9.0)) for 2 minutes. Wet samples were immediately embedded in 55-60°C warm glycerol-gelatin (Sigma-Aldrich, Germany) and cover slips were added. After one night storage at 4°C, cover slips were sealed with commercially available nail polish.

4.5.3.2 Image Acquisition

Images of calcein staining were acquired using the fluorescence microscope BZ-9000 (Keyence, Germany) with 5 fold magnification (2x ocular and 2.5x digital magnification), 480nm excitation and 2.5ms exposure time for calcein and 355nm excitation and 1/1.1ms exposure time for DAPI.

4.6 Immunhistochemistry (IHC)

4.6.1 αMac2 Staining

To examine the amount of macrophages invaded into the intraintimal space, immunohistochemical staining with an antibody against galectin-3 (αMac2, ORIGENE Technologies, Inc., USA) was performed on cryo slices of the aortic root region. The galectin-3 protein is known to be associated with activated macrophages and binds macrophage excreted β-galactosides.

4.6.1.1 Staining Protocol

αMac2 staining was performed on set C of the cryo heart slices. Samples were rehydrated in 1x PBS for 1 hour at RT and subsequently washed in fresh 1xPBS for 5 minutes. For permeabilization, the samples were incubated for 10 minutes in PBST (0.1% TritonX100 in 1x PBS) at RT. The blocking step was operated for 60 minutes at RT in 10% NDS. Afterwards, samples were incubated with the first antibody (αMac2; 1:500 in PBST) at 4°C over night. In the next step, samples were washed 3 times in 1x PBS for 5 minutes at RT. The second antibody (αRat Cy3; 1:1000 in PBST) was added and samples were incubated for 2 hours at RT in a dark chamber. Finally, samples were washed 3 times each for 5 minutes in 1xPBS, air dried and embedded in Vectashield mounting medium with DAPI (Vector Laboratories Inc., USA).

4.6.1.2 Image Acquisition

Images of immunohistochemical staining were acquired using the fluorescence microscope BZ-9000 (Keyence, Germany) with 5 fold magnification (2x ocular and 2.5x digital magnification), 550nm excitation and 3.5ms exposure time for Cy3 (αMac2) and 355nm excitation and 1/1.1ms exposure time for DAPI. For both channels, a black balance in the image center was applied and a dynamic filter ('Enhanced Edge (weak)') was used. For the macrophage analysis, images of 5 consecutive slices were taken.

4.6.1.3 Image Analysis with ImageJ and Data Acquisition

Scaling was performed via the command 'Analyze' > 'Set Scale…' as described for aorta analysis (see **page 32**). In the first step of macrophage analysis, atherosclerotic plaques were selected via 'Freehand selection' tool and the image background was knocked out (black matte). In the second step, channels were split via the command 'Image' > 'Color' > 'Split Channels' and a threshold was set on the red channel: 'Image' > 'Adjust' > 'Threshold…'. The threshold was set from 50-255 and got applied. Subsequently, the area was measured using 'Analyze' > 'Measure'. As a result the total stained macrophagic area was counted per sample and the sum of 5 samples per animal was generated since the inhomogeneous distribution did not allow using means. Hence, the results are given in macrophagic area sum per 5x10µm atherosclerotic plaque.

4.7 Molecular Biology

4.7.1 Extraction of Genomic DNA (gDNA) from Tissue

Buffer	Composition
TE-buffer	10 mM Tris-HCl (pH 8.0), 1mM EDTA
Digestion ('Ear') buffer	100mM Tris (pH 8.5), 5mM EDTA, 200mM NaCl, 0.2% SDS, 1mg/ml proteinase K
TE/RNase buffer	20µg/ml RNase A in TE-buffer (1x)

To extract genomic DNA (gDNA) from tissue biopsies (e.g. tail cuts or ear-biopsies) samples were incubated overnight on shaker at 55°C in 100 µl digestion buffer. The dissolved samples were briefly vortexed and heat-inactivated for 10 min at 95°C. Afterwards cold 600 µl TE/RNase buffer was added, incubated for 15 min at RT and stored either at -20°C or immediately used for genotyping PCRs.

If genotyping PCRs from the extracted gDNA did not obtain clear results, an alternative method for gDNA extraction was used: gDNA precipitation via DNAzol® reagent (Invitrogen, Germany). Therefore, 25mg of deep frozen liver samples was transferred to FastPrepTM lysing matrix tubes (MP Biomedicals, France) containing 1ml of DNAzol® reagent and 5 ceramic beads (2.8mm, VWR International, USA) and homogenized 3 times for 40 seconds in a FastPrep^{TM}-24 instrument (MP Biomedicals, France). Centrifugation of the homogenate at 4°C and 10,000 x g for 10 minutes allowed removal of insoluble tissue fragments, RNA and excess polysaccharides and was followed by transferring the supernatant to a fresh 2ml tube. The precipitation step was operated by adding 0.5ml of 100% ethanol, inverting the sample several times and incubating it for 3 minutes. The visible DNA precipitate was then spooled onto a pipette tip and the supernatant was decanted carefully and aspirated from the tube bottom. Afterwards, gDNA was 2 times washed by adding 1ml of 75% ethanol and inverting 3-6 times. Upright storage of the tube led to the gDNA settling to the tube bottom and ethanol was removed by pipetting. After 10 seconds of air dry, the gDNA was resuspended in 0.4ml 8mM NaOH by slowly passing through a pipette tip and cleaned from insoluble materials by centrifugation at RT and 12,000 x g for 10 minutes. The gDNA containing supernatant was then transferred to a fresh tube and stored either at -20°C or immediately used for genotyping PCRs.

4.7.2 Amplification of DNA Segments

4.7.2.1 Polymerase Chain Reaction for murine ApoE deficiency (3 Primers, 1Reaction)

Deletion of the *ApoE* allele in mice was done by homologous recombination with an expression / selection cassette (neomycin-resistance cassette against ganciclovir-antibiotic treatment). Therefore it is possible to differentiate between unaffected and deleted *ApoE* alleles by a three primer PCR in which one primer is specific for the neo-sequence (ApoE_KO5) and another for the intact Ex4 region (ApoE-WT5) while the third primer attaches to the 3'-UTR (untranslated region) of both alleles (ApoE_3). As a result, PCR products on agarose gel become visible as a 560 bp DNA band for the wild type allele and/or 850 bp DNA band for the knockout allele (**Fig. 7A**).

4.7.2.2 Polymerase Chain Reaction for murine Tph1 deficiency (3 Primers, 1 Reaction)

Deletion of the *Tph1* allele in mice was also done by homologous recombination with a Neo selection cassette, but here, sophisticated cloning strategies using several restriction digestion steps caused a replacement of Ex2 with the shorter Neo selection cassette. This leads to a possible differentiation between unaffected and deleted *Tph1* alleles by a three primer PCR in which one primer binds specifically to the Neo-sequence (Neo3), the second primer binds to the intact gene locus region (GTPH3) and the third primer attaches to the 5'- end of both alleles (GTPH5). This results in PCR products of 590 bp (wild type) and/or 300 bp (knockout) length (**Fig. 7B**).

Protocol for *ApoE* PCR

Mastermix for 1 sample:	
H_2O	9.25µl
Primer ApoE3 (10µM)	0.75µl
Primer ApoE WT5 (10µM)	0.75µl
Primer ApoE KO5 (10µM)	0.75µl
RedTaq	12.5µl
	24.0µl
+	1.0µl DNA

Cycler Protocol:			
Step	Heat Lid		
Initial Denaturation	95°C	3min	
Denaturation	95°C	20sec	X35
Annealing	56°C	20sec	X35
Elongation	72°C	1min	X35
Final Elongation	72°C	10min	
Storage	4-10°C	forever	

Protocol for Tph1 PCR

Mastermix for 1 sample:	
H_2O	18.9µl
Pol-Buffer	2.5µl
dNTPs (5µM)	1.0µl
Primer GTPH5 (7µM)	0.5µl
Primer Neo5 (7µM)	0.5µl
Primer GTPH3 (7µM)	0.5µl
Pol-Taq	0.1µl
	24.0µl
+	1.0µl DNA

Cycler Protocol:			
Step	Heat Lid		
Initial Denaturation	95°C	5min	
Denaturation	95°C	30sec	X35
Annealing	60°C	30sec	X35
Elongation	68°C	40sec	X35
Final Elongation	68°C	5min	
Storage	4-10°C	forever	

4.7.2.3 Polymerase Chain Reaction for murine SERT deficiency (3 Primers, 2 Reactions)

For generation of *Sert*$^{-/-}$ mice a similar homologous recombination approach was used with a Neo cassette replacing Ex2 of the *Sert* gene. Hence, the differentiation between unaffected and deleted alleles is also possible; however the very small difference in size of the two alleles requests for a 3 primer – 2 reactions PCR with one primer pair binding specifically to the Neo-sequence and the 3'-UTR (PCR C: IMR7415 and IMR8899) and one primer pair binding to the wild type Ex2 and the 3'-UTR (PCR D: IMR8890 and IMR8899). As a result, *Sert*$^{-/-}$ PCR only delivers products for knockout samples, while *Sert*$^{+/+}$ PCR only delivers products for wild type samples (**Fig. 7C+D**).

Protocol for Sert PCRs

Mastermix for 1 sample:	WT	KO
H_2O	19.4µl	19.4µl
Pol-Buffer	2.5µl	2.5µl
dNTPs (5µM)	1.0µl	1.0µl
Primer IMR8899 (7µM)	0.5µl	0.5µl
Primer IMR 8890 (7µM)	0.5µl	0.0µl
Primer IMR7415 (7µM)	0.0µl	0.5µl
Pol-Taq	0.1µl	0.1µl
	24.0µl	24.0µl
+	1.0µl DNA	1.0µl DNA

Cycler Protocol:

Step	Heat Lid		
Initial Denaturation	94°C	3min	
Denaturation	94°C	30sec	X35
Annealing	65°C	30sec	X35
Elongation	68°C	30sec	X35
Final Elongation	68°C	2min	
Storage	4-10°C	forever	

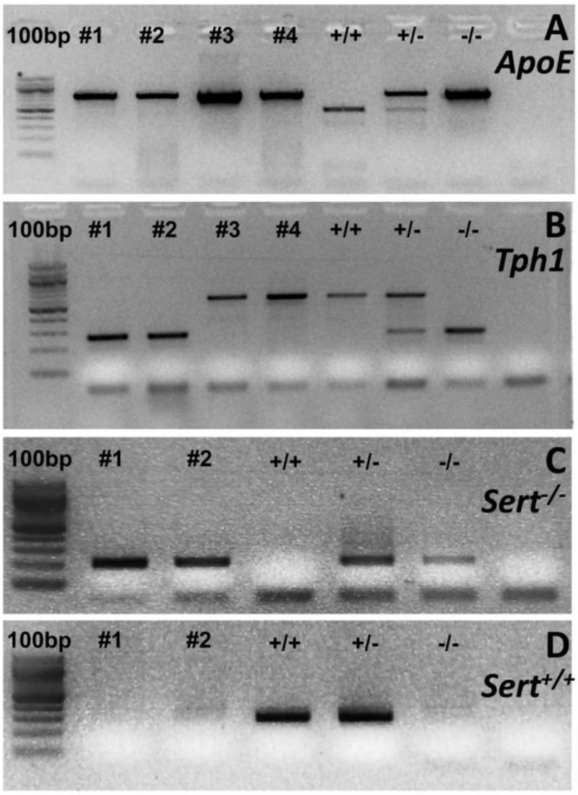

Fig. 7 – Genotyping of *ApoE*, *Tph1* and *Sert* Deficiencies

UV gel images of amplified DNA fragments (PCR products) after PCRs for *ApoE* (**A**), *Tph1* (**B**) and *Sert* (**C** and **D**) deficiencies. 2% agarose gel; 120V for 15 minutes; Light source: UV302; Exposure time: 1s (*ApoE*), 2.4s (*Tph1*), 4.5s (*Sert*); Marker: 100 base pair DNA ladder; #1 - #4: animal sample numbers, in which PCR was performed; +/+: homozygous wild type control DNA; +/-: heterozygous control DNA; -/- homozygous knockout control DNA. **A:** ApoE PCR products: wild type (560bp) and knockout (850bp); **B:** Tph1 PCR products: wild type (590bp) and knockout (300bp); **C:** *Sert*$^{-/-}$ PCR product: knockout (210bp); **D:** *Sert*$^{+/+}$ PCR product: wild type (318bp).

4.7.3 Tissue Homogenization and RNA Extraction (via TRIzol®)

Compound	Composition
0.1% DEPC	ddH_2O, C6H10O5
Chloroform	99% CHCl3
75% Ethanol (DEPC)	75% undenatured ethanol, 30% DEPC (0.1%)
Isopropanol	99% C3H8O
TRIzol®	30-60% phenol, 15-40% guanidinium thiocyanate, 7-13% ammonium thiocyanate
1x PBS	0.8% NaCl, 0.02% KCl, 0.14% Na2HPO4, 0.18% Na2HPO4-2H2O, 0.03% KH2PO4

For RNA extraction from different tissues and volumes, a tissue homogenization protocol containing TRIzol® (Life Technologies, USA) was used. 50mg of tissue (spleen, liver, intestine, thymus, brain and heart) as well the entire amount of extracted blood vessels (*arteria carotis communis, arteria femoralis, aorta* (thoracic aorta and arch)*, vena cava, vena saphena arteria mesentrica, arteria pulmonaria* and *vena porta*) and *nervus vagus* was transferred to FastPrepTM lysing matrix tubes (MP Biomedicals, France) containing 1ml of TRIzol® reagent and 5 ceramic beads (2.8mm, VWR International, USA) respectively one 1/4" Ceramic Sphere Banded Satellite (MP Biomedicals Inc., USA; for aortas) and homogenized 3 times for 40 seconds respectively 5 times for 40 seconds (spleen and aorta) in a FastPrep^{TM}-24 instrument (MP Biomedicals, France). Homogenates were incubated for 5 minutes at RT and subsequently replenished with 0.2ml chloroform. Each sample was vortexed for 15 seconds and incubated for 10 minutes at RT. Afterwards, samples were centrifuged at 12,000 x g for 10 minutes at 4°C and the supernatant (aqueous phase containing only RNA) was transferred to a fresh 1.5ml tube. RNA was then precipitated by adding 0.5ml of ice cold isopropanol, inverting the tubes several times and incubating for 10 minutes at 4°C. The following centrifugation step at 12,000 x g for 10 minutes at 4°C led to the RNA forming a white gel-like pellet at the tube bottom and the supernatant was removed to the greatest possible amount. The RNA pellet was then washed by adding 1ml of 75% ethanol (DEPC) and centrifugation at 12,000 x g for 10 minutes at 4°C. This step was repeated 2-3 times. Afterwards, ethanol was removed and the pellets air dried for 20 minutes under the hood. Resuspension was performed in 50µl respectively 10µl (vessels and *n. vagus*) DEPC-H_2O and by 10 minutes incubation at 55°C and on the shaker.

Concentration and purity of the resuspended RNA was measured using a NanoDrop^{TM} 1000 spectrophotometer (Peqlab, Germany). 1 µl of the respective RNA solution in DEPC-H_2O was rayed and optical densities (OD) at 230, 260 and 280 nm were measured. A 260/280 ratio of ~2.0 was considered “pure” RNA. Lower ratios indicated contaminations of proteins, phenols, and other components absorbing strongly at 280 nm. Those samples were excluded if possible. The ratio of 260/230 was used as a second parameter for contaminations and was supposed to be around 1.8-2.2. Lower values were also indicating co-purified contaminants and samples were excluded if possible. Measurements at 340 nm were used for normalization and DEPC-H_2O was used to blank. RNA was stored at -80°C until use.

4.7.4 DNAse Treatment

Compound	Composition
DNAse I	DNase I recombinant, RNase-free
Rnasin	RNase-free Ribonuclease Inhibitor
DNAse I reaction buffer (10x)	10mM Tris-HCl, 2.5 mM MgCl2, 0.5mM CaCl2

To clean RNA samples from possible DNA contamination, a DNAse digestion was performed using the endonuclease DNase I (New England Biolabs GmbH, Germany). A 20µl reaction solution (Master Mix - MM) was prepared for each sample containing 0.5µl DNAse I, 0.3µl RNAsin, 2.0µl DNAse I reaction buffer (10x) and RNA solution and nuclease free H_2O in a proportion resulting in 500ng RNA/µl MM. Samples were incubated at 25°C for 30 minutes, followed by a heating stop of the reaction at 75°C for 5 minutes. RNA concentration and purity was measured as described above (see **page 39**).

4.7.5 cDNA Synthesis

MM for 1 reaction			Thermo cycler protocol		
M-MLV 5x reaction buffer	4.0	µl	**Primer annealing**	25°C	15 min
dNTPs (5mM)	2.5	µl	**DNA polymerization**	37°C	60 min
Rnasin	0.5	µl	**Enzyme deactivation**	70°C	15 min
M-MLV (200U)	0.8	µl	**Storage**	4°C	forever

Synthesis of complementary DNA (cDNA) from RNA samples was performed following this protocol: 1µl of random hexamer (RH) primer was combined with volumes of RNA sample and nuclease free H_2O such that a final total RNA amount of 2µg was present in each 12.2 µl reaction and the final cDNA concentration was 100ng cDNA/µl. In a first step, the secondary structure of the RNA was melted for 5 minutes at 70°C, followed by a quick cool-down on ice to prevent the secondary structure from reforming. 7.8µl of the MM was added to each sample and cDNA synthesis was achieved via the adequate thermo cycler protocol.

4.7.6 Quantitative Polymerase Chain Reaction (qPCR) Analysis

As preparation for qPCR analysis, a primer optimization on 100ng cDNA was performed using standard PCR protocol with gradient annealing temperatures (52.0-65.0°C, see **Fig. 8A**) and primer testing in several tissues with an annealing temperature of 60°C (**Fig. 8B**). qPCR analysis was performed on cDNA samples from blood vessels (*arteria carotis communis, arteria femoralis, aorta* (thoracic aorta and arch), *vena cava, vena saphena arteria mesentrica, arteria pulmonaria and vena porta*) and *nervus vagus*, as well as from multiple organs (spleen, liver, intestine, thymus, brain and heart) of male B6, FVB/N, *B6/Tph1*$^{-/-}$ and *FVB/N/Tph1*$^{-/-}$ mice (5-6 per group and experiment) at the age of 8-12 weeks. Primers were used for the 5-HT receptors 1A, 1B, 1D, 2A, 2B, 2C, 3A, 3B, 4, 5A, 6, 7 as well as for the 5-HT related substances MAO A, SERT, TPH1 and TPH2. 5µl of diluted cDNA was added to 6.11µl of qPCR MM resulting in a concentration of 10ng cDNA per reaction. For qPCR a 2 step temperature protocol was performed with 15 seconds of denaturation at 95°C and 60 seconds of annealing at 60°C and 40 cycles using the Real time PCR system QuantStudio™ 5 (Applied Biosystems™/Thermo Fisher, USA). Melting curve analysis and primer efficiency analysis via standard curve method were performed for each primer and data were analyzed via ddCT method using the QuantStudio™ Design & Analysis Software 1.3.1 (Applied Biosystems™/Thermo Fisher, USA).

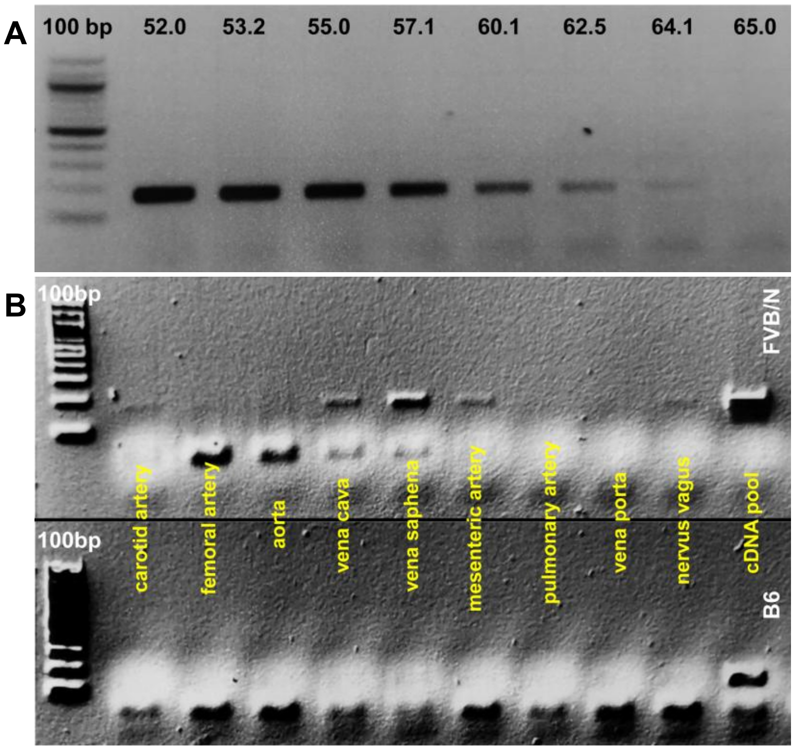

Fig. 8 – Primer Optimization for qPCR
Gradient PCR (**A**) and primer testing in various tissues (**B**) as preparation for qPCR analysis. 3% agarose gel; Light source: UV302; Exposure time: 0.5s (**A**), 0.4s (**B, upper panel**) and 1.9s (**B, lower panel**); Marker: 100 base pair ladder. **A:** Example for gradient PCR performed with primers for 5-HTr 2A in cDNA pool (spleen, liver, gut, thymus and brain); 52.0 – 65.0: Annealing temperatures in °C. **B:** Example for PCR products from one PCR run (anneal: 60°C) with primers for 5-HTr 1A, performed in several tissues (carotid artery – cDNA pool) of FVB/N (upper panel) and B6 (lower panel).

4.7.7 Lipid Extraction and Quantification (via FOLCH)

Lipid extraction via FOLCH solution with subsequent total lipid quantification as well as preparation and execution of colorimetric assays for hepatic cholesterol, triglycerides and NEFA was performed in close collaboration with Prof. Dr. Luíza A. Rabêlo and Dr. Valéria Nunes de Souza.

For lipid extraction, approximately 100mg from similar liver samples (sample L1, see Fig. 6) was isolated, weighed and transferred to their 20-fold volume of a 2:1 chlorofrom/methanol solution. Liver samples were homogenized using a tissue lyser system and 400µl of methanol was added. The samples were centrifuged at 3,000 x g for 10 minutes at RT and subsequently the supernatant was collected while the sediment was discarded. 800µL of chloroform and 640µL of 0.73% NaCl were added and the sample was centrifuged once more at 3,000 x g for 10 minutes at RT. The upper phase was discarded and washing was performed 3 times by adding 600µl FOLCH solution, centrifuging (3,000 x g, 10 minutes, RT) and discarding of the upper phase. Afterwards, the samples were dried by covering them with perforated aluminum foil and incubate them at 37°C over night. Total lipid amount was measured by weighing the dried samples and comparing them to the originally applied liver sample volume (g/g).

For detailed lipid analysis (colorimetric assays of cholesterol, triglycerides and NEFA), the lipid pellet was resuspended in 500µl isopropanol and vortexed for 20 seconds. The suspension was transferred to 2ml tubes and diluted in 1x PBS (1:20 for cholesterol, 1:40 for triglycerides and 1:10 for NEFA). Samples were stored at -20°C until use.

4.7.8 Enzyme Linked Colorimetric Assays

4.7.8.1 Cholesterol Assay

100µl duplicates of ddH_2O and 1x PBS blanks as well as of the standard curve (P1-P7) were pipetted on ice into a 96-well flat bottom microplate (96-well clear microplate F-bottom, Sarstedt AG & Co.KG, Germany). Further, 100µl duplicates of the previously prepared liver lipid dilution samples were added to the wells following a previously determined scheme. In the next step, 100µl of the cholesterol reagent was added to all wells with a multichannel pipette (Research Plus Multichannel Pipette, Eppendorf AG, Germany) and possible blisters were removed as quickly as possible by using a small pipette tip. Samples incubated for 20 minutes at 37°C and in a dark chamber. Finally, absorbance was read at 492nm in the Microplate reader Infinite® M200 (Tecan Trading AG, Switzerland) and cholesterol concentrations were recalculated to the original lipid concentration.

4.7.8.2 Triglycerides (TG) Assay

100µl duplicates of ddH_2O and 1x PBS blanks as well as of the standard curve (P1-P7) were pipetted on ice into a 96-well flat bottom microplate (96-well clear microplate F-bottom, Sarstedt AG & Co.KG, Germany). Further, 100µl duplicates of the previously prepared liver lipid dilution samples were added to the wells following a previously determined scheme. In the next step, 100µl of the triglyceride reagent was added to all wells with a multichannel pipette (Research Plus Multichannel Pipette, Eppendorf AG, Germany) and possible blisters were removed as quickly as possible by using a small pipette tip. Samples incubated for 10 minutes at 37°C and in a dark chamber. Finally, absorbance was read at 492nm in the

Microplate reader Infinite® M200 (Tecan Trading AG, Switzerland) and triglyceride concentrations were recalculated to the original lipid concentration.

4.7.8.3 Not Esterified Fatty Acids (NEFA) Assay

5µl duplicates of ddH_2O blank as well as of the standard curve (P1-P7) were pipetted on ice into a 96-well flat bottom microplate (96-well clear microplate F-bottom, Sarstedt AG & Co.KG, Germany). Further, 5µl duplicates of the previously prepared liver lipid dilution samples were added to the wells following a previously determined scheme. In the next step, 150µl of the reagent 1 from the NEFA kit was added to all wells with a multichannel pipette (Research Plus Multichannel Pipette, Eppendorf AG, Germany) and the samples incubated for 3 minutes at 37°C. Afterwards, 75µl of the reagent 2 from the NEFA kit was added to each sample and possible blisters were removed as quickly as possible by using a small pipette tip. Samples incubated for 4 minutes and 30 seconds at 37°C. Finally, absorbance was read at 546nm and 600nm in the Microplate reader Infinite® M200 (Tecan Trading AG, Switzerland) and NEFA concentrations were extrapolated from the difference of absorbance values (546nm and 600nm) and the originally diluted lipid concentration.

4.7.8.4 Colorimetric Calcium Measurement in Aortas

After *en face* preparation, aortic arches and thoracic aortas were transferred to 200µl of 0.6N HCl were they incubated for at least 14 days at 4°C. HCl dissolved possible calcium deposits out of the aortas. Following the instructions of the Randox Calcium assay kit (Randox Laboratories Ltd, United Kingdom), a fresh 1:1 R1/R2 reaction reagent was prepared and 500µl of it were added to 12.5µl sample, respectively 12.5µl of 0.6N HCl blank. For the standard curve, 40µl standard solution were mixed with 800µl of R1/R2 and from that S2-S7 were generated vie 1:1 dilution. 150µl duplicates of standards (S1-S7), 0.6N HCl blank and samples were added to a 96-well flat bottom microplate (96-well clear microplate F-bottom, Sarstedt AG & Co.KG, Germany) and absorbance was immediately measured at 562nm in the Microplate reader Infinite® M200 (Tecan Trading AG, Switzerland). Measurements were compared to standard curve and directly converted to total calcium amount of aortas.

4.8 Statistics

Statistical analyses were performed in Prism5 (GraphPad Software, USA), PASW Statistics 18 (SPSS18, IBM, Germany) and Statistica 8 (StatSoft (Europe) GmbH, Germany). For all tests the significance threshold was set to $\alpha \leq 0.05$, probabilities of error between 0.05 and 0.099 were considered as statistical trends. If applicable, two-tailed tests were always performed.

4.8.1 Outlier Analysis in *Excel* and *GraphPad QuickCalcs*

Outliers were detected by graphical presentation in histograms and boxplot-diagrams (criteria for outliers: >3.0 x interquartile range (IQR)). For numerical identification of outliers, either outlier analysis in *Excel* (criteria for outliers: >1.5 x interquartile range (IQR)) or *Grubb's* test for outliers at GraphPad QuickCalcs (https://www.graphpad.com/quickcalcs/Grubbs1.cfm) with a significance level of $\alpha \leq 0.05$ was performed. Only if typos could not be corrected and outliers were biological incomprehensible, data-points or respective animal was excluded from the analysis.

4.8.2 Determination of Distribution Type in *Statistica*

Distribution type was determined via *Kolmogorow-Smirnow & Lilliefors* test for normality. The following statistical tests as well as the graphical data representation were selected for the respective results of these pre-tests, e.g. parametrical tests and data representation as mean ± SEM or non-parametrical tests and median ± IQR.

4.8.3 Two-group Analysis in *GraphPad*

Two group analyses were performed using *unpaired t-test* (T, parametrical test for unconnected data), after checking for homologous or heterologous variance using the *F-test*. *Mann-Whitney U-test* (U, non-parametrical data) was used if application of *unpaired t-test* was not allowed due to inappropriate data distribution or variance homogeneity. Both tests were operated in Prism5.

4.8.4 Multi-group Analysis in *GraphPad*

For comparisons involving more than two groups, but one variable, *One-way ANOVA* (parametrical data sets) or *Kruskal–Wallis One-way analysis of variance by ranks* (non-parametrical data sets) were used. For group analysis an adequate post-Hoc test was performed subsequently (e.g. *Tukey's Multiple Comparison* or *Dunn's Multiple Comparison* Post-Hoc test).

4.8.5 Correlations in *SPSS*

Correlations between data-sets were calculated separately for each experimental group either with *Pearson's product-moment* or *Spearman's rank correlation coefficient* (depending on distribution type). An r^2-score between 1.0 and 0.8 was taken as positive correlation while an r^2-score between 0.8 and 0.7 was defined as tendency, if the alpha-level of $p<0.05$ was crossed.

5 Results

5.1 The Serotonin System in Vessels of *Tph1* deficient Mice in different Genetic Backgrounds

At first, a characterization of the serotonergic system in vessels of wild type and *Tph1* deficient mice on two different genetic background strains (B6 and FVB/N) was elaborated. Therefore, RNA expression levels of 12 5-HT receptors and 4 other 5-HT related proteins were quantified via qPCR in different vascular beds. For this purpose the respective primers were designed and PCR protocols were established in 10 different vascular tissues and pool RNAs from brain and liver (1:1). This comprised optimization of the primer concentrations and annealing temperatures via gradient PCR. Only after successful optimization of the PCR protocol, qPCR was performed on cDNA from all 10 tissues and primer efficiencies (via standard curve method) and RNA expression levels relative to wild type B6 animals were quantified.

5.1.1 5-HT Receptor Distribution in Vessels of B6 and FVB/N Mice

In the first step of primer optimization equal amounts of cDNA were used for all tissues and PCR products were applied to agarose gels (see **Fig. 8B**) which allowed a semiquantitative comparison of the resulting DNA bands and gave a first impression of the distribution of 5-HT receptors and other 5-HT related genes MAO A, SERT, TPH1 and TPH2. The results are summarized in **Tab. 5**.

The most striking finding here is the great alteration of 5-HT receptor distribution among the different blood vessel types of the two tested mouse strains: For instance, strong bands could be detected for 5-HTr 2A and 2B in *arteria femoralis* and *aorta* of FVB/N mice, but none or only faint bands could be found in respective vessels of B6 mice. The same is true for 5-HTr 3A in *vena cava* and by trend for 5-HTr 1A, 1D and 2B in *vena saphena*. On the other hand there are 5-HTr 1B and 1D (see **Tab. 5**) which exhibit stronger bands on the gel in the *aorta* of B6 than in FVB/N and in the *arteria mesenterica* bands were stronger in B6 than in FVB/N for 5-HTr 1D and 2A. Differences could also be detected in the pool RNA (liver and brain, 1:1): Stronger bands for FVB/N for 5-HTr 1A, 2B, 3A, 4, 5A, 6 and 7 and for MAO A, SERT and TPH1. However, B6 had presumably more mRNA in the pool for 5-HTr 1B, 2C and for TPH2. These first findings demonstrate clear differences between 5-HT receptor distribution in the vessels of B6 and FVB/N mice.

The almost exclusive expression of the 5-HTr 3A in samples of *nervus vagus* could be confirmed and served as a second methodological control. Generally, 5-HT receptors 3B – 7 gave only poor results in the regular PCR protocol in both strains and *arteria carotis communis* and *vena porta* appeared to express 5-HT receptor and 5-HT related gene RNAs only at very low levels (see **Tab. 5**).

						DNA band in… (B6 / FVB/N)									
Gene	**Primer FW**	**Primer REV**	**cDNA [bp]**	**gDNA [bp]**	**Anneal [°C]**	***arteria carotis communis***	***arteria femoralis***	***aorta***	***vena cava***	***vena saphena***	***arteria mesenterica***	***arteria pulmonaria***	***vena porta***	***nervus vagus***	**cDNA pool**
Mouse *HTr1a*	CCGATCTCATGGTGTCAGTG	GGTGATTGCCCAGTACCTGT	176	176	52-62.5 (best: **57.1**)	**-/(+)**	**-/(+)**	**-/-**	**-/+**	**-/++**	**-/+**	**-/-**	**-/-**	**-/(+)**	**++/++++**
Mouse *HTr1b*	ATGCGGTGGAGTATTCTGCT	TCACAAAGCAGTCCAGCATC	147	147	52-60.1 (best: **52.0**)	**-/-**	**-/+**	**++/-**	**-/-**	**-/-**	**-/-**	**-/(+)**	**-/-**	**-/-**	**+++/++**
Mouse *HTr1d*	CACGGACCTCCTGGTTTCTA	GCCCAGTATCTGTCCAGAGC	171	171	52-60.1 (best: **55.0**)	**-/(+)**	**-/(+)**	**(+)/-**	**-/+**	**-/++**	**+/(+)**	**-/-**	**-/-**	**(+)/(+)**	**++/++**
Mouse *HTr2a*	TCATCATGGCAGTGTCCCTA	AGGTAAATCCAGACGGCACA	178	2820	52-57.1 (best: **52.0**)	**-/-**	**-/+++**	**++/++++**	**-/-**	**-/+**	**+/-**	**-/+**	**-/+**	**-/-**	**+++/++**
Mouse *HTr2b*	GCAGATTTGCTGGTTGGATT	AGGGAAATGGCACAGAGATG	158	7911	53.2-57.1 (best:**55.0**)	**-/-**	**-/++++**	**+/++++**	**(+)/+**	**(+)/++**	**-/+**	**(+)/+**	**(+)/+**	**-/-**	**-/+**
Mouse *HTr2c*	CCATTGCTGATATGCTGGTG	CATGATGGACGCAGTTGAAA	143	93515	52-60.1 (best: **55.0**)	**-/-**	**-/-**	**-/-**	**-/-**	**-/-**	**-/-**	**-/-**	**-/-**	**-/-**	**+++/+**
Mouse *HTr3a*	CGGCAGTACTGGACTGATGA	TCACCTCGATGATGCACGTA	173	1705	52-60.1 (best: **55.0**)	**-/-**	**-/-**	**-/+**	**-/+++**	**-/+**	**-/-**	**-/+**	**-/-**	**+/+**	**+/++**
Mouse *HTr3b*	ATCCAGAACTGCAGCCTCAC	GCTGCCACTCACTGTCATTC	130	893	n.a.	**-/-**	**-/-**	**-/-**	**-/-**	**-/-**	**-/-**	**-/-**	**-/-**	**-/-**	**-/-**
Mouse *HTr4*	TCGATCTTTCACCTGTGCTG	CCTTGCATTATGGGGAGAAA	161	14452	52-57.1 (best: **55.0**)	**-/-**	**-/-**	**-/-**	**-/-**	**-/-**	**-/-**	**-/-**	**-/-**	**-/-**	**-/+**
Mouse *HTr5a*	CAGGAAGACCAACAGCGTCT	CGTATCCCCTTCTGTCTGGA	124	7687	52-57.1 (best: **55.0**)	**-/-**	**-/-**	**-/-**	**-/-**	**-/+**	**-/-**	**-/-**	**-/-**	**-/-**	**-/++**
Mouse *HTr6*	GGTGCCATCTGCTTCACCTA	GGTGGTCAGACGCCTACTGT	174	11982	52-65 (best: **55.0-60.1**)	**-/-**	**-/-**	**-/-**	**-/-**	**-/-**	**-/-**	**-/-**	**-/-**	**-/-**	**-/+++**
Mouse *HTr7*	CTTCTGCAACGTCTTCATCG	TTGGCCATACATTTCCCATT	144	86784	52-57.1 (best: **52.0**)	**-/-**	**-/-**	**-/-**	**-/-**	**-/+**	**-/-**	**-/-**	**-/-**	**-/-**	**-/+++**
Mouse *MaoA*	TGTGAGGCAGTGTGGAGGTA	TTATCCCCAAGGAGGACCAT	120	2311	53.2-62.5 (best: **57.1**)	**n.a./+**	**n.a./++**	**n.a./-**	**n.a./-**	**n.a./+**	**n.a./-**	**n.a./+**	**n.a./-**	**n.a./-**	**-/++**
Mouse *Slc6a4* (Sert)	CTGGACCAGCTGCAAGAACT	CCTGGAGTCCCTTTGACTGA	152	1805	52-64.1 (best: **57.1**)	**n.a./+**	**n.a./-**	**n.a./-**	**n.a./+**	**n.a./+**	**n.a./-**	**n.a./+**	**n.a./-**	**n.a./-**	**+/++++**
Mouse *Tph1*	GTGGCTATCGGGAAGACAAC	GGGGATCTGAACTGTGTCTCA	177	3159	52-64.1 (best: **55.0-57.1**)	**n.a./-**	**n.a./++**	**n.a./-**	**n.a./+**	**n.a./+**	**n.a./-**	**n.a./-**	**n.a./+**	**n.a./-**	**+/+++**
Mouse *Tph2*	CGGGAGCTCTCCAAACTCTA	AGGTAGCCAGCCACTGGTC	173	5130	52-65 (best: **57.1-60.1**)	**n.a./-**	**n.a./-**	**n.a./-**	**n.a./-**	**n.a./-**	**n.a./-**	**n.a./-**	**n.a./-**	**n.a./-**	**+++/++**

Tab. 5 – 5-HT Receptor Distribution in B6 and FVB/N
Overview of all tested 5-HT receptors and the related substances Mao A, SERT, TPH1 and TPH2 in 10 different tissues of B6 and FVB/N mice optically quantified via gel bands of PCR products. The table additionally gives all tested primers with sequence, cDNA and gDNA fragments, optimal annealing temperature and PCR product result (gel band) for **B6/FVB/N**. **-:** no band detectable; **(+):** only very faint band; **+:** faint band; **++:** regular band; **+++:** strong band; **++++:** very strong band; **n.a.:** not applicable.

5.1.2 RNA Expression Levels of 5-HT Receptor Subtypes 1 and 2

As the RT-PCR data suggested, qPCR and determination of RNA expression levels was only successful for 5-HTr 1B, 1D, 2A and 2B, but surprisingly not for 5-HTr 1A. Furthermore, the mentioned 5-HT receptor RNA levels could only be quantified in RNA extracts from *aorta*, *arteria femoralis*, *arteria mesenterica* and *vena cava*, but surprisingly not in samples from *vena saphena* (cf. Tab. 5). Pooled samples from brain and liver were successfully used for standard curve calculation and all tested primers (except 5-HTr 3B) featured efficiencies of 80-100% (data not shown). Samples from B6, FVB/N, *B6/Tph1*$^{-/-}$ and *FVB/N/Tph1*$^{-/-}$ animals were examined and ddCT values were extrapolated from each sample and normalized to B6 and the housekeeping gene *GAPDH* to define relative RNA expression levels.

Relative RNA expression levels appear to be quite variable among different tissues, but surprisingly, as well between different genetic background strains. The here presented data provide evidence for two major phenomena: First, FVB/N animals, as well as *Tph1*$^{-/-}$ animals bred in the FVB/N background tend to have higher RNA expression levels for most 5-HT receptor types and in the majority of the tested vessels. However, the second observation was that in most cases the inter-group variances are too high to allow the differences to reach statistical significance. Hence, individual factors seem to play an important role. This was true for all tested genetic groups and organs, such that genotype or organ specific tissue processing issues could be widely excluded (see Fig. 9).

In the *aorta* 5-HT receptor RNAs appear to be expressed at similar levels in all tested genotypes (Fig. 9A-D). Only in *FVB/N/Tph1*$^{-/-}$, receptors 1D and 2B tend to exhibit higher relative expression levels than the other genetic groups (Fig. 9B and D), this was statistically significant for 5-HTr 2B compared to *B6/Tph1*$^{-/-}$(Fig. 9D).

In the *arteria femoralis* (see Fig. 9E-H) the situation is different: The relative expression level for 5-HTr 1D is more than 10-fold increased in *FVB/N/Tph1*$^{-/-}$ compared to B6 and significantly increased compared to *B6/Tph1*$^{-/-}$(Fig. 9F). On the other hand, relative 5-HTr 2B expression is decreased in all groups compared to B6 (Fig. 9H: $p<0.1$ trend for FVB/N). Relative expression levels for 5-HTr 1B and 2A appear to be similar for all groups in *arteria femoralis* (see Fig. 9E and G).

In the *arteria mesenterica* (Fig. 9I-L) a trend is visible for FVB/N and *FVB/N/Tph1*$^{-/-}$ showing higher relative expression levels for all receptors compared to the two B6 groups. This was statistically significant for 5-HTr 2A at $p\leq0.01$ for *FVB/N/Tph1*$^{-/-}$ compared to *B6/Tph1*$^{-/-}$ (Fig. 9K).

In *vena cava* (Fig. 9M-P) the relative RNA expression of 5-HTr 1B and 2A is elevated in all groups compared to B6 (Fig. 9O: statistic trend, $p<0.1$ for 5-HTr 2A in FVB/N). Levels of 5-HTr 1D and 2B are relatively lower or comparable to B6 (Fig. 9N and P).

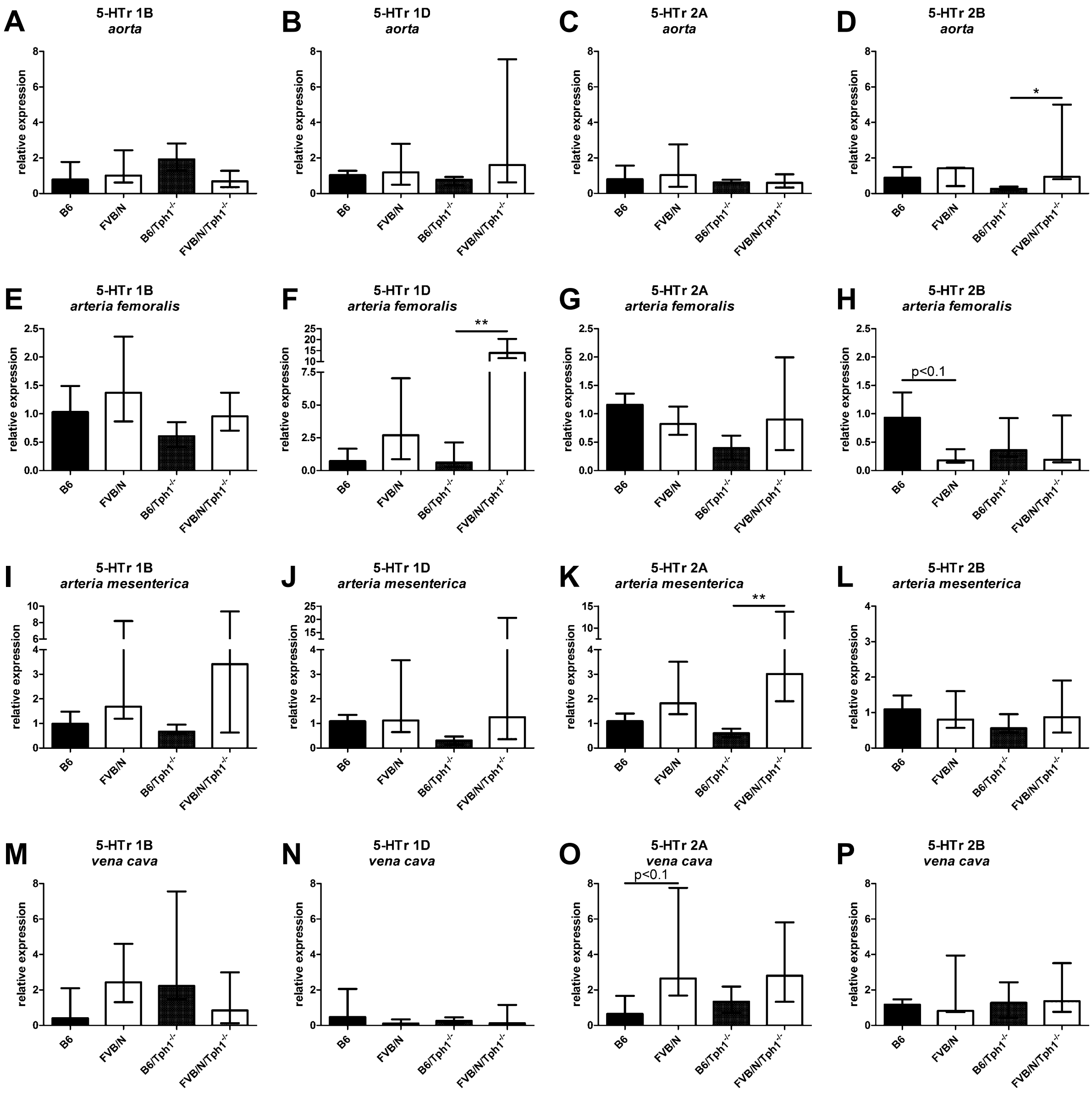

Fig. 9 – 5-HT Receptor RNA Levels in Different Blood Vessel Types measured by qPCR
Relative RNA expression levels normalized to *GAPDH* and compared to B6. Graphic display of RNA expression levels in *aorta* (**A-D**), *arteria femoralis* (**E-H**), *arteria mesenterica* (**I-L**) and *vena cava* (**M-P**) of B6, FVB/N, *B6/Tph1*$^{-/-}$ and *FVB/N/Tph1*$^{-/-}$ mice. Bars represent **Medians**; error bars show the interquartile range (**IQR**). Closed bars represent B6 (4-5n), open bars FVB/N (3-5n), dark grey *B6/Tph1*$^{-/-}$ (5-6n) and light grey *FVB/N/Tph1*$^{-/-}$ (5-6n). Sample size varied with applicable sample number per qPCR run and tissue. *$p \leq 0.05$; **$p \leq 0.01$; *Kruskal-Wallis* with subsequent *Dunn's Multiple Comparison* test (trends are indicated with $p \leq 0.1$).

Concluding, the results for qPCR are very variable but with a trend of FVB/N and *FVB/N/Tph1*$^{-/-}$ expressing relatively more 5-HT receptor RNA than B6 and *B6/Tph1*$^{-/-}$ what supports the findings from first quantification of DNA bands on agarose gels (cf. Tab. 5).

5.1.3 5-HTr 1B and 2A RNA Expression Levels after Tissue Cleaning

In order to exclude contributions of adventitial tissue to the RNA expression of 5-HT system components aortas were cleaned from the surrounding fat tissue. For this analysis the tissue cleaning protocol was applied to freshly collected aortas (aortic arch and thoracic aorta) from animals of all 4 genetic groups.

Again, quantification of relative RNA expression levels in cleaned aortas was only possible for receptor types 1B, 1D and 2A (Fig. 10), but not for 5-HTr 2B - even though all available 5-HTr primers were tested and achieved good results for standard curves in pooled cDNA from liver and brain (data not shown). Due to several samples performed only poorly during qPCR (threshold cycle larger than 40), the analysis for 5-HTr 1D was only possible for some samples and sample sizes varied from 2 to 4 per group. For 5-HTr 1B and 2A qPCR analysis could be performed unobstructed and the comparable low variability of data even allowed a parametric statistical analysis. These first results strongly support the idea of 5-HTr 1B and 2A being the major players in mammalian blood vessels.

It could be shown that the relative RNA expression for 5-HTr 1B is twice as high in FVB/N as in B6, but surprisingly, it is on a comparable level in *FVB/N/Tph1$^{-/-}$* and B6. Interestingly, in *B6/Tph1$^{-/-}$* the RNA expression is significantly increased (more than 3-fold) compared to B6. Additional unpaired t-tests revealed that *FVB/N/Tph1$^{-/-}$* RNA expression is even significantly lower than in FVB/N and *B6/Tph1$^{-/-}$* (Fig. 10A).

As mentioned, the analysis for 5-HTr 1D was impaired, but there might be a tendency of *FBV/N/Tph1$^{-/-}$* animals exhibiting elevated RNA expression levels compared to the other groups. FVB/N as well as *B6/Tph1$^{-/-}$* show slightly decreased expression levels compared to B6 (Fig. 10B). Due to very low sample size, none of the results for 5-HTr 1D could be statistically proven.

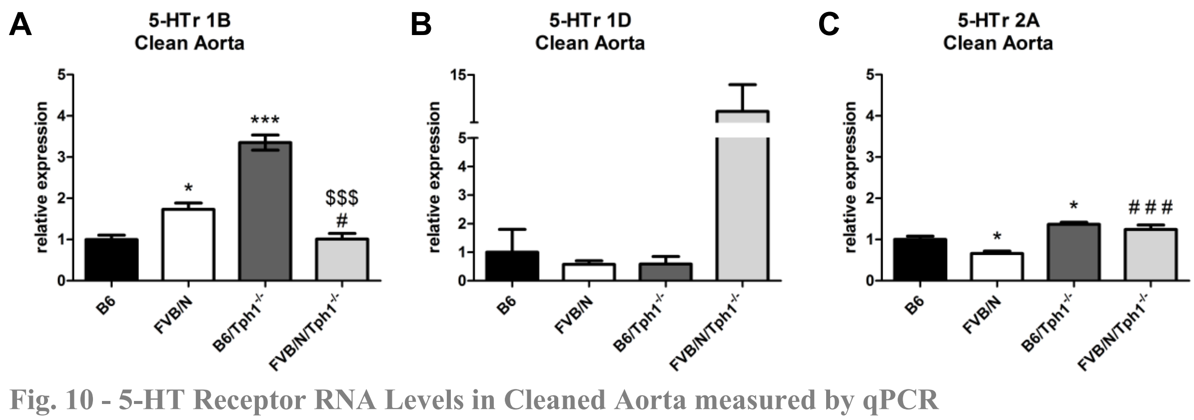

Fig. 10 - 5-HT Receptor RNA Levels in Cleaned Aorta measured by qPCR
Relative RNA expression levels normalized to *GAPDH* and compared to B6. Graphic display of RNA expression levels for 5-HTr 1B (**A**), 1D (**B**) and 2A (**C**) in cleaned aortas of B6, FVB/N, *B6/Tph1$^{-/-}$* and *FVB/N/Tph1$^{-/-}$* mice. Bars represent **Means**; error bars show the standard deviation of the mean (**SEM**). Closed bars represent B6 (2-5n), open bars FVB/N (3-5n), dark grey *B6/Tph1$^{-/-}$* (4-6n) and light grey *FVB/N/Tph1$^{-/-}$* (2-4n). Sample size varied with applicable sample number per qPCR run and was always lowest for 5-HTr 1D. Single unpaired t-tests: *p≤0.05; ***p≤0.001 for comparison with B6, #p≤0.05; ###p≤0.001 for comparison with FVB/N; $$$p≤0.001 for comparison with B6/Tph1$^{-/-}$.

Relative RNA expression level for 5-HTr 2A was significantly lower in FVB/N than in B6, but significantly raised in *B6/Tph1*$^{-/-}$. Interestingly, *FVB/N/Tph1*$^{-/-}$ appeared to exhibit strongly significantly higher relative RNA expression than FVB/N. These results clearly show that 5-HTr 2A RNA expression in *Tph1* deficient animals in elevated compared to their wild type controls (**Fig. 10C**).

In summary, the detection of RNA expression alterations between groups of animals could be performed more precisely after a tissue cleaning protocol. The genetic background strains appear to express 5-HTr RNA differently and so do the *Tph1* deficient animals generated in these strains, but not always in a comparable manner. Results from the first qPCR analysis in uncleaned tissues could be at least partly confirmed (cf. **Fig. 9** and **Fig. 10**), but data from the RT-PCR assays differed from these results (cf. **Tab. 5** and **Fig. 10**).

5.2 Characterization of Newly Established *ApoE/Tph1*$^{-/-}$ and *ApoE/Sert*$^{-/-}$ Animals

The double knockout mouse lines *ApoE/Tph1*$^{-/-}$ and *ApoE/Sert*$^{-/-}$ were generated by breeding and the genotype for each animal was determined via PCR as described above (see **page 37**). The following data sets give an overview of the *ApoE/Tph1*$^{-/-}$ and *ApoE/Sert*$^{-/-}$ physiology in aged animals (45 weeks and older) with regard to atherosclerosis development.

5.2.1 Bodyweight and Blood Glucose Levels

Bodyweight of representative groups of B6, *ApoE*$^{-/-}$, *ApoE/Tph1*$^{-/-}$ and *ApoE/Sert*$^{-/-}$ males and females was measured at the age of 45 weeks and before any experimental procedure. Furthermore, fasting blood glucose was measured in similarly untreated *ApoE*$^{-/-}$, *ApoE/Tph1*$^{-/-}$ and *ApoE/Sert*$^{-/-}$ males and females (only one *ApoE/Tph1*$^{-/-}$ animal) to avoid elevation of blood glucose levels due to stress. The results are summarized in Fig. 11.

In males the median bodyweight in B6 animals was 36.95g. The median bodyweight of *ApoE*$^{-/-}$ (36.30g) and *ApoE/Sert*$^{-/-}$ (34.60g) males did not significantly differ from B6. However, *ApoE/Tph1*$^{-/-}$ males appeared to have a significantly lower median bodyweight (31.80g) than B6 and *ApoE*$^{-/-}$ males (Fig. 11A). In females the median bodyweights were measured at 30.90g (B6), 27.80g (*ApoE*$^{-/-}$), 24.80g (*ApoE/Tph1*$^{-/-}$) and 28.65g (*ApoE/Sert*$^{-/-}$). Hence, *ApoE/Tph1*$^{-/-}$ females were significantly lighter than B6 controls (Fig. 11B).

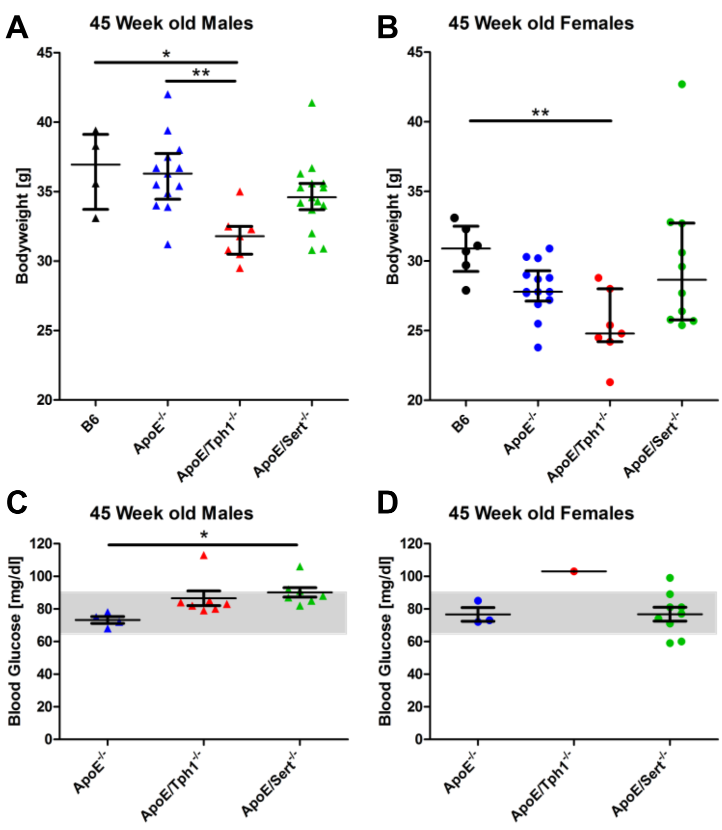

Fig. 11 – Bodyweight and Blood Glucose in 45 Week old Double Knockout Animals

Median bodyweight with **IQR** (**A** and **B**) and **mean** fasted blood glucose with **SEM** (**C** and **D**) in untreated, 45 week old B6, *ApoE*$^{-/-}$, *ApoE/Tph1*$^{-/-}$ and *ApoE/Sert*$^{-/-}$ males and females. Bodyweight: *$p \leq 0.05$; **$p \leq 0.01$; *Kruskal-Wallis* with subsequent *Dunn's Multiple Comparison* test. Blood Glucose: *$p \leq 0.05$; *One-way ANOVA* with *Tukey's Multiple Comparison* test. Grey area: normal range for fasted B6.

Male fasted blood glucose levels in all groups ranged around normal fasted blood glucose of adult B6 mice (65 – 90 mg/dl; Sun et al., 2016), but were elevated by trend in *ApoE/Tph1*$^{-/-}$ and significantly in *ApoE/Sert*$^{-/-}$compared to *ApoE*$^{-/-}$(Fig. 11C). In females, fasted blood glucose levels in *ApoE*$^{-/-}$ and *ApoE/Sert*$^{-/-}$ were similarly distributed in the normal range. However, the only examined *ApoE/Tph1*$^{-/-}$ female (due to instrument failure) appeared to have an elevated blood glucose value (Fig. 11D).

5.2.2 Plasma Cholesterol and Triglycerides

To investigate whether levels of free cholesterol and triglycerides in the blood of double knockouts at the age of 45 weeks differ from B6 controls, plasma of representative groups was examined photometrically (see **page 28**).

The results in **Fig. 12A and B** show clearly, that fasting plasma cholesterol levels in all three groups and both sexes are highly significantly increased compared to fasting B6 control which ranges slightly below the normal physiological values for B6 mice (117 – 164 mg/dl in *ad libitum* fed mice, Weibust, 1973). In males it could be shown that *ApoE/Sert*$^{-/-}$ exhibits even higher plasma cholesterol levels compared to *ApoE*$^{-/-}$ ($p \leq 0.05$) and *ApoE/Tph1*$^{-/-}$ ($p \leq 0.05$). In females this effect could not be verified. However, *ApoE/Tph1*$^{-/-}$ animals of both sexes tend to exhibit slightly lower plasma cholesterol levels than *ApoE*$^{-/-}$ and *ApoE/Sert*$^{-/-}$; this is even significant when female *ApoE/Tph1*$^{-/-}$ vs. *ApoE*$^{-/-}$ animals are statistically re-analyzed via single two-tailed t test ($p \leq 0.05$, *Mann-Whitney-U* test, data not shown).

Plasma triglycerides in male and female *ApoE*$^{-/-}$, *ApoE/Tph1*$^{-/-}$ and *ApoE/Sert*$^{-/-}$ animals are not drastically altered when compared to B6 and range around innate levels of B6 (37 – 109 mg/dl, (Zhang et al., 1992)). However, all tested groups of females appear to have generally lower plasma triglyceride levels than males. In males, *ApoE*$^{-/-}$ and *ApoE/Sert*$^{-/-}$ could be demonstrated to have higher plasma triglycerides levels than *ApoE/Tph1*$^{-/-}$ (see **Fig. 12C**; re-analysis of *ApoE*$^{-/-}$ vs. *ApoE/Tph1*$^{-/-}$, *Mann-Whitney-U* test: $p \leq 0.05$). In females this effect is not significant (**Fig. 12D**).

Concluding, the results strongly support the image of *ApoE* deficiency leading to high plasma cholesterol levels and elevated plasma triglyceride levels in regular *ApoE*$^{-/-}$ as well as in the double knockouts *ApoE/Tph1*$^{-/-}$ and *ApoE/Sert*$^{-/-}$ compared to B6 animals. However, the effects seem to be even increased in *ApoE/Sert*$^{-/-}$, whereas *ApoE/Tph1*$^{-/-}$ animals could be shown to be at least partly protected.

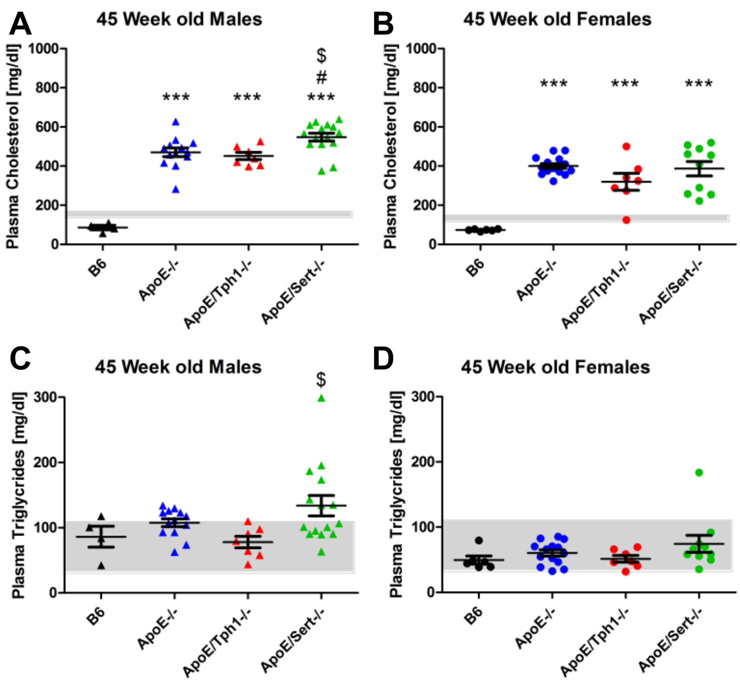

Fig. 12 – Plasma Cholesterol and Triglycerides in 45 Week old Double Knockout Animals
Summarized results for photometric measurement of fasting plasma cholesterol (**A** and **B**) and triglycerides (**C** and **D**) in untreated, 45 week old B6, *ApoE*$^{-/-}$, *ApoE/Tph1*$^{-/-}$ and *ApoE/Sert*$^{-/-}$ males (▲) and females (●). Grey area shows normal physiological range of measured parameters for *ad libitum* fed B6 mice. Lines represent **means**, error bars depict **SEM**. ***$p \leq 0.001$ (vs. B6); #$p \leq 0.05$ (vs. *ApoE*$^{-/-}$); \$$p \leq 0.05$ (vs. *ApoE/Tph1*$^{-/-}$); *One-way ANOVA* with *Tukey's Multiple Comparison* test.

5.2.3 Liver Weight and Plasma Liver Parameters

Since blood cholesterol, triglycerides and liver status are closely connected, it was very important to investigate the liver status, as done via relative organ weight measurement, and levels of liver enzymes aspartate transaminase (AST) and alanine transaminase (ALT) in plasma, which are used as indicators for possible liver damage. The results for the liver status in all groups of 45 week old animals are summarized in Fig. 13.

The relative liver weight (normalized to total bodyweight) in all animals ranged from 4 to 6 % and was very similar in all tested genetic groups of males (see Fig. 13A), but significantly increased in *ApoE/Tph1*$^{-/-}$ females compared to *ApoE*$^{-/-}$ and *ApoE/Sert*$^{-/-}$ (see Fig. 13B). The level of AST in *ApoE*$^{-/-}$ males and females lied above the normal range of 50 – 100 U/l (Fraulob et al., 2010; Maletzki et al., 2019), whereas it stayed within the normal range in *ApoE/Tph1*$^{-/-}$ and *ApoE/Sert*$^{-/-}$ males and *ApoE/Tph1*$^{-/-}$ females. However, *ApoE/Sert*$^{-/-}$ males were shown to exhibit significantly lower AST values than *ApoE/Tph1*$^{-/-}$ males. In females, the difference of AST levels in between *ApoE*$^{-/-}$ and *ApoE/Tph1*$^{-/-}$ was statistically significant (Fig. 13C and D). ALT levels could be detected inside of the normal range of 25 – 60 U/l (Fraulob et al., 2010; Maletzki et al., 2019) for all tested groups. However, male *ApoE/Sert*$^{-/-}$ mice appeared to have significantly lower ALT levels compared to *ApoE/Tph1*$^{-/-}$(Fig. 13E and F). The *De Ritis* quotient (AST/ALT) was at comparable levels in all tested groups and close to the normal value of 2 (Maletzki et al., 2019). Only in females, it tended to be slightly raised (Fig. 13G and H).

Summing up, liver status was comparable in all tested groups and liver enzyme levels were close to normal range. Nevertheless, it needs to be highlighted, that *ApoE/Sert*$^{-/-}$ males tend to be protected from ALT and AST increase and liver status is slightly worse in females.

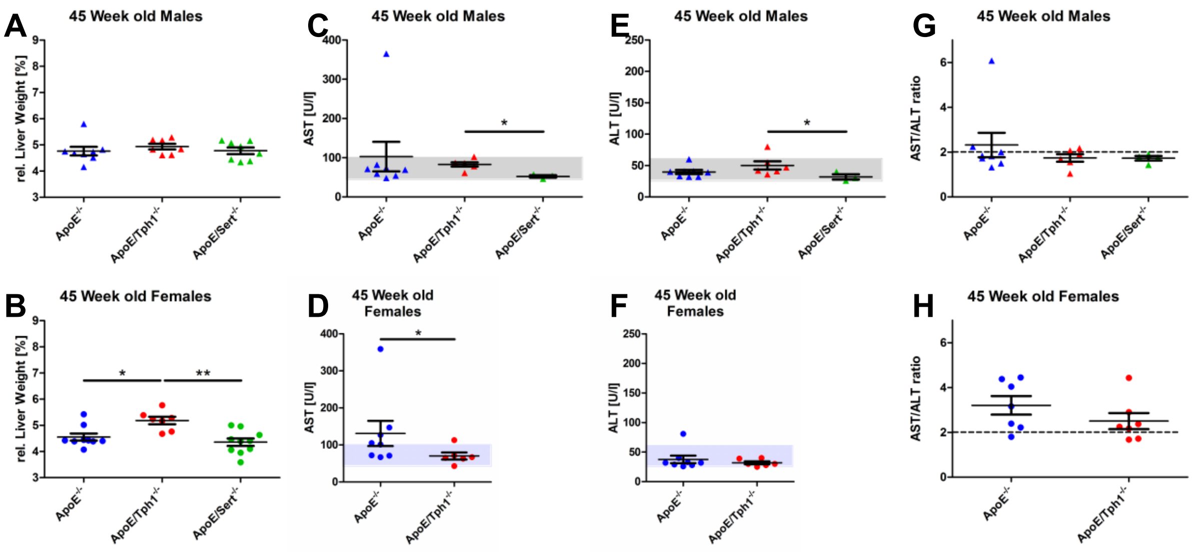

Fig. 13 – Liver Status in 45 Week old Double Knockout Animals
Relative liver weight (**A** and **B**) and liver enzymes AST (**C** and **D**), ALT (**E** and **F**) and AST/ALT ratio (*De Ritis* quotient; **G** and **H**) measured photometrically in plasma of male (▲) and female (●) mice. Lines and error bars: **mean** ± **SEM**; grey areas in C – F and dashed line in G and H represent normal levels in B6 mice. Relative liver weight: *p≤0.05; **p≤0.01; *One-way ANOVA* with *Tukey's Multiple Comparison* test. AST and ALT in males (**C** and **E**): *p≤0.05; *Kruskal-Wallis* with subsequent *Dunn's Multiple Comparison* test. AST in females (**D**): *p≤0.05; *Mann-Whitney-U* test.

5.2.4 Atherosclerotic Plaque Formation in Whole Aorta

The major focus of this study was the elucidation of possible correlations between the lifelong systemic absence of 5-HT in the periphery and the development of atherosclerotic lesions. Therefore, the analysis of atherosclerotic plaques in tissues like the aortic arch, preferentially performed in an *en face* preparation (**Fig. 14A and B**), is indispensable. Aortic arches of representative groups of *ApoE*$^{-/-}$, *ApoE/Tph1*$^{-/-}$ and *ApoE/Sert*$^{-/-}$ males and females were dissected, processed to *en face* specimens and analyzed for atherosclerotic plaque size as described above (see **page 32**); results are presented in **Fig. 14**.

Males and females of all tested groups develop aortic plaques similarly (2 – 20% of the aortic surface covered by atherosclerotic plaque) and with comparable distribution along the dissected part of the aortic arch (data not shown). However, in both groups, males and females of *ApoE/Sert*$^{-/-}$ genotype could be demonstrated to develop significantly larger aortic plaques (**Fig. 14C and D**). In males, this difference is statistically significant for *ApoE/Sert*$^{-/-}$ vs. *ApoE/Tph1*$^{-/-}$, not least because of *ApoE/Tph1*$^{-/-}$ tending to develop relatively smaller aortic plaques than *ApoE*$^{-/-}$(**Fig. 14C**). In females, *ApoE/Sert*$^{-/-}$ were shown to have significantly larg-

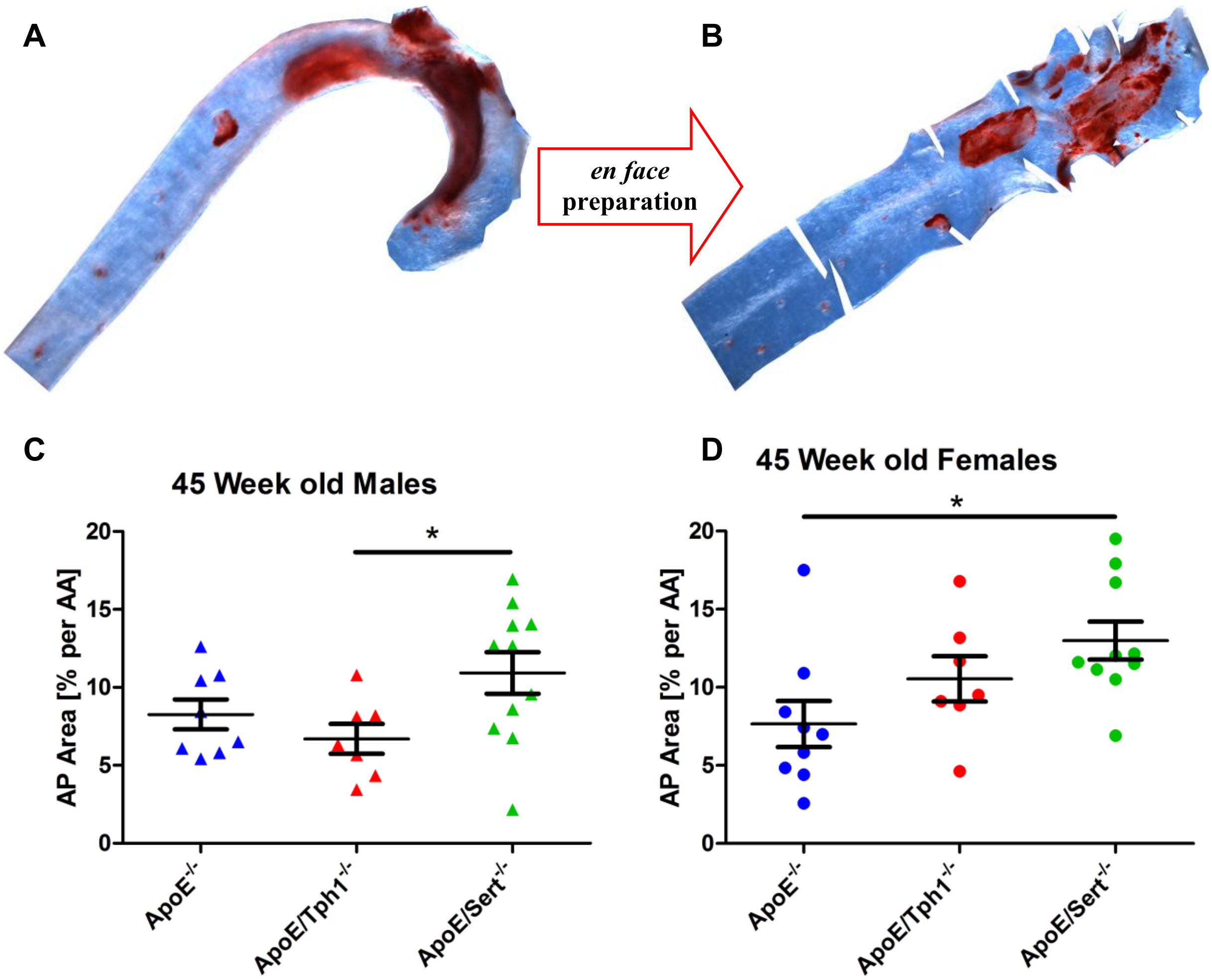

Fig. 14 – Aortic Plaques in 45 Week old Double Knockout Animals
Representative ORO stained *en face* preparation of an aortic arch from an *ApoE/Sert*$^{-/-}$ female with atherosclerotic plaques in **red** (**A** and **B**) and results for aortic plaque analysis in males (**C**) and females (**D**). Lines indicate **Mean** relative aortic plaque size with **SEM** (error bars). *p≤0.05; single unpaired t-tests.

er aortic plaques compared to *ApoE*$^{-/-}$. This is also true because of *ApoE/Tph1*$^{-/-}$ females tending to exhibit larger aortic plaques than *ApoE*$^{-/-}$ controls (**Fig. 14D**).

Concluding, in aortas of the tested animal groups the largest atherosclerotic plaques could be detected in *ApoE/Sert*$^{-/-}$ animals, independently from animals' sex. A similar tendency was seen in *ApoE/Tph1*$^{-/-}$ females, but not in *ApoE/Tph1*$^{-/-}$ males.

5.2.5 Atherosclerotic Plaque Formation at Aortic Roots

For deeper analysis of atherosclerotic status and processes in the 45 weeks old animal groups, but as well in 100 weeks old males (B6, *Tph1*$^{-/-}$, *ApoE*$^{-/-}$and *ApoE/Tph1*$^{-/-}$), 10µm cryo slices of the aortic root region where generated and subsequently processed. In order to perform atherosclerotic plaque size analysis, histological Oil Red O (ORO) staining (**Fig. 15C**) was applied to one set of 10 slices per animal and from these the mean atherosclerotic plaque size was calculated and summarized in **Fig. 15A,B and D**.

Surprisingly, no statistically significant difference in between the genetic groups of 45 week old animals could be detected. However, the pattern of *ApoE/Sert*$^{-/-}$ exhibiting bigger atherosclerotic plaques than *ApoE/Tph1*$^{-/-}$ could again be observed by trend in samples of the aortic root (**Fig. 15A and B**), similarly to aortic arches (cf. **Fig. 14C and D**). Nevertheless, none of the double knockout groups appeared to have altered atherosclerotic plaque size in the aortic root region compared to *ApoE*$^{-/-}$. Interestingly, 45 week old males and females of all tested genetic groups developed atherosclerotic lesions of comparable size, only in *ApoE*$^{-/-}$ a sex difference could be found with females having significantly larger atherosclerotic plaques than males ($p \leq 0.01$, *Mann-Whitney-U* test, data not shown).

In 100 week old males no statistically significant alteration of atherosclerotic plaque size could be detected for *ApoE/Tph1*$^{-/-}$ compared to *ApoE*$^{-/-}$ (**Fig. 15D**). *ApoE/Sert*$^{-/-}$ males could not be examined because of too small sample size occurring naturally in this very advanced age. However, it could very clearly be demonstrated that B6 and *Tph1*$^{-/-}$ males do not develop atherosclerotic plaques of mentionable size, even at the age of 100 weeks (**Fig. 15D**). Hence, B6 and *Tph1*$^{-/-}$ control groups were no longer used for this project. 100 week old *ApoE*$^{-/-}$ and *ApoE/Tph1*$^{-/-}$ males were the only tested animal groups where calcification in atherosclerotic plaques could be observed occasionally (**Fig. 15C, arrow head**).

In summary, there were no drastic alterations in atherosclerotic plaque size in animals lacking peripheral 5-HT. Therefore, further analysis of atherosclerotic plaque composition, such as calcification, collagen and macrophage amount was performed.

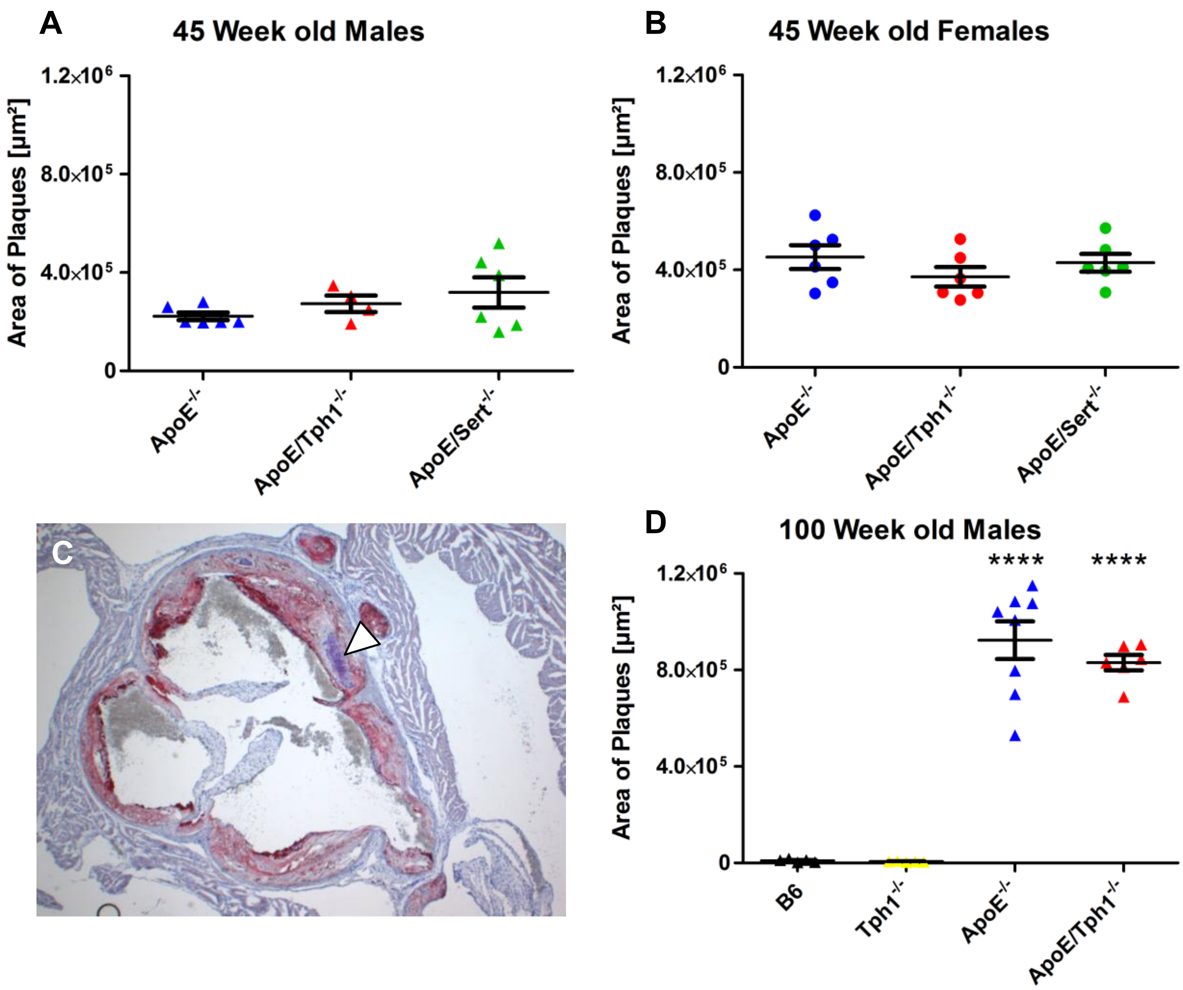

Fig. 15 – Atherosclerotic Plaques at Aortic Root in 45 and 100 Week old Animals
Mean total area of ORO stained atherosclerotic plaques, extrapolated from 10 cryo slices (10µm) of the aortic root (aortic valve area) per animal. Lines represent **Means**, error bars **SEM** of 45 week old males (▲, **A**), 45 week old females (●, **B**) and 100 week old males (▲, **C**). ****$p \leq 0.0001$; *One-way ANOVA* with *Tukey's Multiple Comparison* test. Representative 10µm cryo slice of a 100 week old *ApoE*$^{-/-}$ animal (**D**), red areas: atherosclerotic plaques, arrow head: purple stained calcification.

5.2.6 Aortic Calcification

The analysis of calcification in cryo slices of the aortic root region via Calcein staining (cf. Fig. 16A – C) failed due to issues during tissue processing caused by the physical characteristics of calcified atherosclerotic plaques. A more promising technique was the colorimetric calcium assay, which was performed in aortic arches and thoracic aorta of 45 week old *ApoE*$^{-/-}$, *ApoE/Tph1*$^{-/-}$ and *ApoE/Sert*$^{-/-}$ mice; results are illustrated in Fig. 16D and E.

Remarkably, calcification could not be detected in *ApoE*$^{-/-}$and *ApoE/Tph1*$^{-/-}$ males and in the majority of *ApoE/Sert*$^{-/-}$ males (Fig. 16D). In females, calcification in aortic plaques occurred more often with highest values in *ApoE*$^{-/-}$ and *ApoE/Tph1*$^{-/-}$ (Fig. 16E). In *ApoE/Sert*$^{-/-}$ females, calcification was significantly lower than in *ApoE/Tph1*$^{-/-}$ females (Fig. 16E).

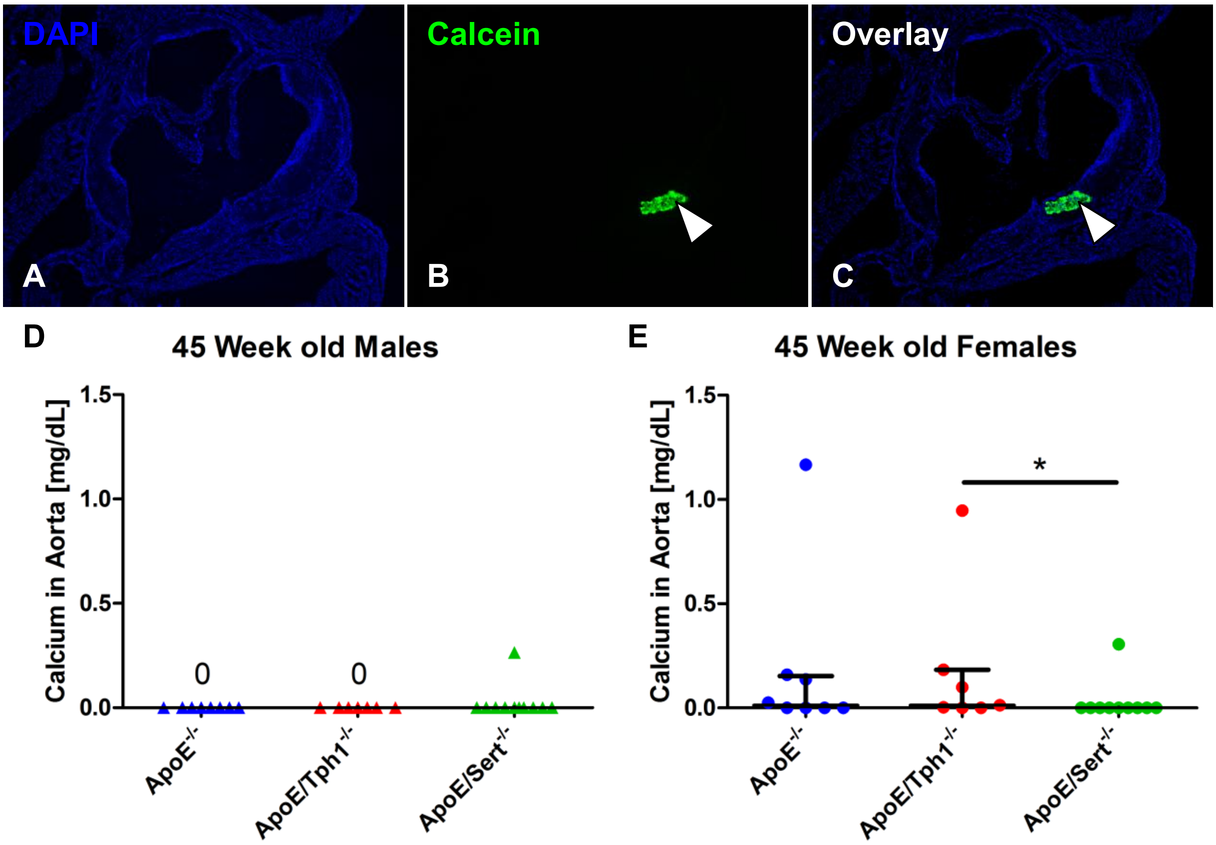

Fig. 16 – Calcification in 45 Week old Double Knockout Animals
A – C: Representative example of fluorescent Calcein staining in 10µm aortic root slices of a 100 week old *ApoE*$^{-/-}$ male with **blue cell nuclei (DAPI)** and **green calcification (Calcein)**. Arrow head: location of calcification inside of atherosclerotic plaque. (Images are only illustrative and were not used for any data analysis.) **D and E:** Total calcium amounts in aortic arches of males (**D**) and females (**F**) measured via photometric assay. Lines indicate **medians**, error bars indicate **IQR**. In some groups calcium could not be detected at all (0), hence, statistical analysis could not be performed. *p≤0.05; single *Mann-Whitney-U* test.

5.2.7 Collagen Fibers and Macrophages

For the composition of atherosclerotic plaques two intraintimal compartments are of importance: First, the amount of collagen fibers, which play a major role in the atherosclerotic plaque stability and can be detected via image analysis of Masson's trichrome stained samples. And second, the quantity of macrophages, which are known to accumulate inside of atherosclerotic plaques and can be immunohistochemically flagged and analyzed. Both types of examination were performed in sets of 5 cryo slices per animal in males and females of *ApoE*$^{-/-}$, *ApoE/Tph1*$^{-/-}$ and *ApoE/Sert*$^{-/-}$; results are summarized in Fig. 18 and Fig. 17.

Analysis of Masson's trichrome stained 10µm cryo slices (Fig. 18A) revealed that mean relative collagen amounts of atherosclerotic plaques in male *ApoE*$^{-/-}$ (58.7%) and *ApoE/Sert*$^{-/-}$ (60.8%) mice are quite similar, whereas male *ApoE/Tph1*$^{-/-}$ (69.6%) tend to exhibit relatively more collagen inside their plaques. This observation could not be statistically proven (Fig. 18B).

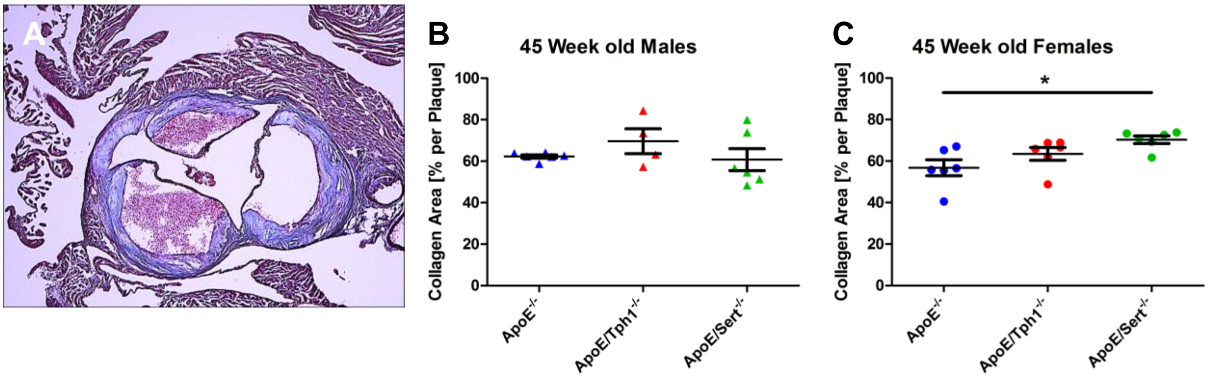

Fig. 18 – Collagen in Atherosclerotic Plaques of 45 Week old Double Knockout Animals
Representative 10µm slice (aortic root) of an *ApoE/Sert*$^{-/-}$ female stained via Masson's trichrome protocol (**A**). **Collagen** is stained in blue. Mean relative collagen amount per plaque area in males (**B**) and females (**C**); extrapolated from set of 5 slices for each animal. Lines and error bars represent means and SEM. *p≤0.05; *One-way ANOVA* with *Tukey's Multiple Comparison* test.

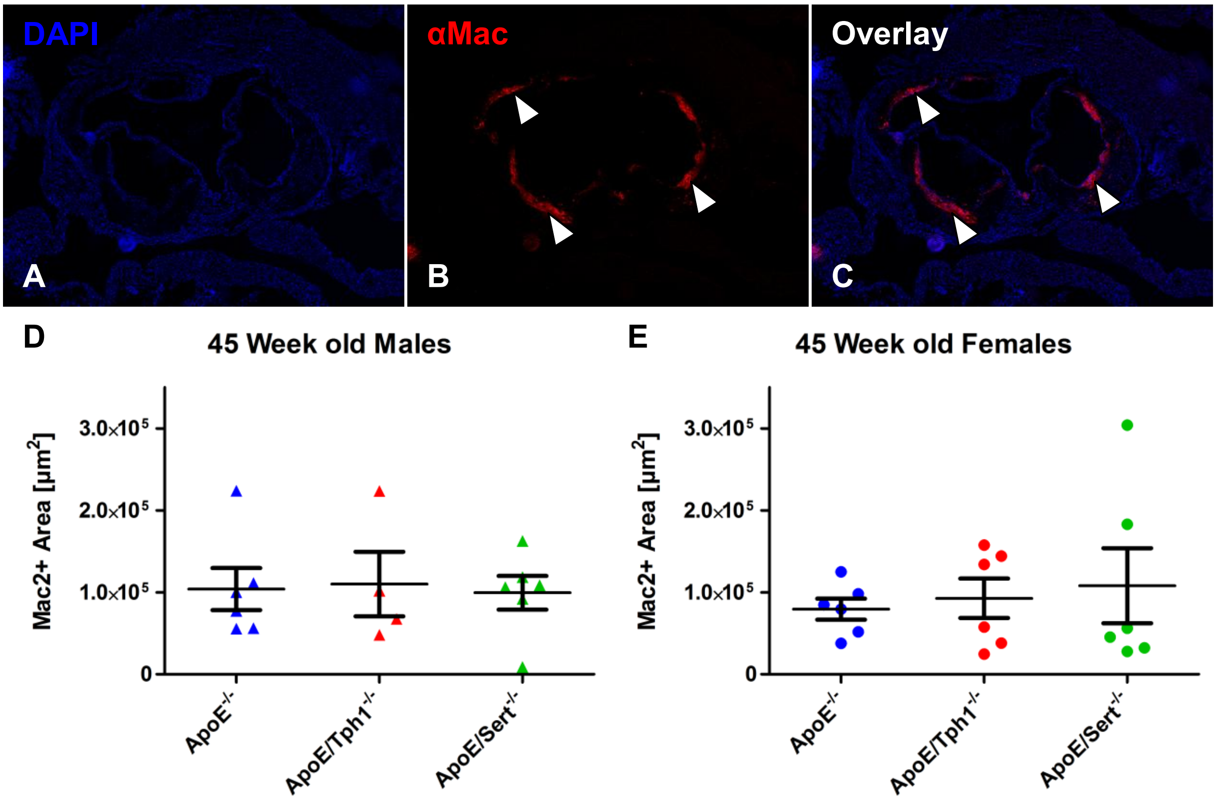

Fig. 17 – Macrophages in Atherosclerotic Plaques of 45 Week old Double Knockout Animals
A - C: Representative 10µm slice (aortic root) of an *ApoE/Sert*$^{-/-}$ female immunohistochemically stained against macrophages (αMac2) with **blue cell nuclei (DAPI)** and **red macrophages**. Arrow heads point at intraintimal macrophage areas. **D + E:** Quantification of total intraintimal macrophage area from 5 specimens per animal for males (▲) and females (●). Lines and error bars indicate **Means** and **SEM**.

In females, *ApoE*$^{-/-}$ (55.5%) appeared to have similar relative collagen amounts as observed in males of the same genotype. The mean relative collagen amount in *ApoE/Tph1*$^{-/-}$ females tended to be elevated (62.0%) and was significantly increased in *ApoE/Sert*$^{-/-}$ females (69.3%; Fig. 18C).

Immunohistochemical staining of 10µm cryo slices of the aortic root region with an antibody binding to macrophages (αMac2, see Fig. 17A - C) and the subsequent analysis of the total amount of Mac2 positive area in 5 slices per animal showed that there are no statistically significant alterations in macrophage amount or distribution inside the atherosclerotic plaques in any of the tested genetic animal groups (**Fig. 17D and E**).

Concluding, analysis of atherosclerotic plaque composition in aortic root cryo slices of *ApoE*$^{-/-}$, *ApoE/Tph1*$^{-/-}$ and *ApoE/Sert*$^{-/-}$ animals could not definitely answer the question for an effect of peripheral 5-HT absence on atherosclerotic processes. However, as reported for the majority of the described experiments in 45 week old double knockout animals, the *ApoE/Sert*$^{-/-}$ group tended to stand out from the other groups with regard to plaque composition and was shown to have higher levels of intraintimal collagen.

5.3 Physiological Alterations in *ApoE/Tph1*$^{-/-}$ Animals after Long-term Western Diet

The Western or High Fat/High Cholesterol diet (WD) enables the experimenter to artificially induce hypercholesterolemia and atherosclerosis in animals at a relatively young age and in a very quick way – first atherosclerotic lesions are detectable after 4 weeks of diet. For this project, young (10 week old) male and female *ApoE*$^{-/-}$and *ApoE/Tph1*$^{-/-}$ mice got fed Western diet for either 8 or 12 weeks. Physiological changes, especially atherosclerotic processes, were analyzed in tissues of these animals and in 22 week old control groups.

5.3.1 Bodyweight, Body Fat and Blood Glucose Levels

Total bodyweight of all animals was documented before and after 8 respectively 12 weeks of WD. Furthermore, animals of all groups underwent body composition analysis (BCA) via non-invasive *Time-Domain-Nuclear-Magnetic-Resonance* imaging (TD-NMR) after 8 and after 12 weeks of WD, shortly before the end of the respective experiment. Blood glucose levels were detected in overnight fasted animals. All results are summarized in Fig. 19, Fig. 20 and Fig. 21.

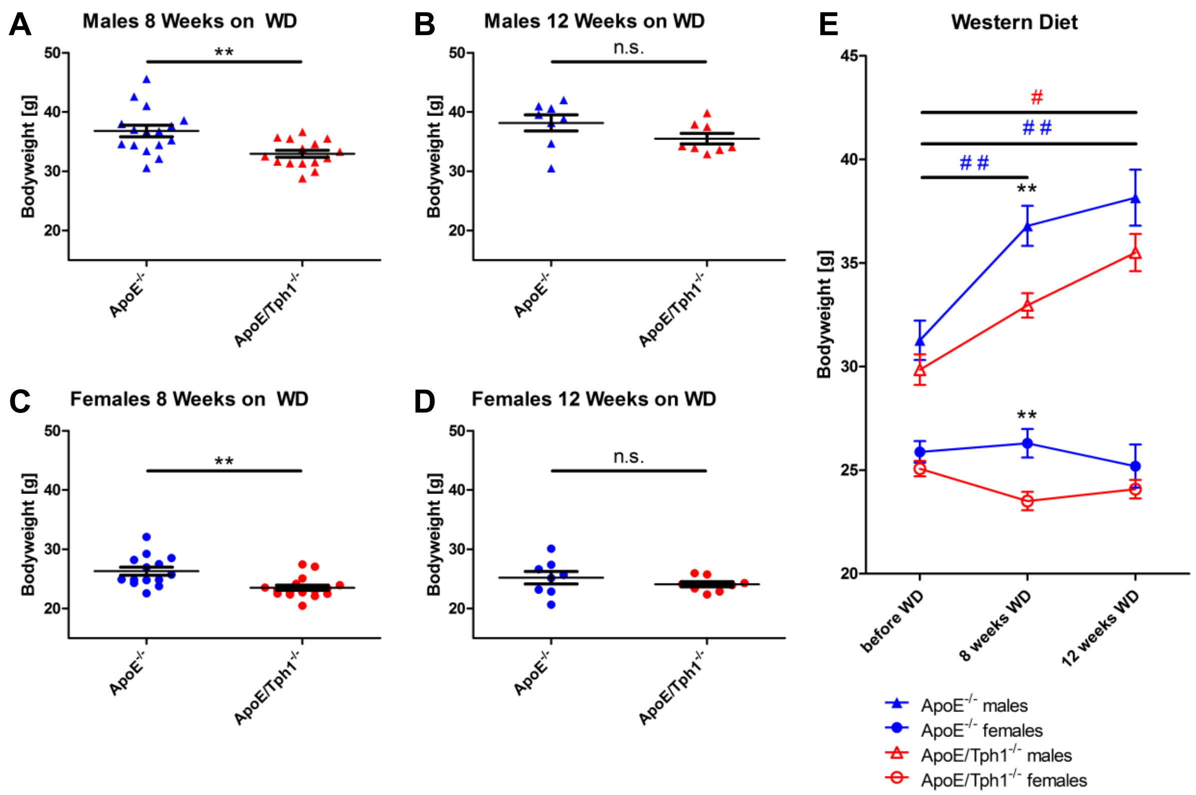

Fig. 19 – Bodyweight in *ApoE/Tph1*$^{-/-}$ animals after 8 and 12 Weeks of Western Diet
Graphical representation of mean bodyweight in male and female *ApoE/Tph1*$^{-/-}$ mice after 8 (**A** and **C**) and 12 weeks (**B** and **D**) of Western diet (WD), compared to age matched *ApoE*$^{-/-}$ controls. Lines indicate means, error bars SEM; **p≤0.01; n.s.: not significant; unpaired t-test. **E:** One-graph comparison of all tested animal groups before and after 8 and 12 weeks of WD. Closed icons represent *ApoE*$^{-/-}$; open icons represent *ApoE/Tph1*$^{-/-}$; **p≤0.01 vs. *ApoE*$^{-/-}$ (same sex);); #p≤0.05; ##p≤0.01 vs. 'before WD'; *One-way ANOVA* with *Tukey's Multiple Comparison* test.

Results of the bodyweight measurements clearly showed that in both sexes the 5-HT lacking *ApoE/Tph1*$^{-/-}$ group was significantly lighter after 8 weeks of WD compared to *ApoE*$^{-/-}$ (**Fig. 19A and C**). Interestingly, this effect was only observed by trend after 12 weeks of WD in both sexes (**Fig. 19B and D**). The summary of all tested groups before and after 8 and 12 weeks of WD revealed that males significantly gain bodyweight under WD, whereas females are about to keep their initial bodyweight (**Fig. 19E**).

The body composition analysis (BCA) in WD treated *ApoE*$^{-/-}$ and *ApoE/Tph1*$^{-/-}$ mice showed that in all tested animal groups relative body fat (**Fig. 20A – D**) and water (**Fig. 20E – H**) amounts are reduced in *ApoE/Tph1*$^{-/-}$ mice, whereas relative muscle portion (**Fig. 20I - L**) appeared to be higher in *ApoE/Tph1*$^{-/-}$ compared to *ApoE*$^{-/-}$. Surprisingly, the described effects where stronger in both sexes after 8 weeks of WD than after 12, but could only be statistically confirmed by trend for *ApoE/Tph1*$^{-/-}$ females after 8 weeks of WD (**Fig. 20C and G**). One more finding that should be highlighted at this point is the tendency of females exhibiting relatively less body fat (p=0.1; unpaired t-test; females 8 weeks vs. 12 weeks; data not shown) and relatively more muscles (p=0.06; unpaired t-test; females 8 weeks vs. 12 weeks; data not shown) after 12 than after 8 weeks of WD. In males, the opposite effect was observed (cf. **Fig. 20B and D** and **Fig. 20F and H**).

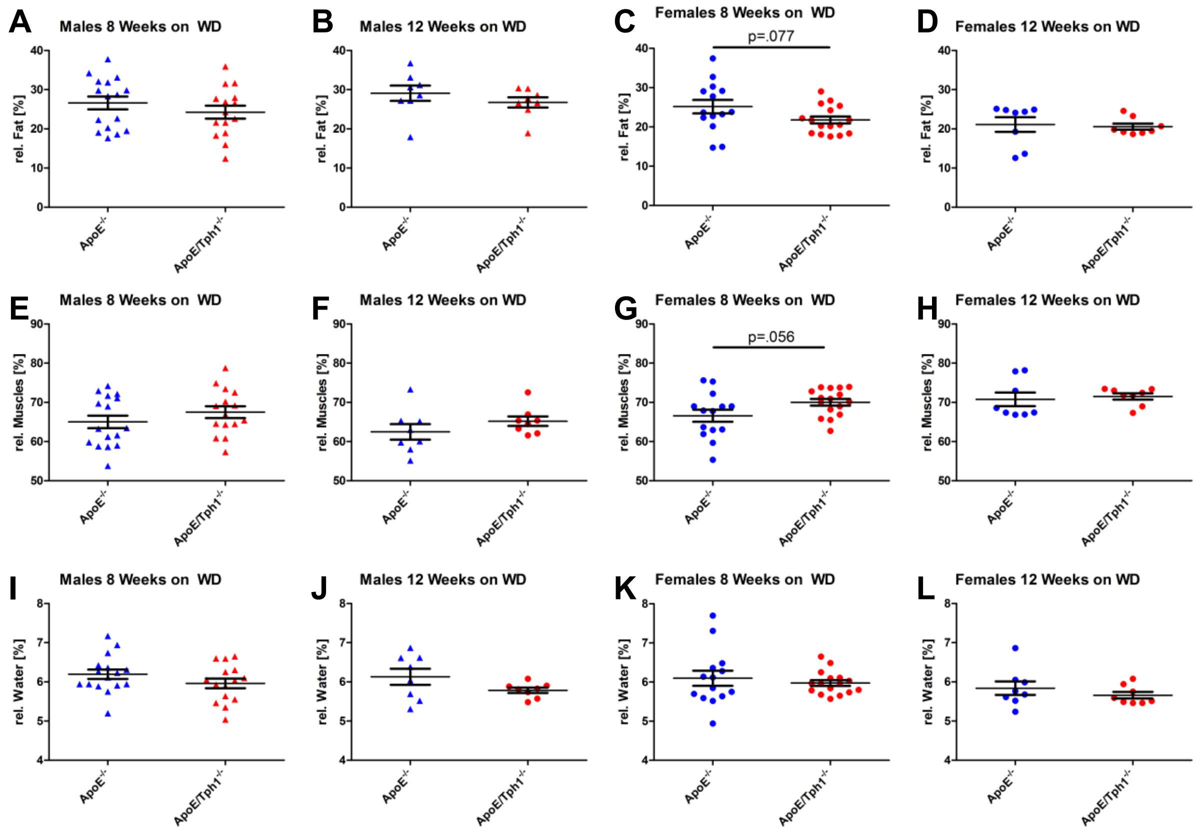

Fig. 20 – Body Composition Analysis in *ApoE/Tph1*$^{-/-}$ animals after 8 and 12 Weeks of Western Diet
Results of the body composition analysis in all groups after 8 and 12 weeks of WD. **A – D: Means** and **SEM** of relative body fat amount; **E – H: Means** and **SEM** of relative amount of muscles; **I – L: Means** and **SEM** of relative water amount. All groups were statistically tested *ApoE*$^{-/-}$ vs. *ApoE/Tph1*$^{-/-}$ via *unpaired t-test*, trends are indicated by p values.

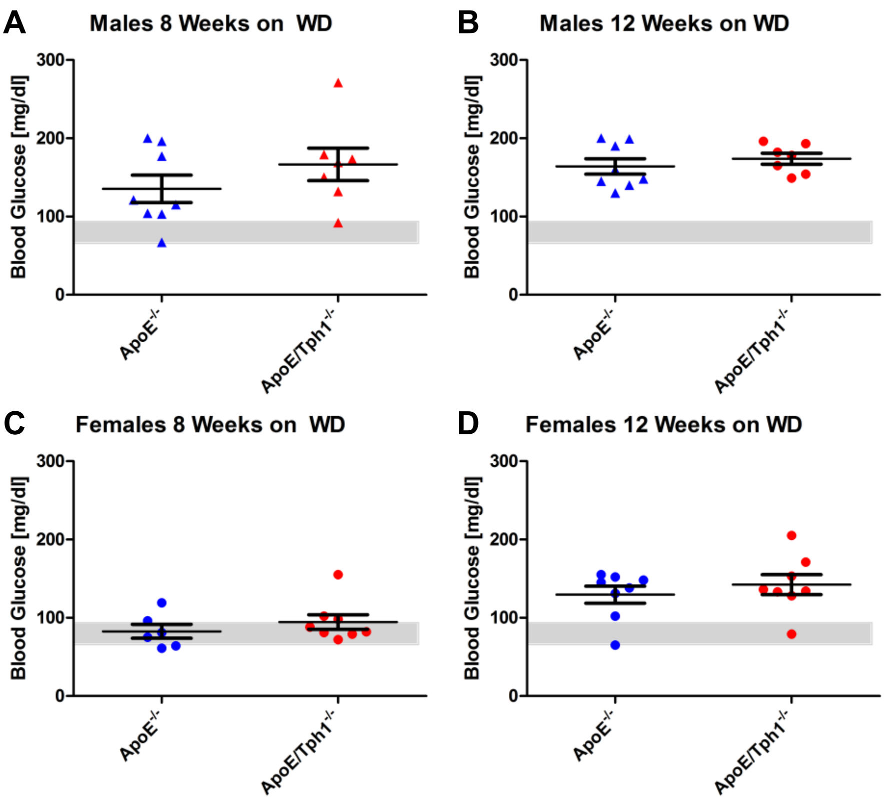

Fig. 21 – Blood Glucose in *ApoE/Tph1*$^{-/-}$ animals after 8 and 12 Weeks of Western Diet Fasted blood glucose levels in males (**A** and **B**) and females (**C** and **D**) after 8 and 12 weeks of WD. Lines indicate **Means**, error bars **SEM**. Grey area: normal blood glucose range for fasted B6 animals.

Data indicate that in all tested groups (except females after 8 weeks) the mean fasted blood glucose level after WD is increased over normal B6 range. Interestingly, *ApoE/Tph1*$^{-/-}$ animals of all groups exhibited slightly but not significantly higher blood glucose levels than *ApoE*$^{-/-}$ controls (Fig. 21). Comparing both experiments with each other showed that females of both genotypes had higher blood glucose levels after 12 weeks of WD than after 8 weeks ($p \leq 0.05$; *One-way ANOVA* with *Tukey's Multiple Comparison* test).

5.3.2 Plasma Cholesterol and Triglycerides

Photometric detection of cholesterol in the plasma of *ApoE*$^{-/-}$ and *ApoE/Tph1*$^{-/-}$ animals after WD and in age matched control groups of same genotypes, revealed that, as expected, plasma cholesterol was drastically increased in animals lacking ApoE, compared to normal B6 levels (Fig. 22A - D). Plasma triglycerides in the same animal groups were shown to be approximately at normal B6 levels (Fig. 22E - H).

Furthermore, it could be statistically proven that 12 weeks of WD caused elevated plasma cholesterol values in all treated animal groups similarly, when compared to untreated animals of the same genotype (Fig. 22B and D). Contrasting, levels of plasma triglycerides appeared to be decreased by trend after 12 weeks of WD, compared to untreated mice (Fig. 22F and H).

In *ApoE/Tph1*$^{-/-}$ animals of both sexes it could be shown that after 8 weeks of WD, plasma cholesterol is decreased by trend (Fig. 22A and C) and also plasma triglycerides are significantly lower than in *ApoE*$^{-/-}$ mice (Fig. 22E and G).

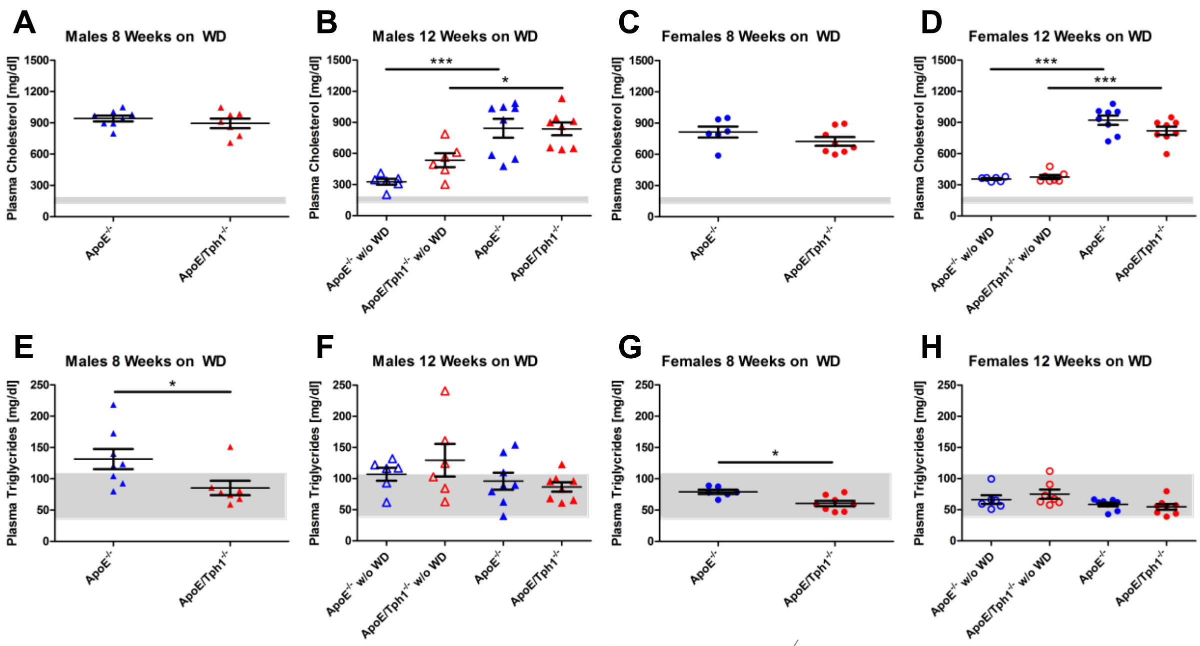

Fig. 22 – Plasma Cholesterol and Triglycerides in *ApoE/Tph1*$^{-/-}$ animals after 8 and 12 Weeks of Western Diet

Photometrically measured total amounts of cholesterol (**A – D**) and triglycerides (**E – H**) in plasma of *ApoE*$^{-/-}$and *ApoE/Tph1*$^{-/-}$ male (▲) and female (●) mice after 8 and 12 weeks of WD. Graphs for animals after 12 weeks of WD additionally contain data from 22 week old control groups which did not obtain WD (open icons). Lines indicate **means**, error bars represent **SEM**. Grey area depicts normal ranges of plasma cholesterol (118 – 164 mg/dl) and triglycerides (37 – 109 mg/dl). *p≤0.05; ***p≤0.001; *One-way ANOVA* with *Tukey's Multiple Comparison* test.

5.3.3 Hepatic Cholesterol

Colorimetric quantification in liver extracts from *ApoE*$^{-/-}$ and *ApoE/Tph1*$^{-/-}$ animals after 8 and 12 weeks of WD suggested that there is a trend for *ApoE/Tph1*$^{-/-}$ to develop lower hepatic cholesterol levels than *ApoE*$^{-/-}$ animals (Fig. 23A - D).

Very interestingly, females of both genotypes exhibited drastically increased hepatic cholesterol levels after 8 weeks of WD compared to all other experimental groups (p≤0.001; *One-way ANOVA* with *Tukey's Multiple Comparison* test), including females after 12 weeks of WD (Fig. 23C).

5.3.4 Hepatic Triglyceride, Non-esterified Free Fatty Acid and Total Lipid Levels

Data from different colorimetric assays revealed that a general trend for decreased hepatic lipid parameters is visible in male *ApoE/Tph1*$^{-/-}$ mice after 12 weeks of WD and in females *ApoE/Tph1*$^{-/-}$ mice after 8 weeks of WD (Fig. 23B + C; F + G; J + K and N + O).

In detail, the presented data show that while hepatic triglycerides could be detected at similar levels for *ApoE*$^{-/-}$ and *ApoE/Tph1*$^{-/-}$ males after 8 weeks of WD (Fig. 23E) and for *ApoE*$^{-/-}$ and *ApoE/Tph1*$^{-/-}$ females after 12 weeks of WD (Fig. 23H), they are significantly lower in *ApoE/Tph1*$^{-/-}$ males after 12 weeks of WD (Fig. 23F).

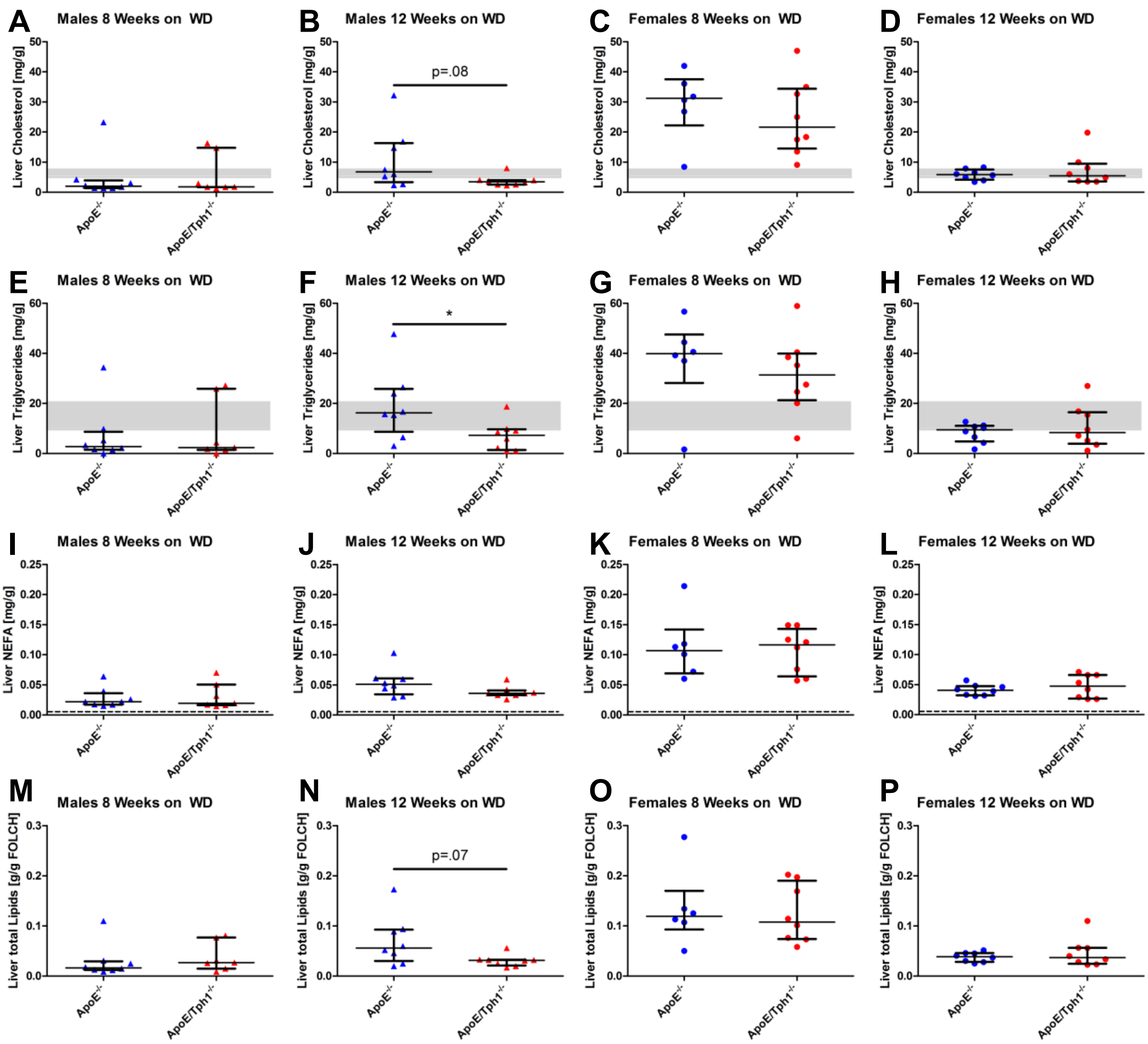

Fig. 23 – Hepatic Cholesterol, Triglycerides, NEFA and Total Lipids in *ApoE/Tph1$^{-/-}$* animals after 8 and 12 Weeks of Western Diet
Results of enzyme-linked colorimetric measurements for cholesterol (**A - D**), triglycerides (**E – H**), NEFA (non-esterified fatty acids) (**I – L**) and total lipids (**M – P**) in extracts from *ApoE$^{-/-}$* and *ApoE/Tph1$^{-/-}$* livers. Lines represent **medians**, error bars depict **IQR**. *p≤0.05; *Mann-Whitney-U* test; trends are indicated by respective p values. Grey areas/dashed lines represent physiological ranges of respective substance in healthy wild type (B6) liver if applicable.

The same was shown for hepatic not esterified free fatty acids (NEFA): Equal levels in livers of *ApoE$^{-/-}$* and *ApoE/Tph1$^{-/-}$* males after 8 weeks of WD (Fig. 23I) and for *ApoE$^{-/-}$* and *ApoE/Tph1$^{-/-}$* females after 12 weeks of WD (Fig. 23L) and slightly, statistically not provable, decreased NEFA levels in *ApoE/Tph1$^{-/-}$* males after 12 weeks of WD (Fig. 23J).

The amount of total lipids after Folch's extraction from liver was comparable in *ApoE$^{-/-}$* and *ApoE/Tph1$^{-/-}$* males after 8 weeks of WD (Fig. 23M) and in *ApoE$^{-/-}$* and *ApoE/Tph1$^{-/-}$* females after 12 weeks of WD (Fig. 23P). However, total hepatic lipids in *ApoE/Tph1$^{-/-}$* males after 12 weeks of WD tended to be decreased compared to *ApoE$^{-/-}$* (Fig. 23N).

A noticeable effect that occurred during all executed enzyme-linked colorimetric analyses in liver extracts was the clearly visible tendency of both female groups after 8 weeks of WD to have drastically increased liver parameters than animals from all other experimental groups: As mentioned, *ApoE*$^{-/-}$ and *ApoE/Tph1*$^{-/-}$ females after 8 weeks of WD were shown to have elevated hepatic cholesterol (**Fig. 23C**; p=0.0005; *Mann-Whitney-U* test; females 8 weeks vs. females 12 weeks), but also hepatic triglycerides (**Fig. 23G**; p<0.0001; *Mann-Whitney-U* test; females 8 weeks vs. females 12 weeks), NEFA (**Fig. 23K**; p<0.0001; *Mann-Whitney-U* test; females 8 weeks vs. females 12 weeks) and total lipids after Folch's extraction (**Fig. 23O**). Except from NEFA, those parameters were all shown to be slightly lower in *ApoE/Tph1*$^{-/-}$ females than in *ApoE*$^{-/-}$.

5.3.5 Liver Weight and Plasma Liver Parameters

Also in WD treated animals, the liver status was examined via relative liver weight documentation and measurement of plasma AST and ALT and the resulting *De Ritis* quotient (AST/ALT; normal value for B6: 2) to determine to what extend the long term WD administration affects liver health in *ApoE*$^{-/-}$ and *ApoE/Tph1*$^{-/-}$ mice. The results are summarized in **Fig. 24**.

It could be shown that independently from sex or WD duration, *ApoE/Tph1*$^{-/-}$ animals tend to exhibit lower relative liver weight than *ApoE*$^{-/-}$ (**Fig. 24A - D**). This effect was even significant in *ApoE/Tph1*$^{-/-}$ females after 12 weeks of WD (**Fig. 24D**).

The liver parameter AST was elevated above normal B6 values in nearly all tested groups after WD and reached highest levels in *ApoE*$^{-/-}$ males after 8 weeks of WD (**Fig. 24E**). Interestingly, *ApoE/Tph1*$^{-/-}$ males and females after 12 weeks of WD had approximately normal AST levels, while levels in both *ApoE*$^{-/-}$ groups were comparably higher (**Fig. 24F and H**).

ALT levels were similarly elevated above normal range in almost all tested groups after WD (**Fig. 24I - L**), but again, after 12 weeks of WD, male and female *ApoE/Tph1*$^{-/-}$ mice appeared to have plasma ALT at normal levels (**Fig. 24J and L**). Generally, there was a tendency of *ApoE/Tph1*$^{-/-}$ to have lower plasma ALT than *ApoE*$^{-/-}$ (**Fig. 24J**).

Calculation of the *De Ritis* quotient, a marker for liver damage if raised above a value of 2 (**Fig. 24M – P**, dashed lines), revealed that animals of all groups had AST/ALT ratios very close to normal level. However, after 8 weeks of WD, mean *De Ritis* quotients in *ApoE*$^{-/-}$ males and females were slightly increased: Males at 2.13, females at 2.31, whereas levels in *ApoE/Tph1*$^{-/-}$ animals of both sexes appeared to be normal (**Fig. 24M and O**). Interestingly, in *ApoE*$^{-/-}$ males after 12 weeks of WD the *De Ritis* quotient was with 1.71 slightly lower than normal (**Fig. 24N**).

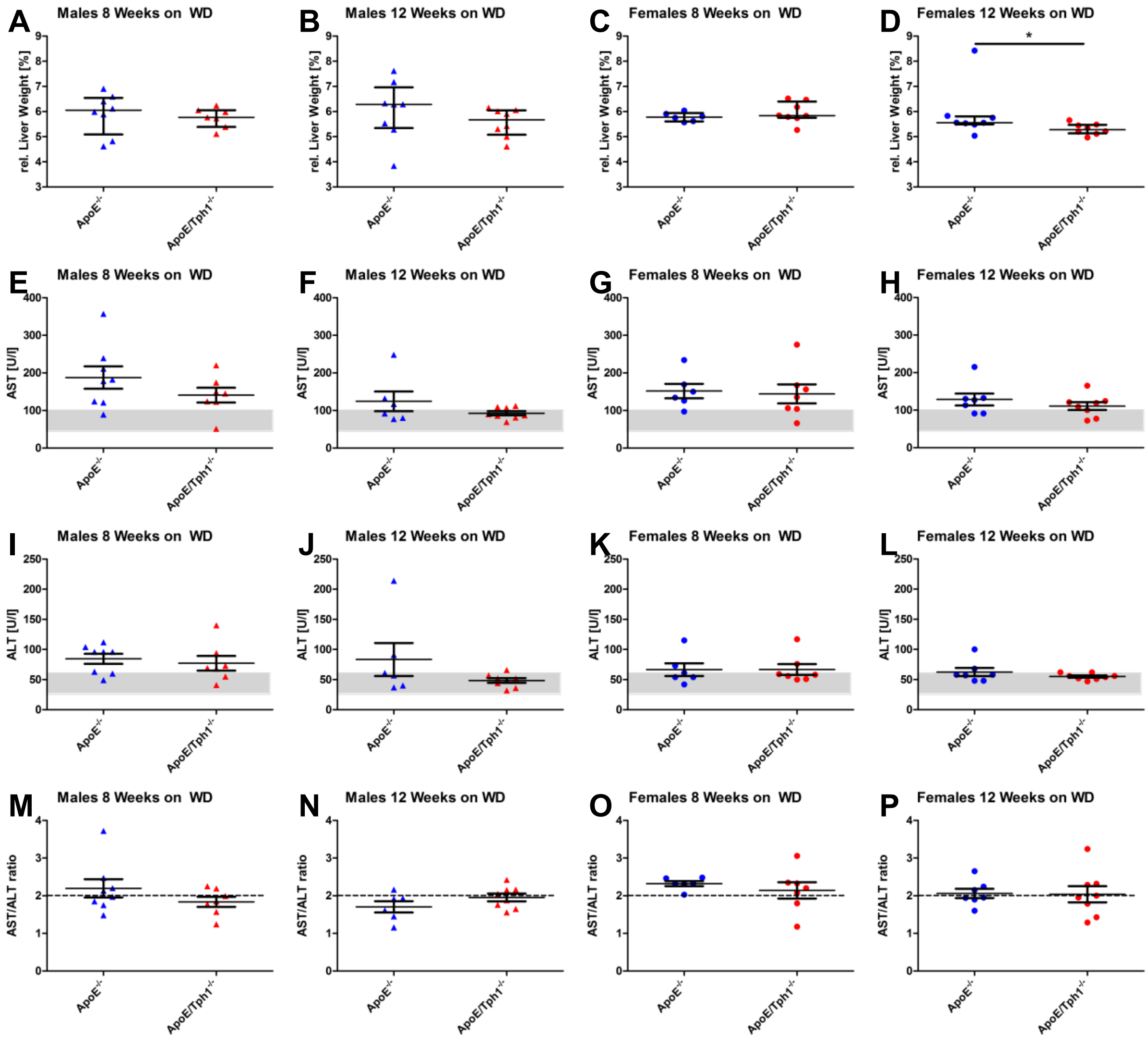

Fig. 24 – Liver Status in *ApoE/Tph1*$^{-/-}$ animals after 8 and 12 Weeks of Western Diet
Relative liver weight (**A - D**) and liver enzymes AST (**E - H**), ALT (**I - L**) and AST/ALT ratio (*De Ritis* quotient; **M - P**) measured photometrically in plasma of male (▲) and female (●) mice. **A – D:** Lines represent **medians**, error bars show **IQR**; **E – P:** Lines and error bars represent **means** ± **SEM**; grey areas in A - L and dashed line in M - P represent normal levels in B6 mice. **A – D:** *p≤0.05; *Mann-Whitney-U* test.

5.3.6 Aortic Plaque Development under Long-term Western Diet

Relative size of atherosclerotic plaques and their distribution along the vessel compartment was analyzed via ORO staining with subsequent en face preparation of equally dissected fragments of aortic arches and thoracic aorta (entire aortic arch plus exactly 15mm after the bifurcation of *arteria subclavia*). Results from microscopic image analysis of aortic plaque size are illustrated in Fig. 25.

After 8 weeks of WD, there was no obvious difference in aortic plaque size between *ApoE*$^{-/-}$ and *ApoE/Tph1*$^{-/-}$ males (Fig. 25A).

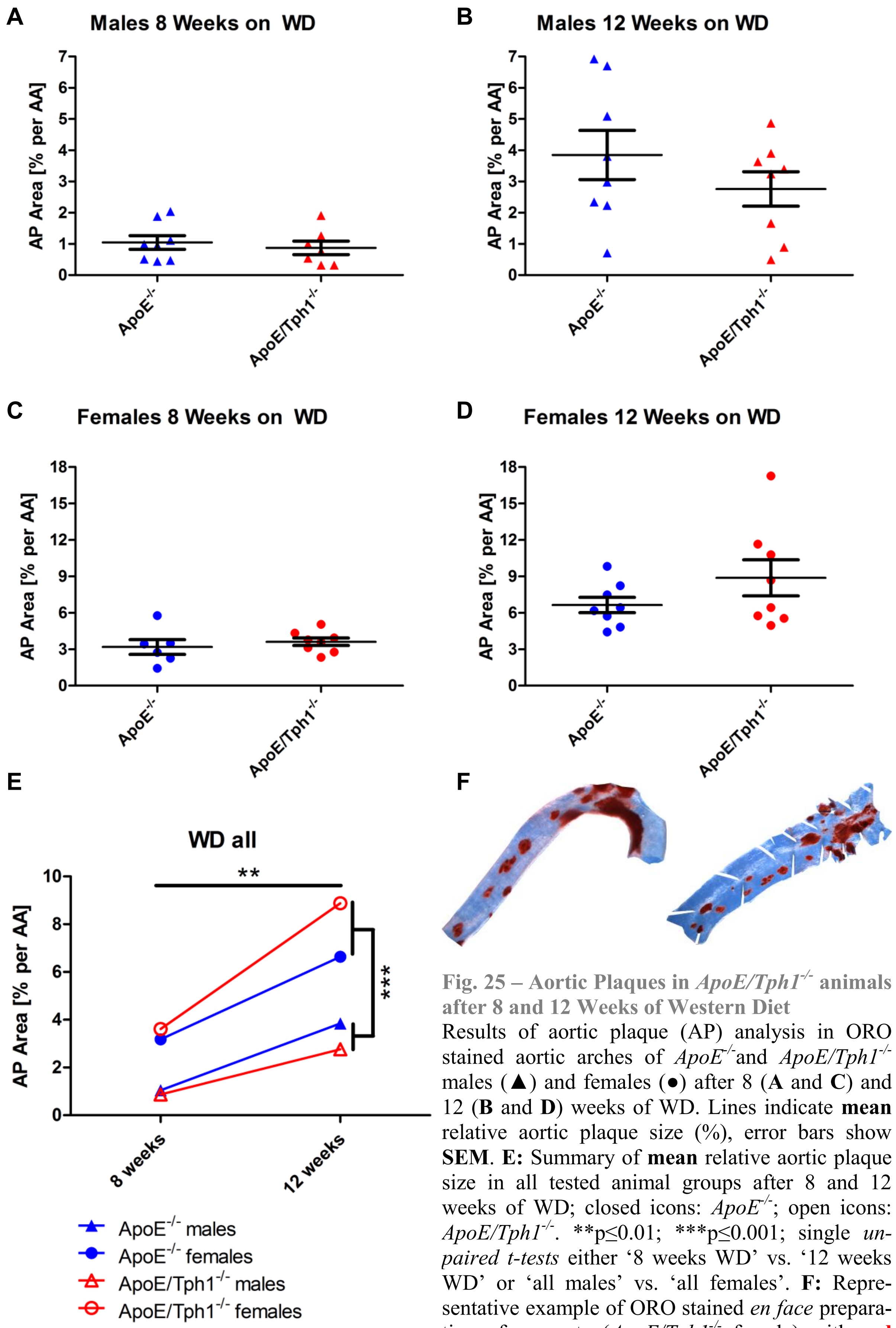

Fig. 25 – Aortic Plaques in *ApoE/Tph1*$^{-/-}$ animals after 8 and 12 Weeks of Western Diet

Results of aortic plaque (AP) analysis in ORO stained aortic arches of *ApoE*$^{-/-}$and *ApoE/Tph1*$^{-/-}$ males (▲) and females (●) after 8 (**A** and **C**) and 12 (**B** and **D**) weeks of WD. Lines indicate **mean** relative aortic plaque size (%), error bars show **SEM**. **E:** Summary of **mean** relative aortic plaque size in all tested animal groups after 8 and 12 weeks of WD; closed icons: *ApoE*$^{-/-}$; open icons: *ApoE/Tph1*$^{-/-}$. **p≤0.01; ***p≤0.001; single *unpaired t-tests* either '8 weeks WD' vs. '12 weeks WD' or 'all males' vs. 'all females'. **F:** Representative example of ORO stained *en face* preparation of an aorta (*ApoE/Tph1*$^{-/-}$ female) with **red** atherosclerotic plaques.

However, after 12 weeks of WD, the relative size of aortic plaques was increased in both genotypes compared to the 8 week groups, but apparently to a slightly lower extend in *ApoE/Tph1*$^{-/-}$ males (p=0.28; **Fig. 25B**). Due to large data variation, this effect could not be statistically proven.

In females, the mean aortic plaque size was at similar levels in *ApoE*$^{-/-}$ and *ApoE/Tph1*$^{-/-}$ after 8 weeks of WD (**Fig. 25C**). Also, both tested female groups developed larger aortic plaques after 12 weeks of WD compared to the 8 week groups, but surprisingly, *ApoE/Tph1*$^{-/-}$ females tended to have an increased relative aortic plaque size compared to *ApoE*$^{-/-}$ (p=0.19; **Fig. 25D**). This finding contrasts with the results from male *ApoE/Tph1*$^{-/-}$ mice after 12 weeks of WD.

Generally, all tested animal groups exhibited significantly larger aortic plaques after 12 weeks of WD than after 8 weeks (**Fig. 25E**) and females of both genotypes were proven to develop highly significantly larger aortic plaques than males (**Fig. 25E**).

Atherosclerotic plaques appeared to be similarly distributed along the analyzed compartments of aortic arch and thoracic aorta of both, males and females of both tested genotypes and after 8 and 12 weeks of WD: The majority of plaques was located at the aortic arch (up to 90%) and scattered small plaques could be detected at the thoracic aorta (exemplified in **Fig. 25F**).

5.3.7 Aortic Calcification after Western Diet

Photometric examination of calcium amounts in extracts from aortas showed that calcium accumulation in aortic plaques appears only very rarely in *ApoE*$^{-/-}$ and *ApoE/Tph1*$^{-/-}$ animals after WD (**Fig. 26**). The only experimental groups in which some animals developed markedly calcification were males after 12 weeks of WD (**Fig. 26B**). Out of 29 tested female mice, there was only one exhibiting a measurable calcium amount in extract of the aorta (**Fig. 26C and D**).

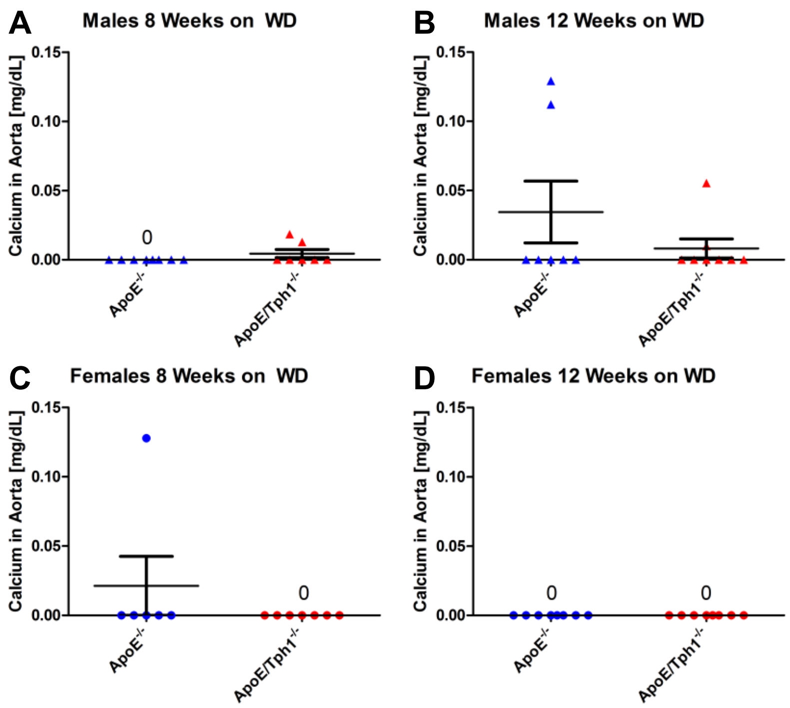

Fig. 26 – Calcification in *ApoE/Tph1*$^{-/-}$ animals after 8 and 12 Weeks of Western Diet
Total calcium amounts in aortic arches of males (**A** and **B**) and females (**C** and **D**) measured via photometric assay in aortic extracts. Lines indicate **means**, error bars indicate **SEM**. In some groups calcium could not be detected at all (0), hence, statistical analysis could not be performed.

5.4 Conclusion of Results

There are three major results of this study:

First, it could clearly be shown that some 5-HT receptors are differently distributed in vessels of B6 and FVB/N animals and hence, in *Tph1* deficient animals generated in these background strains. This was convincingly shown for 5-HT receptor subtypes 1B and 2A in aorta: 5-HTr 1B RNA expression was 2-fold increased in FVB/N and even more than 3-fold increased in *B6/Tph1*$^{-/-}$ animals compared to B6. 5-HTr 2A RNA expression was decreased in FVB/N, but increased in *B6/Tph1*$^{-/-}$ compared to B6 (see **Tab. 6**).

Second, in 45 week old *ApoE* deficient animals, it could be demonstrated that *Tph1* deficiency results in significantly decreased bodyweight, plasma cholesterol and AST levels and significantly increased relative liver weight, whereas *Sert* deficiency causes significant increases in blood glucose, plasma cholesterol, atherosclerotic plaque size in aortas and collagen amounts in atherosclerotic plaques. The majority of these effects appear to have a sex dependent compound (see **Tab. 6**).

And third, in *ApoE/Tph1*$^{-/-}$ animals after long term Western Diet, it was shown that bodyweight was significantly reduced, plasma and hepatic cholesterol as well as hepatic triglyceride and total lipid levels were significantly lower, and relative liver weight was also significantly reduced in comparison to *ApoE*$^{-/-}$ mice (see **Tab. 6**). Sex differences, including contrasting non-significant trends for reduced atherosclerotic plaque size in *ApoE/Tph1*$^{-/-}$ males and increased atherosclerotic plaque size in *ApoE/Tph1*$^{-/-}$ females, were detected in these groups as well.

Tab. 6 – Summary of Complete Study Results

Overview of all results, gained from the present study. Male *Tph1*$^{-/-}$ mice are described with either a higher (↑) or lower (↓) relative RNA expression of the respective receptor, compared to B6 or FVB/N males. Male and female *ApoE/Tph1*$^{-/-}$ and *ApoE/Sert*$^{-/-}$ mice are described with either an increase/higher level of the examined feature (↑ or (↑) in case of weak effects), a decrease/lower level of the examined feature (↑ or (↑) in case of weak effects) or an equality of the examined feature (-) in comparison to the respective *ApoE*$^{-/-}$ group. Missing data are indicated with n.a. (not applicable).

	Males		**Females**	
	Tph1$^{-/-}$			
Expression in Aorta:				
5-HTr 1B	↑(B6), ↓(FVB/N)		n.a.	
5-HTr 1D	↓(B6), ↑(FVB/N)		n.a.	
5-HTr 2A	↑(B6), ↑(FVB/N)		n.a.	
5-HTr 2B	↓(B6), ↓(FVB/N)		n.a.	
45 Week old Animals:	***ApoE/Tph1***$^{-/-}$	***ApoE/Sert***$^{-/-}$	***ApoE/Tph1***$^{-/-}$	***ApoE/Sert***$^{-/-}$
Bodyweight	↓	(↓)	(↓)	(↑)
Blood Glucose	(↑)	↑	(↑)	-
Plasma Cholesterol	-	↑	↓	-
Plasma Triglycerides	(↓)	(↑)	(↓)	(↑)
Rel. Liver Weight	-	-	↑	-
AST	(↓)	(↓)	↓	n.a.
ALT	(↑)	(↓)	-	n.a.
De Ritis Quotient	(↓)	(↓)	(↓)	n.a.
Aortic Plaques	(↓)	(↑)	(↑)	↑
Plaques Aortic Root	(↑)	(↑)	(↓)	-
Calcification	-	-	-	(↓)
Plaque Collagen	(↑)	-	(↑)	↑
Plaque Macrophages	-	-	-	(↑)
After long term WD:				
Bodyweight	↓	n.a.	↓	n.a.
Blood Glucose	(↑)	n.a.	(↑)	n.a.
Rel. Body Fat	(↓)	n.a.	(↓)	n.a.
Rel. Muscles	(↑)	n.a.	(↑)	n.a.
Rel. Water	(↓)	n.a.	(↓)	n.a.
Plasma Cholesterol	(↓)	n.a.	(↓)	n.a.
Plasma Triglycerides	↓	n.a.	↓	n.a.
Hepatic Cholesterol	↓	n.a.	(↓)	n.a.
Hepatic Triglycerides	↓	n.a.	(↓)	n.a.
Hepatic NEFA	(↓)	n.a.	(↑)	n.a.
Hepatic Lipids	↓	n.a.	-	n.a.
Rel. Liver Weight	(↓)	n.a.	↓	n.a.
AST	(↓)	n.a.	(↓)	n.a.
ALT	(↓)	n.a.	-	n.a.
De Ritis Quotient	-	n.a.	-	n.a.
Aortic Plaques	(↓)	n.a.	(↑)	n.a.
Calcification	-	n.a.	-	n.a.

6 Discussion

6.1 Differently Expressed 5-HT Receptors in B6 and FVB/N Mice and their Possible Effects

As this study could cogently demonstrate, the distribution of 5-HT receptors in mouse vessels is not invariable between different genetic background strains (e.g. B6 and FVB/N) and within genetically modified mouse lines generated in these strains. While alterations of 5-HT receptor distribution and expression were expected for *Tph1* deficient animals in different genetic background similarly, it was very surprising that 5-HT receptors in vessels of B6 and FVB/N mice seem to be expressed differently, depending on background strain, genetic modification and the receptor subtype itself.

Classically, it could have been supposed, that under the lifelong drastic 5-HT reduction, as true in *Tph1*$^{-/-}$ animals, 5-HT receptors are upregulated as an innate mechanism of the cells to increase the 5-HT sensitivity and ensure 5-HT dependent physiological processes, such as blood pressure regulation. Alternatively, it was also conceivable that the lack of peripheral 5-HT synthesis from the beginning on caused developmental alterations in the animals' systems and 5-HT receptors may have been downregulated to save resources and allow replacement through other signaling pathways.

An effect, such as the one shown for 5-HTr 1B in the aorta of B6, FVB/N and the two knockouts: *B6/Tph1*$^{-/-}$ and *FVB/N/Tph1*$^{-/-}$, where receptor expression is upregulated in *B6/Tph1*$^{-/-}$, but downregulated in *FVB/N/Tph1*$^{-/-}$, seems to be conflicting at the first sight, but may appear reasonable in the light of intra background strain homeostasis: While the cellular strategy of B6 is to upregulate the 5-HTr 1B under *Tph1* deficiency to increase cell sensitivity for 5-HT; it might be more effective for FVB/N animals which already have a 2-fold higher amount of 5-HTr 1B, to downregulate the receptor expression under *Tph1* deficiency in favor of other signaling mechanisms and to save the energy which would be necessary for 5-HTr 1B maintenance.

This explanation becomes even more convincing when looking at the case of 5-HTr 2A. Here, the initial situation is a different one: Receptor expression in FVB/N is lower than in B6 animals and under *Tph1* deficiency both lines upregulate expression to a similar level. It might be that the classical strategy of vascular cells (endothelial) of both background strains is the upregulation of 5-HT receptor synthesis under *Tph1* deficiency, but since they start already at different expression levels it might only be suitable to upregulate 5-HT receptor expression if a particular level is not exceeded.

In case of 5-HTr 1B in FVB/N mice, this particular level could have been reached, hence the vessels did not upregulate the receptor expression under *Tph1* deficiency, but downregulated it.

The fact that the serotonergic system in vessels differs between the genetic background strains B6 and FVB/N and their *Tph1*$^{-/-}$ variants also matches the latest findings of our partner group in Lübeck. There, it could be shown that *FVB/N/Tph1*$^{-/-}$animals develop higher levels of dystrophic cardiac calcification than FVB/N after freeze-thaw injury, but interestingly, this could not be shown for B6 and *B6/Tph1$^{-/-}$* animals (Aherrahrou & Alenina, unpublished data). Also, the here presented data from *ApoE$^{-/-}$* and *ApoE/Tph1$^{-/-}$* animals, bred in B6 background, suggest that calcification in atherosclerotic plaques in the aorta occurs very rarely and is not increased in *Tph1* deficient animals compared to *ApoE$^{-/-}$* alone. The possible protective effect of B6 genetic background against calcification events, which was also reported in other studies (Cooley, 2007; Sontag et al., 2014), may be linked to the altered serotonergic situation in the vessels of B6 compared to FVB/N in which these events happen to a larger extent. It might very well be that the 5-HT receptors involved in calcification are only upregulated in *FVB/N/Tph1$^{-/-}$* animals, following the before described cellular strategy. A downregulation of calcification protective 5-HT receptors in *FVB/N/Tph1$^{-/-}$* animals is also conceivable.

In summary, for future cardiovascular research it might be of great importance that 5-HT receptor subtypes are differently expressed in vessels of different mouse strains, such as B6 and FVB/N and hence, the omnipresent hormone 5-HT is potentially able to cause completely different effects in these strains, as well as in genetically modified lines that base on these strains. Further analysis in different blood vessel types and on additional 5-HT receptors needs to be done to elucidate the relationship of 5-HT receptors in different mouse strains and their potential effects on atherosclerotic processes, as well as on angiogenesis.

For this study, it was very important to show that the physiological situation in vessels of genetically modified animals (here *Tph1$^{-/-}$*) can not only be influenced by the lack of direct effects of the respective substance (here 5-HT signaling), but can further be changed indirectly by altered receptor expression and subsequently by altered substance sensitivity. Since it was reported that 5-HT in *Tph1* deficient animals is alternatively synthesized (via phenylalanine hydroxylase, see Matthes & Bader, 2018), a changed vessel morphology with overexpressed receptors (as shown for 5-HTr 1B) could cause completely unexpected effects on e.g. atherosclerotic processes. This means that even if the animal is *Tph1* deficient and initially lacks the majority of peripheral 5-HT (up to 10% are left!) only small amounts of 5-HT from the duodenum or other than the primary synthesis sources could cause enormous serotonergic effects in the vessels. Hence, a 5-HT lack must not automatically result in an absence of 5-HT signaling.

6.2 Effects of 5-HT Deficiency on Metabolic and Atherosclerotic Processes in aged *ApoE* deficient Animals

A homozygous deficiency of the *ApoE* gene in mice (of B6 background) is widely known to cause not just hypercholesterolemia (Plump et al., 1992; Zhang et al., 1992), followed by a development of all stages of atherosclerosis (Nakashima et al., 1994), but also lowered bodyweight levels (reviewed in Pendse et al., 2009) , increased parameters for liver steatosis (Kampschulte et al., 2014) and a tendency for lowered fasting blood glucose levels (Kawashima et al., 2009; Li et al., 2011). All these effects could be consistently reproduced in this study in naturally aged *ApoE*$^{-/-}$ animals of both sexes. The novel approach of this study was to elucidate whether a peripheral 5-HT absence in *ApoE*$^{-/-}$ animals leads to changes in this characteristic phenotype.

The great chance of this study was the accessibility of two different murine models for 5-HT reduction/absence: First, the *Tph1*$^{-/-}$ mouse which lacks peripheral 5-HT synthesis and was shown to exhibit lowered bodyweight levels and body fat accumulation (Crane et al., 2015; Watanabe et al., 2016), an exacerbation of induced liver toxicity (Zhang et al., 2015) and decreased insulin secretion, hence higher blood glucose levels (under high fat diet) (Kim et al., 2015). And second, the *Sert*$^{-/-}$ mouse which lacks the 5-HT transporter (SERT) and was demonstrated to exhibit a complete absence of blood 5-HT (Chen et al., 2001). *Sert*$^{-/-}$ mice could be shown to develop higher bodyweight, body fat levels, blood glucose and liver steatosis than controls, even though they had reduced food intake (Chen et al., 2012). None of the two peripherally 5-HT lacking mouse models was characterized for impacts on atherosclerosis before and the establishment of double knockout mouse lines allowed a direct comparison between *ApoE*$^{-/-}$, *ApoE/Tph1*$^{-/-}$ and *ApoE/Sert*$^{-/-}$ with regard to atherosclerotic processes.

6.2.1 Metabolic Effects in Double Knockouts

In this study it was shown that *ApoE*$^{-/-}$ animals tend to have lower bodyweight than wild type controls, what was earlier discussed to be due to an impaired delivery of very low density lipoproteins (VLDL) to adipocytes in *ApoE*$^{-/-}$ (Pendse et al., 2009). Further, it could be shown that *ApoE/Tph1*$^{-/-}$ animals exhibit significantly lower bodyweight levels than *ApoE*$^{-/-}$ what is presumably caused by the earlier demonstrated increase of mitochondria uncoupling protein 1 (UCP1) mediated thermogenesis in brown adipose tissue (BAT) under *Tph1* inhibition (Crane et al., 2015). Surprisingly, *ApoE/Sert*$^{-/-}$ animals were demonstrated to have bodyweight levels comparable to *ApoE*$^{-/-}$, hence, lower than B6 controls. This could be explained by the earlier reported *Sert*$^{-/-}$ -related decrease in food intake, what was not documented in this study or by the alternatively balanced nutrient partitioning towards fat but without an overall increase in body mass in *Sert* deficient mice (Chen et al., 2012). Combined with the impaired fat metabolism, caused by *ApoE* deficiency, this may lead to a lowered bodyweight in *ApoE/Sert*$^{-/-}$ animals compared to B6 controls. Data for blood glucose in 45 week old animals suggest that while *ApoE*$^{-/-}$ mice exhibit normal to low values, *ApoE/Tph1*$^{-/-}$ and *ApoE/Sert*$^{-/-}$ mice, tend to exhibit hyperglycemic phenotypes what completely goes in line with the findings of Paulmann et al., 2009, showing that 5-HT and serotonylation being crucial for insulin secretion and blood glucose homeostasis.

The elevated plasma cholesterol levels in all tested groups of mice completely match the idea of ApoE being crucial for maintenance of blood cholesterol balance, but it needs to be highlighted that, at least in males, *ApoE/Sert*$^{-/-}$ exhibited even higher plasma cholesterol values what might be caused by either the mentioned altered nutrition balance or by a generally impaired locomotive behavior in *Sert* deficient animals (Kalueff et al., 2007). A similar trend was revealed for plasma triglycerides which were slightly increased in all tested *ApoE* deficient males, but significantly elevated in *ApoE/Sert*$^{-/-}$ males, what might also be due to hypolocomotion. These findings could also explain why the *ApoE/Sert*$^{-/-}$ group was shown to develop significantly bigger atherosclerotic plaques in the aortas.

Naturally, plasma cholesterol and triglycerides have large impact on liver homeostasis and vice versa (reviewed in Arguello et al., 2015 and Trapani et al., 2012). Hence, it could have been supposed that relative liver weight, as well as plasma liver parameters AST and ALT and the resulting *De Ritis* quotient are increased in *ApoE/Sert*$^{-/-}$ males which were shown to exhibit elevated cholesterol and triglyceride levels in plasma compared to *ApoE*$^{-/-}$. Interestingly, the opposite was the case: *ApoE/Sert*$^{-/-}$ males exhibited very low liver values. One possible explanation is that the impairment of 5-HT uptake to hepatocytes attenuates liver damage what is also supported by the findings of Nocito et al., 2007. Another very interesting finding was the relatively high liver weight in *ApoE/Tph1*$^{-/-}$ females, as well as the quite low AST value in this group. It might be that even though *ApoE* deficiency leads to increased liver damage parameters, the reduction of peripheral 5-HT acts protective on liver cells, as demonstrated for *Tph1*$^{-/-}$ mice (Lesurtel et al., 2006; Nocito et al., 2007). This could presumably be caused by beneficial effects on liver perfusion or hepatic fibrosis (Lesurtel et al., 2012).

6.2.2 Effects on Atherosclerosis in Double Knockouts

As mentioned, one of the most striking findings in this study was the significantly increased relative aortic plaque size in both, *ApoE/Sert*$^{-/-}$ males and females. This finding completely correlates with the results of Rami and colleagues, which were published in 2018. In this study it was reported, that the chronic treatment of *ApoE*$^{-/-}$ animals with the SSRI fluoxetine (SERT inhibitor) promotes atherosclerotic plaque formation after HFD. Increased atherosclerotic plaque size and adhesion of myeloid cells to the vessel wall together with an enhanced C-C motif chemokine ligand 5 (CCL5) -induced integrin activation and consequently increased vascular permeability and leukocyte recruitment indicated that fluoxetine treatment promoted atherosclerotic phenotypes in *ApoE*$^{-/-}$ mice after HFD. Further, the study showed that these effects were strongest after 2 and 4 weeks of HFD, hence in the onset of atherogenesis, and became weaker after 16 weeks of HFD. This also matches the results of the present study where the proatherogenic effect of the genetic SERT inhibition was not visible in cryo slices of the aortic root: Here, all tested groups appeared to have quite large (10 times larger than in animals after 2 weeks of HFD from Rami et al., 2018) atherosclerotic plaques. Earlier studies reported that the aortic root is one of the predilected areas of atherosclerotic plaque development (Nakashima et al., 1994; Whitman, 2004). Hence, it might be that at the age of 45 weeks, the development of atherosclerotic plaques at the aortic root area was so advanced in all genetic groups that potential differences between them could no longer be detected and that in whole aortas the differences were still visible because of the third dimension (longitudinal plane) which was examined.

Another very interesting question is whether the proatherogenic effect in *ApoE/Sert*$^{-/-}$ animals is linked to 5-HT absence. Since the genetically induced *Sert* deficiency in mice used in this study, as well as the pharmacologically induced SERT inhibition via fluoxetine and additionally via escitalopram in mice (Rami et al., 2018) and further the pharmacologically induced SERT inhibition via sertraline in monkeys (Shively et al., 2015) resulted in increased atherosclerotic lesion size, it is very likely that the blocking of SERT generally promotes atherogenesis. And since it was shown that blood levels of 5-HT in *Sert*$^{-/-}$ animals reach zero (Chen et al., 2001), whereas in *Tph1*$^{-/-}$ animals they do not go lower than 4-10% (Walther et al., 2003a) of wild type levels it appears to be plausible that the total 5-HT absence plays a role in the proatherogenic effect of SERT inhibition. It further also explains why this study could not report a similar proatherogenic effect of *Tph1* deficiency.

Putting everything into context, it appears more than plausible that *ApoE/Sert*$^{-/-}$ animals which presumably lack the complete blood 5-HT, appeared to have very high plasma cholesterol and triglyceride levels and which were earlier shown to have an imbalanced nutrient partitioning towards fat tissue (Chen et al., 2012) and an impaired locomotive activity (Kalueff et al., 2007), develop larger atherosclerotic lesions under *ApoE* deficiency than animals without these deficits. It could further be discussed whether the inhibition of SERT, what also affects the CNS and PNS causes altered sleep behavior, vessel contractility or other effects that influence atherosclerotic processes (reviewed in Kadoya & Koyama, 2019 and Sheng & Zhu, 2018).

Further, it is comprehensible that *ApoE/Tph1*$^{-/-}$ males which lack the proatherogenic factor due to an assumed remainder of blood 5-HT and which were shown to accumulate less body fat and have by trend lower plasma cholesterol and triglyceride levels than *ApoE*$^{-/-}$ males, tended to develop smaller atherosclerotic lesions. Nevertheless, this whole concept seems to be exclusively working in males, since female *ApoE/Tph1*$^{-/-}$ mice were indeed also shown to accumulate less body fat and by trend lower plasma cholesterol and triglyceride levels, but atherosclerotic lesions in their aortas tended to be of increased size compared to those in *ApoE*$^{-/-}$ females. The classical known sex difference in atherosclerosis pathogenesis only occurs in young animals (16 weeks of age), but disappears in aged animals (Caligiuri et al., 1999; Paigen et al., 1987) probably due to lower steroid hormone levels in aged females. The 45 week old animals in this study did also only exhibit non-significant differences in lesion size between males and females; hence it is unlikely that *Tph1* deficiency only boosts an existing independent phenomenon. A possible explanation might be found in the altered 5-HT receptor distribution which could be substantiated in vessels of *Tph1* deficient animals. If it is assumed that under *Tph1* deficiency, particular 5-HT receptors are not only alternatively expressed in the vessels, but also in other tissues, such as gonads, this may lead to changed gonadal hormone production or sensitivity which might then influence the onset and the progression of atherosclerosis (Sirotkin & Schaeffer, 1997; Paigen et al., 1987).

The detailed analysis of atherosclerotic plaque composition revealed that while in males both groups with impaired 5-HT homeostasis did not exhibit alterations of calcification, plaque collagen or intraintimal macrophages. However, *ApoE/Sert*$^{-/-}$ females tended to have lower calcification levels and non-significantly elevated collagen and macrophage counts compared to *ApoE*$^{-/-}$ females. It is known that the female steroid hormone 17β-estradiol has a protective effects on vascular calcification (Peng et al. in 2017), but how this should be exclusively present in *ApoE/Sert*$^{-/-}$ females remains unclear and needs further research. For the observed increase of plaque collagen content an interesting explanation was discussed in 2009 by Pavone et al., who found elevated cardiac fibrosis in *Sert*$^{-/-}$ animals and hypothesized that this could be caused by a local 5-HT excess (due to the inhibition of 5-HT transport), which increased 5-HTr 2A activation which was then followed by an activation of TGF-beta 1[9] signaling and consequently by an up-regulation of the α-SMA[10] protein and collagen production. Why this effect could exclusively be observed in female *ApoE/Sert*$^{-/-}$ mice remains unclear. It is likely that complex interactions between metabolic alterations, such as increased cholesterol and altered steroid hormone levels caused by *ApoE* deficiency and 5-HT deficiency (in *Tph1*$^{-/-}$) / temporary 5-HT excess (in *Sert*$^{-/-}$) cause cross effects on multifactorial processes, such as atherogenesis. The uptake of oxidized LDL into macrophages for example, is affected by 5-HT and very concentration sensitive (Aviram et al., 1992). If it is assumed, that female mice generally produce lower 5-HT amounts than males and a *Sert* deficiency causes temporary increased levels of free 5-HT (e.g. after food intake), it might be that this results in the optimal 5-HT concentration for intraintimal macrophages to ingest oxidized LDL and form transient foam cells in the intimal space to a larger extend than any other examined animal group, what could explain the finding of this study.

[9] TGF-beta 1: First isoform of the transforming growth factor-beta family, which controls proliferation, differentiation and other functions in many cell types via TGF-beta receptors.
[10] α-SMA: Alpha smooth muscle actin is the predominant actin isoform within VSMCs.

6.3 Western Diet Regime Discloses Contrary Effects of 5-HT Absence

6.3.1 Diminished Body Fat Accumulation in *Tph1* and *ApoE* deficient Animals

Similarly as in aged animals, *ApoE/Tph1*$^{-/-}$ animals of both sexes were shown to exhibit significantly lower bodyweight under WD than *ApoE*$^{-/-}$ animals. In consistence with this finding were the relative body fat levels also lower in *ApoE/Tph1*$^{-/-}$ animals, whereas the amount of muscle mass was higher than in *ApoE*$^{-/-}$. As mentioned above, it was reported earlier that *Tph1* deficiency leads to lower body fat accumulation under high fat diet (HFD) due to an upregulation of UCP1 and the subsequent activation of UCP1 dependent thermogenesis in BAT (Crane et al., 2015; Oh et al., 2015; Watanabe et al., 2016). This effect appears to be so stable in itself that even the changed lipid metabolism under *ApoE* deficiency could not disrupt it. The same can be stated for blood glucose levels in *ApoE/Tph1*$^{-/-}$ animals of both sexes under WD: They are consistently higher (but never statistically significant) in *ApoE/Tph1*$^{-/-}$ than in *ApoE*$^{-/-}$. The lack of peripheral 5-HT affects serotonylation-dependent insulin secretion and hence, causes hyperglycemic phenotypes, not only in *Tph1*$^{-/-}$ (Paulmann et al., 2009; Watanabe, Rose, & Aso, 2011) but also in *ApoE/Tph1*$^{-/-}$ animals.

Interestingly, females of both genotypes appeared to be protected from WD induced obesity and even lost bodyweight after 8 weeks of WD (more prominent effect in *ApoE/Tph1*$^{-/-}$ females). It is very likely that here again an interplay of several physiological phenomena becomes visible: First, female mice could be shown to be partly protected from obese phenotype under HFD. This was discussed to be caused by gonadal hormones, such as estradiol, since ovariectomized females did not show any protective effect (Hong et al., 2009). Female protection against obesity, genetically combined with an impaired delivery of VLDL to adipocytes, caused by *ApoE* deficiency (Pendse et al., 2009) might lead an impairment of bodyweight gain in tested female mice. Further, the bodyweight loss in *ApoE/Tph1*$^{-/-}$ females after 8 weeks of WD is supposably caused by the reported upregulated thermogenesis in these animals (Crane et al., 2015).

6.3.2 Effects of *Tph1* Deficiency on Lipid Metabolism under Western Diet

Under long term WD, fasting plasma cholesterol levels in *ApoE* deficient animals reach drastically high values of 900mg/dl and above. This was supposed as ApoE is the major lipoprotein clearance mediator in the mouse (Plump et al., 1992) and a lack of ApoE results in increasing circulating LDL and VLDL levels due to a diminished uptake to the liver and other tissues. In contrast, plasma triglyceride levels in *ApoE* deficient animals under WD were shown to be at normal range and even lower by trend than in normal diet controls. Only in *ApoE*$^{-/-}$ males after 8 weeks of WD plasma triglyceride levels were elevated above normal range as expected for all *ApoE* deficient groups since ApoE is also essential for triglyceride transport and uptake to liver and other peripheral tissues (von Zychlinski et al., 2014). However, *ApoE/Tph1*$^{-/-}$ animals under WD tended to exhibit slightly lower plasma cholesterol levels and significantly lower plasma triglyceride levels after 8 weeks of WD. Interestingly, peripheral 5-HT was shown to decrease plasma lipids, such as cholesterol and triglycerides, postprandially by stimulation of e.g. hepatocytes. Regulation of plasma lipid concentrations was discussed to be mediated by different 5-HT receptor types (reviewed in Watanabe et al., 2011) and hence, alternatively expressed 5-HT receptors in *Tph1* deficient animals (as demonstrated in this study) together with an alternative 5-HT synthesis pathway (Matthes & Bader, 2018) might lead to alterations in lipid uptake and consequently in plasma lipid concentrations.

Another interesting approach is the analysis of different metabolic balance or coping strategies in the different animal models: While *ApoE*$^{-/-}$ males for example, were shown to exhibit higher plasma triglyceride levels after 8 weeks than after 12 weeks of WD, *ApoE*$^{-/-}$ and *ApoE/Tph1*$^{-/-}$ females were clearly demonstrated to exhibit higher hepatic lipids (cholesterol, triglycerides, NEFA and total lipids) after 8 than after 12 weeks of WD. It was reported before, that plasma as well as hepatic cholesterol levels increase under HFD, but can drop to relatively low levels in wild type mice after 6-8 weeks of the diet (Campbell et al., 1982). Hence, it might be possible that depending on genotype and sex, this metabolic balance mechanism is impaired.

6.3.3 No clear Effect of *Tph1* Deficiency on Atherosclerosis after Long Term WD

Similarly as in 45 week old animals, it was shown that while male *ApoE/Tph1*$^{-/-}$ mice exhibit smaller atherosclerotic lesions in the aortic arch than controls, female *ApoE/Tph1*$^{-/-}$ mice exhibit larger aortic plaques than controls even if this effect was neither statistically significant in 45 week old animals nor in animals after long term WD (8 or 12 weeks). Possible explanations might be the lower body fat and cholesterol accumulation only in *ApoE/Tph1*$^{-/-}$ mice. It might be that greater animal cohorts will result in statistically significant results for a sex and *Tph1* deficiency dependent protective effect from atherosclerotic processes in males and for the opposite effect in females. Additionally, future studies should definitely focus on WD treatment in *ApoE/Sert*$^{-/-}$ animals to strengthen the idea of *Sert* deficiency being a crucial proatherogenic factor und to elucidate the underlying mechanisms.

However, this study clearly confirmed that there is a strong sex difference in atherosclerotic phenotype induced by *ApoE* deficiency which is most prominent at young age (animals under WD) and becomes smaller at advanced age (45 week old animals). As discussed previously, this effect appears to be more influenced by immunological factors that are affected by the female gonadal hormone 17β-estradiol than by hormonal effects on the lipoprotein metabolism. As the hormonal status in both males and females changes with age, it was discussed that age- and sex-dependent variations of cell-mediated immune responses could modulate the onset and the progression of atherosclerosis (Caligiuri et al., 1999).

7 Conclusion

Since this study was created more exploratory than confirmatory, it is important to mention that the reported results (statistically significant as well as biologically relevant) cover a wide spectrum of atherosclerosis related biological processes affected by genetic modifications in the used animal models, but not all of them. Further research will be needed to elucidate and confirm the findings and deepen the insights especially into the underlying mechanisms.

Nevertheless, it could be clearly shown that peripheral 5-HT reduction and absence have strong effects on general vascular physiology and atherosclerosis relevant parameters, but only a complete 5-HT absence (as assumed in *Sert* deficient animals) affects atherogenesis itself. However, there are more factors than simply ‘5-HT or no 5-HT’, that need to be considered: This study proved that animal background strains, sex and age, genetically induced or artificially accelerated pathogenesis as well as type of 5-HT absence (via *Tph* or *Sert*) play important roles in the disease process and characteristics. The latter is the most promising projection for future research, since *ApoE/Tph1*$^{-/-}$ and *ApoE/Sert*$^{-/-}$ animals partly delivered very contrasting results. While the transgenic inhibition of 5-HT synthesis in *ApoE* deficient animals (*ApoE/Tph1*$^{-/-}$ mice) did not affect atherogenesis mentionable, the inhibition of intra cellular 5-HT transport in these animals (*ApoE/Sert*$^{-/-}$ mice) delivered clearly proatherogenic effects and might be a target for future therapeutic approaches including SERT enhancement (e.g. via tianeptine; Mennini et al., 1987).

As an overall conclusion it can be stated that 5-HT is not a main determinant of atherosclerosis but small 5-HT dependent alterations were found in this study.

Appendix

Table of Abbreviations

5-HIAA	5-hydroxyindole acetic acid
5-HIAL	5-hydroxyindole acetaldehyde
5-HT	5-hydroxytryptamine (serotonin)
5-HT$_{[\#]}$	5-HT receptor subtype # (number)
5-HTP	5-hydroxytryptophan
5-HTr	5-HT receptor
5-HTr [#]	5-HT receptor subtype # (number)
5-HTT	serotonin transporter (also SERT)
AA (Fig. 14 and 25)	aortic arch
AADC	aromatic amino acid decarboxylase
ACAT-1	acyl-coenzyme A:cholesterol acyltransferase-1
ALDH	aldehyde dehydrogenase
ALT	alanine aminotransferase
ANOVA	analysis of variance
AP	atherosclerotic plaque
Apo	apolipoprotein
apoB$_{100}$	human apolipoprotein B (full length)
ApoE	apolipoprotein E
ApoE	ApoE gene
ApoE$^{-/-}$	*ApoE* knockout
ApoE/Sert$^{-/-}$	*ApoE* and *Sert* double knockout
ApoE/Tph1$^{-/-}$	*ApoE* and *Tph1* double knockout
AST	aspartate aminotransferase
B6	see C57Bl/6
B6/Tph1$^{-/-}$	*Tph1* knockout in B6 background
BAT	brown adipose tissue
BBB	blood brain barrier
BCA	body composition analysis
BH$_4$	tetrahydrobiopterin
bp	base pairs
C (Fig. 4)	collagen
C57Bl/6	wild type black 6 (B6)
CCL5	C-C motif chemokine ligand 5
cDNA	complementary DNA
CE	cholesterol esters
CETP	cholesterylester transfer protein
cf.	*confer* (compare)
CNS	central nervous system
CVD	cardiovascular disease
ddH$_2$**O**	double distilled water
DNA	deoxyribonucleic acid
EC	enterochromaffin cells
EC (Fig. 4)	endothelial cell
ECM	extracellular matrix
ENS	enteric nervous system
Ex[#]	exon # (number)
F1-F2	visceral fat samples
FB	fibroblast
FC	free cholesterol
FC (Fig. 4)	foam cell
Fig.	figure
FVB/N	wild type Friend virus B
FVB/N/Tph1$^{-/-}$	*Tph1* knockout in FVB/N background
GAPDH	glyceraldehyde 3-phosphate dehydrogenase (housekeeping gene)
GCH1	GTP cyclohydrolase 1
gDNA	genomic DNA
GPCR	G-protein coupled seven transmembrane receptors
GTPase	guanosine triphosphate hydrolase
HDL	high-density liporprotein
HFD	high fat diet
i.p.	intraperitoneal
IDO 1	indoleamine dioxygenase 1
IDO 2	indoleamine dioxygenase 2
IQR	interquartile range
IUPHAR	International Union of Basic and Clinical Pharmacology
IVC	individually ventilated cage
KO	knockout
L1-L4	liver samples
LAGeSo	Landesamt für Gesundheit und Soziales
LDL	low-density lipoprotein
LGIC	ligand gated ion channel
LNAA	large neutral amino acids
LNAAT	large neutral amino acid transporter
Mac	macrophage
MAO-A	monoamine oxidase A
MAO-B	monoamine oxidase B
MC	mast cell
MM	master mix
Mono	monocyte
MPO	myeloperoxidase
n.a.	not applicable
NEFA	not esterified fatty acids

NIH	National Institutes of Health
NMR	nuclear magnetic resonance
NO	nitric oxide
NP	neutrophil
ORO	Oil red O staining
ox.LDL	oxidized LDL
PAH	phenylalanin hydroxylase
PCR	polymerase chain reaction
PDGF-B	platelet-derived growth factor B
PH	pulmonary hypertension
PL	platelet
PND	post natal day
PNS	peripheral nervous system
PTPS	6-pyruvoyl-5,6,7,8-tetrahydropterin
qBH2	quinoid dihydrobiopterin
qPCR	real time quantitative PCR
RH	random hexamer
RhoA	Ras homolog gene family, member A
RN	raphe nuclei
RNA	ribonucleic acid
rpm	revolutions per minute
RT	room temperature (20-25°C)
SEM	standard error of the mean
SERT	serotonin transporter (also 5-HTT)
Sert$^{-/-}$	*Sert* knockout
Slc6a4	solute carrier family 6 member 4 (gene name for *Sert*)
Slc6a4$^{-/-}$	see *Sert$^{-/-}$*
SMC	smooth muscle cell
SSRI	selective serotonin reuptake inhibitor
Tab.	table
TD-NMR	time-domain-nuclear-magnetic-resonance imaging
TG	transglutaminases
TGF-beta	transforming growth factor-beta
TH	tyrosine hydroxylase
TPH	tryptophan hydroxylase
TPH1	tryptophan hydroxylase 1 (periphery)
Tph1	TPH1 gene
Tph1$^{-/-}$	*Tph1* knockout
TPH2	tryptophan hydroxylase 2 (CNS)
Tph2	TPH2 gene
Trp	L-Tryptophan
UCP1	uncoupling protein 1
UTR	untranslated region
VLDL	very low- density lipoprotein
VMAT	vesicular monoamine transporters
VMAT 1	vesicular monoamine transporter 1
VMAT 2	vesicular monoamine transporter 2
VSMC	vascular smooth muscle cell
WD	Western type diet
WHO	World Health Organization
α-SMA	alpha smooth muscle actin

Table of Figures

Table of Tables

Table of References

Ahern, G. P. (2011). 5-HT and the Immune System. *Current Opinion in Pharmacology*, *11*(1), 29–33. https://doi.org/10.1016/j.coph.2011.02.004

Aherrahrou, Z., & Schunkert, H. (2013). Genetics of atherosclerosis and vascular calcification go hand-in-hand. *Atherosclerosis*, *228*(2), 325–326. https://doi.org/10.1016/J.ATHEROSCLEROSIS.2012.10.029

Amento, E. P., Ehsani, N., Palmer, H., & Libby, P. (1991). Cytokines and growth factors positively and negatively regulate interstitial collagen gene expression in human vascular smooth muscle cells. *Arteriosclerosis and Thrombosis: A Journal of Vascular Biology*, *11*(5), 1223–1230. https://doi.org/10.1161/01.ATV.11.5.1223

Arguello, G., Balboa, E., Arrese, M., & Zanlungo, S. (2015). Recent insights on the role of cholesterol in non-alcoholic fatty liver disease. *Biochimica et Biophysica Acta (BBA) - Molecular Basis of Disease*, *1852*(9), 1765–1778. https://doi.org/10.1016/J.BBADIS.2015.05.015

Aviram, M., Fuhrman, B., Maor, I., & Brook, G. J. (1992). Serotonin increases macrophage uptake of oxidized low density lipoprotein. *European Journal of Clinical Chemistry and Clinical Biochemistry : Journal of the Forum of European Clinical Chemistry Societies*, *30*(2), 55–61. Retrieved from http://www.ncbi.nlm.nih.gov/pubmed/1581411

Ball, H. J., Yuasa, H. J., Austin, C. J. D., Weiser, S., & Hunt, N. H. (2009). Indoleamine 2,3-dioxygenase-2; a new enzyme in the kynurenine pathway. *The International Journal of Biochemistry & Cell Biology*, *41*(3), 467–471. https://doi.org/10.1016/J.BIOCEL.2008.01.005

Barnes, N. M., & Sharp, T. (1999). A review of central 5-HT receptors and their function. *Neuropharmacology*, *38*(8), 1083–1152. https://doi.org/10.1016/S0028-3908(99)00010-6

Barthels, M. (Ed.). (2012). 3 Physiologie der Thrombozyten. In *Das Gerinnungskompendium*. https://doi.org/10.1055/b-0034-15016

Becker, R. C. (2008). Editor's page: fundamentals in neurocardiology - The brain–platelet–coronary artery interface. *Journal of Thrombosis and Thrombolysis*, *26*(1), 74–77. https://doi.org/10.1007/s11239-008-0255-5

Beis, D. (2014). *Phenotypical Analysis of Animal-Models with Genetic Changes of Tryptophan Hydroxylase 2 (Tph2) Expression*.

Bengel, D., Murphy, D. L., Andrews, A. M., Wichems, C. H., Feltner, D., Heils, A., … Lesch, K. P. (1998). Altered brain serotonin homeostasis and locomotor insensitivity to 3,4-methylenedioxymethamphetamine ('ecstasy') in serotonin transporter-deficient mice. *Molecular Pharmacology*, *53*(4), 649–655. https://doi.org/10.1124/mol.53.4.649

Bishop, C. A., & O'shea, M. (1983). Serotonin immunoreactive neurons in the central nervous system of an insect (Periplaneta americana). *Journal of Neurobiology*, *14*(4), 251–269. https://doi.org/10.1002/neu.480140402

Bottalico, B., Larsson, I., Brodszki, J., Hernandez-Andrade, E., Casslén, B., Marsál, K., & Hansson, S. . (2004). Norepinephrine Transporter (NET), Serotonin Transporter (SERT), Vesicular Monoamine Transporter (VMAT2) and Organic Cation Transporters (OCT1, 2 and EMT) in Human Placenta from Pre-eclamptic and Normotensive Pregnancies. *Placenta*, *25*(6), 518–529. https://doi.org/10.1016/J.PLACENTA.2003.10.017

Brady, S. T., Siegel, G. J., Albers, R. W. (Robert W., & Price, D. L. (Donald L. (2012). *Basic neurochemistry : principles of molecular, cellular, and medical neurobiology*. Retrieved from https://books.google.de/books?hl=de&lr=&id=jtmUQWt4mssC&oi=fnd&pg=PP1&dq=Basic+neurochemistry+:+principles+of+molecular,+cellular,+and+medical+neurobiology&ots=JjeYkbwrmk&sig=JodRhP4MQyi6oO6myl_RHm7kT88#v=onepage&q=Basic neurochemistry %3A principles of m

Buznikov, G. A., Lambert, W. H., & Lauder, J. M. (2001). Serotonin and serotonin-like substances as regulators of early embryogenesis and morphogenesis. *Cell and Tissue Research*, *305*(2), 177–186. https://doi.org/10.1007/s004410100408

Cadirci, E., Halici, Z., Bayir, Y., Albayrak, A., Karakus, E., Polat, B., … Gundogdu, C. (2013). Peripheral 5-HT7 receptors as a new target for prevention of lung injury and mortality in septic rats. *Immunobiology*, *218*(10), 1271–1283. https://doi.org/10.1016/J.IMBIO.2013.04.012

Caligiuri, G., Nicoletti, A., Zhou, X., Törnberg, I., & Hansson, G. K. (1999). Effects of sex and age on atherosclerosis and autoimmunity in apoE-deficient mice. *Atherosclerosis*, *145*(2), 301–308. https://doi.org/10.1016/S0021-9150(99)00081-7

Campbell, A. E., Loria, R. M., Madge, G. E., & Kaplan, A. M. (1982). Dietary hepatic cholesterol elevation: Effects on coxsackievirus B infection and inflammation. *Infection and Immunity*, *37*(1), 307–317.

Cesura, A. M., Bertocci, B., & Da Prada, M. (1990). Binding of [3H]dihydrotetrabenazine and [125I]azidoiodoketanserin photoaffinity labeling of the monoamine transporter of platelet 5-HT organelles. *European Journal of Pharmacology*, *186*(1), 95–104. https://doi.org/10.1016/0014-2999(90)94064-5

Charles, A., Rounds, S., & Farber, H. W. (1991). Neutrophil chemoattractant production by cultured serotonin-stimulated bovine and human endothelial cells. *The American Journal of Physiology*, *261*(2 Pt 1), L133-9. https://doi.org/10.1152/ajplung.1991.261.2.L133

Chen, J. J., Li, Z., Pan, H., Murphy, D. L., Tamir, H., Koepsell, H., & Gershon, M. D. (2001). Maintenance of serotonin in the intestinal mucosa and ganglia of mice that lack the high-affinity serotonin transporter: Abnormal intestinal motility and the expression of cation transporters. *The Journal of Neuroscience : The Official Journal of the Society for Neuroscience*, *21*(16), 6348–6361. https://doi.org/10.1523/JNEUROSCI.21-16-06348.2001

Chen, X., Margolis, K. J., Gershon, M. D., Schwartz, G. J., & Sze, J. Y. (2012). Reduced serotonin reuptake transporter (SERT) function causes insulin resistance and hepatic steatosis independent of food intake. *PloS One*, *7*(3), e32511. https://doi.org/10.1371/journal.pone.0032511

Clavien, P. A. (2008). Liver regeneration: A spotlight on the novel role of platelets and serotonin. *Swiss Medical Weekly*, *138*(25–26), 361–370.

Cooley, B. C. (2007). in Vein Grafts and Wire-Injured Arteries. *Circulation Journal*, *71*(October), 1649–1652.

Côté, F., Thévenot, E., Fligny, C., Fromes, Y., Darmon, M., Ripoche, M.-A., … Vodjdani, G. (2003). Disruption of the nonneuronal tph1 gene demonstrates the importance of peripheral serotonin in cardiac function. *Proceedings of the National Academy of Sciences of the United States of America*, *100*(23), 13525–13530. https://doi.org/10.1073/pnas.2233056100

Crane, J. D., Palanivel, R., Mottillo, E. P., Bujak, A. L., Wang, H., Ford, R. J., … Steinberg, G. R. (2015). Inhibiting peripheral serotonin synthesis reduces obesity and metabolic dysfunction by promoting brown adipose tissue thermogenesis. *Nature Medicine*, *21*(2), 166–172. https://doi.org/10.1038/nm.3766

Cui, Y., Niziolek, P. J., MacDonald, B. T., Zylstra, C. R., Alenina, N., Robinson, D. R., … Robling, A. G. (2011). Lrp5 functions in bone to regulate bone mass. *Nature Medicine*, *17*(6), 684–691. https://doi.org/10.1038/nm.2388

Dees, C., Akhmetshina, A., Zerr, P., Reich, N., Palumbo, K., Horn, A., … Distler, J. H. W. (2011). Platelet-derived serotonin links vascular disease and tissue fibrosis. *The Journal of Experimental Medicine*, *208*(5), 961–972. https://doi.org/10.1084/jem.20101629

Derrick, J. R., Pollard, H. S., & Moore, R. M. (1959). The Pattern of Arteriosclerotic Narrowing of the Celiac and Superior Mesenteric Arteries. *Annals of Surgery*, *149*(5), 684. Retrieved from https://www.ncbi.nlm.nih.gov/pmc/articles/PMC1451070/?page=1

Duleu, S., Mangas, A., Sevin, F., Veyret, B., Bessede, A., & Geffard, M. (2010). Circulating Antibodies to IDO/THO Pathway Metabolites in Alzheimer's Disease. *International Journal of Alzheimer's Disease*, *2010*. https://doi.org/10.4061/2010/501541

Endemann, D. H., & Schiffrin, E. L. (2004). Endothelial Dysfunction. *Journal of the American Society of Nephrology*, *15*(8), 1983–1992. https://doi.org/10.1097/01.ASN.0000132474.50966.DA

Erickson, J. D., Schafer, M. K., Bonner, T. I., Eiden, L. E., & Weihe, E. (1996). Distinct pharmacological properties and distribution in neurons and endocrine cells of two isoforms of the human vesicular monoamine transporter. *Proceedings of the National Academy of Sciences of the United States of America*, *93*(10), 5166–5171. https://doi.org/10.1073/pnas.93.10.5166

Erspamer, V., & Asero, B. (1952). Identification of Enteramine, the Specific Hormone of the Enterochromaffin Cell System, as 5-Hydroxytryptamine. *Nature*, *169*, 800–801. https://doi.org/10.1038/169800b0

Falk, E. (1992). Why do plaques rupture? *Circulation*, *86*(6 Suppl), III30-42. Retrieved from http://www.ncbi.nlm.nih.gov/pubmed/1424049

Farrelly, L. A., Thompson, R. E., Zhao, S., Lepack, A. E., Lyu, Y., Bhanu, N. V., … Maze, I. (2019). Histone serotonylation is a permissive modification that enhances TFIID binding to H3K4me3. *Nature*, *567*, 535–539. https://doi.org/10.1111/mec.13536.Application

Fraulob, J. C., Ogg-Diamantino, R., Fernandes-Santos, C., Aguila, M. B., & Mandarim-de-Lacerda, C. A. (2010). A mouse model of metabolic syndrome: Insulin resistance, fatty liver and Non-Alcoholic Fatty Pancreas Disease (NAFPD) in C57BL/6 mice fed a high fat diet. *Journal of Clinical Biochemistry and Nutrition*, *46*(3), 212–223. https://doi.org/10.3164/jcbn.09-83

Frazer, A., & Hensler, J. G. (1999). Large neutral amino acids: dietary effects on brain neurochemistry and function. *Amino Acids*, *45*(3), 419–430. https://doi.org/10.1007/s00726-012-1330-y

Fujimiya, M., & Inui, A. (2000). Peptidergic regulation of gastrointestinal motility in rodents. *Peptides*, *21*(10), 1565–1582. https://doi.org/10.1016/S0196-9781(00)00313-2

Fuster, V., Stein, B., Ambrose, J. A., Badimon, L., Badimon, J. J., & Chesebro, J. H. (1990). Atherosclerotic plaque rupture and thrombosis. Evolving concepts. *Circulation*, *82*(3 Suppl), II47-59. Retrieved from http://www.ncbi.nlm.nih.gov/pubmed/2203564

Gerrity, R. G. (1981). The role of the monocyte in atherogenesis: I. Transition of blood-borne monocytes into foam cells in fatty lesions. *The American Journal of Pathology*, *103*(2), 181–190. Retrieved from http://www.ncbi.nlm.nih.gov/pubmed/7234961

Gershon, M. D. (2004). Review article: serotonin receptors and transporters - roles in normal and abnormal gastrointestinal motility. *Alimentary Pharmacology and Therapeutics*, *20*(s7), 3–14. https://doi.org/10.1111/j.1365-2036.2004.02180.x

Gershon, Michael D. (2012). Serotonin is a sword and a shield of the bowel: serotonin plays offense and defense. *Transactions of the American Clinical and Climatological Association*, *123*, 268–280; discussion 280. Retrieved from http://www.ncbi.nlm.nih.gov/pubmed/23303993

Goldstein, J. L., Ho, Y. K., Basu, S. K., & Brown, M. S. (1979). Binding site on macrophages that mediates uptake and degradation of acetylated low density lipoprotein, producing massive cholesterol deposition. *Proceedings of the National Academy of Sciences*, *76*(1), 333–337. https://doi.org/10.1073/PNAS.76.1.333

Grohmann, M. (2009). *Die Rolle der Tryptophan-Hydroxylase 2 bei der Entstehung psychiatrischer Erkrankungen*. Retrieved from https://refubium.fu-berlin.de/handle/fub188/11579

Guilluy, C., Eddahibi, S., Agard, C., Guignabert, C., Izikki, M., Tu, L., … Pacaud, P. (2009). RhoA and Rho Kinase Activation in Human Pulmonary Hypertension. *American Journal*

of Respiratory and Critical Care Medicine, *179*(12), 1151–1158. https://doi.org/10.1164/rccm.200805-691OC
Gutknecht, L., Kriegebaum, C., Waider, J., Schmitt, A., & Lesch, K.-P. (2009). Spatio-temporal expression of tryptophan hydroxylase isoforms in murine and human brain: Convergent data from Tph2 knockout mice. *European Neuropsychopharmacology*, *19*(4), 266–282. https://doi.org/10.1016/j.euroneuro.2008.12.005
Hansson, G. K., Robertson, A.-K. L., & Söderberg-Nauclér, C. (2006). INFLAMMATION AND ATHEROSCLEROSIS. *Annual Review of Pathology: Mechanisms of Disease*, *1*(1), 297–329. https://doi.org/10.1146/annurev.pathol.1.110304.100100
Hara, K., Hirowatari, Y., Yoshika, M., Komiyama, Y., Tsuka, Y., & Takahashi, H. (2004). The ratio of plasma to whole-blood serotonin may be a novel marker of atherosclerotic cardiovascular disease. *Journal of Laboratory and Clinical Medicine*, *144*(1), 31–37. https://doi.org/10.1016/J.LAB.2004.03.014
Hardebo, J. E., & Owman, C. (1980). Barrier mechanisms for neurotransmitter monoamines and their precursors at the blood- brain interface. *Annals of Neurology*, *8*(1), 1–11. https://doi.org/10.1002/ana.410080102
Hensler, J. G. (2012). Serotonin. *Basic Neurochemistry*, 300–322. https://doi.org/10.1016/B978-0-12-374947-5.00015-8
Holmes, A., Murphy, D. L., & Crawley, J. N. (2003). Abnormal behavioral phenotypes of serotonin transporter knockout mice: Parallels with human anxiety and depression. *Biological Psychiatry*, *54*(10), 953–959. https://doi.org/10.1016/j.biopsych.2003.09.003
Höltje, M., Winter, S., Walther, D., Pahner, I., Hörtnagl, H., Ottersen, O. P., … Ahnert-Hilger, G. (2003). The vesicular monoamine content regulates VMAT2 activity through Galphaq in mouse platelets. Evidence for autoregulation of vesicular transmitter uptake. *The Journal of Biological Chemistry*, *278*(18), 15850–15858. https://doi.org/10.1074/jbc.M212816200
Hong, J., Stubbins, R. E., Smith, R. R., Harvey, A. E., & Núñez, N. P. (2009). Differential susceptibility to obesity between male, female and ovariectomized female mice. *Nutrition Journal*, *8*, 11. https://doi.org/10.1186/1475-2891-8-11
Hummerich, R., & Schloss, P. (2010). Serotonin—more than a neurotransmitter: transglutaminase-mediated serotonylation of C6 glioma cells and fibronectin. *Neurochemistry International*, *57*(1), 67–75. https://doi.org/10.1016/J.NEUINT.2010.04.020
Huo, Y., Schober, A., Forlow, S. B., Smith, D. F., Hyman, M. C., Jung, S., … Ley, K. (2003). Circulating activated platelets exacerbate atherosclerosis in mice deficient in apolipoprotein E. *Nature Medicine*, *9*(1), 61–67. https://doi.org/10.1038/nm810
Kadoya, M., & Koyama, H. (2019). Sleep, Autonomic Nervous Function and Atherosclerosis. *International Journal of Molecular Sciences*, *20*(4). https://doi.org/10.3390/ijms20040794
Kalueff, A. V., Fox, M. A., Gallagher, P. S., & Murphy, D. L. (2007). Hypolocomotion, anxiety and serotonin syndrome-like behavior contribute to the complex phenotype of serotonin transporter knockout mice. *Genes, Brain and Behavior*, *6*(4), 389–400. https://doi.org/10.1111/j.1601-183X.2006.00270.x
Kampschulte, M., Stöckl, C., Langheinrich, A. C., Althöhn, U., Bohle, R. M., Krombach, G. A., … Roderfeld, M. (2014). Western diet in ApoE-LDLR double-deficient mouse model of atherosclerosis leads to hepatic steatosis, fibrosis, and tumorigenesis. *Laboratory Investigation*, *94*(11), 1273–1282. https://doi.org/10.1038/labinvest.2014.112
Kapourchali, F. R., Surendiran, G., Chen, L., Uitz, E., Bahadori, B., & Moghadasian, M. H. (2014). Animal models of atherosclerosis. *World Journal of Clinical Cases*, *2*(5), 126–132. https://doi.org/10.12998/wjcc.v2.i5.126
Kaumann, A. J., & Levy, F. O. (2006). 5-Hydroxytryptamine receptors in the human

cardiovascular system. *Pharmacology & Therapeutics*, *111*(3), 674–706. https://doi.org/10.1016/J.PHARMTHERA.2005.12.004

Kawashima, Y., Chen, J., Sun, H., Lann, D., Hajjar, R. J., Yakar, S., & Leroith, D. (2009). Apolipoprotein E deficiency abrogates insulin resistance in a mouse model of type 2 diabetes mellitus. *Diabetologia*, *52*(7), 1434–1441. https://doi.org/10.1007/s00125-009-1378-8

Kellett, D. O., Stanford, S. C., Machado, B. H., Jordan, D., & Ramage, A. G. (2005). Effect of 5-HT depletion on cardiovascular vagal reflex sensitivity in awake and anesthetized rats. *Brain Research*, *1054*(1), 61–72. https://doi.org/10.1016/J.BRAINRES.2005.06.063

Kelley, J. L., Chi, D. S., Abou-Auda, W., Smith, J. K., & Krishnaswamy, G. (2000). The molecular role of mast cells in atherosclerotic cardiovascular disease. *Molecular Medicine Today*, *6*(8), 304–308. https://doi.org/10.1016/S1357-4310(00)01747-0

Kim, K., Oh, C. M., Ohara-Imaizumi, M., Park, S., Namkung, J., Yadav, V. K., … Kim, H. (2015). Functional role of serotonin in insulin secretion in a diet-induced insulin-resistant state. *Endocrinology*, *156*(2), 444–452. https://doi.org/10.1210/en.2014-1687

Kondaurova, E. M., Naumenko, V. S., & Popova, N. K. (2012). Effect of chronic activation of 5-HT3 receptors on 5-HT3, 5-HT1A and 5-HT2A receptors functional activity and expression of key genes of the brain serotonin system. *Neuroscience Letters*, *522*(1), 52–56. https://doi.org/10.1016/j.neulet.2012.06.015

Kushnir-Sukhov, N. M., Brown, J. M., Wu, Y., Kirshenbaum, A., & Metcalfe, D. D. (2007). Human mast cells are capable of serotonin synthesis and release. *The Journal of Allergy and Clinical Immunology*, *119*(2), 498–499. https://doi.org/10.1016/j.jaci.2006.09.003

Kwidzinski, E., & Bechmann, I. (2007). IDO expression in the brain: a double-edged sword. *Journal of Molecular Medicine*, *85*(12), 1351–1359. https://doi.org/10.1007/s00109-007-0229-7

Kwidzinski, E., Bunse, J., Kovac, A. D., Ullrich, O., Zipps, F., Nitsch, R., & Bechmann, I. (2003). *Ido (indolamine 2,3-dioxygenase) Expression and Function in the CNS*. https://doi.org/10.1007/978-1-4615-0135-0_13

Lee, G. S., Simpson, C., Sun, B.-H., Yao, C., Foer, D., Sullivan, B., … Insogna, K. L. (2014). Measurement of Plasma, Serum, and Platelet Serotonin in Individuals With High Bone Mass and Mutations in LRP5. *Journal of Bone and Mineral Research*, *29*(4), 976–981. https://doi.org/10.1002/jbmr.2086

Lee, S.-L., Wang, W.-W., & Fanburg, B. L. (1998). Superoxide as an Intermediate Signal for Serotonin-Induced Mitogenesis. *Free Radical Biology and Medicine*, *24*(5), 855–858. https://doi.org/10.1016/S0891-5849(97)00359-6

Lesch, K. -P., Wolozin, B. L., Estler, H. C., Murphy, D. L., & Riederer, P. (1993). Isolation of a cDNA encoding the human brain serotonin transporter. *Journal of Neural Transmission*, *91*(1), 67–72. https://doi.org/10.1007/BF01244919

Lesch, Klaus-Peter, & Waider, J. (2012). Serotonin in the Modulation of Neural Plasticity and Networks: Implications for Neurodevelopmental Disorders. *Neuron*, *76*(1), 175–191. https://doi.org/10.1016/J.NEURON.2012.09.013

Lesurtel, M., Graf, R., Aleil, B., Walther, D. J., Tian, Y., Jochum, W., … Clavien, P.-A. (2006). Platelet-Derived Serotonin Mediates Liver Regeneration. *Science*, *312*(5770), 104–107. https://doi.org/10.1126/science.1123842

Lesurtel, M., Soll, C., Humar, B., & Clavien, P.-A. (2012). Serotonin: A double-edged sword for the liver? *The Surgeon*, *10*(2), 107–113. https://doi.org/10.1016/J.SURGE.2011.11.002

Lesurtel, Mickaël, & Clavien, P.-A. (2012). Serotonin: a key molecule in acute and chronic liver injury! *Clinics and Research in Hepatology and Gastroenterology*, *36*(4), 319–322. https://doi.org/10.1016/j.clinre.2012.05.005

Lesurtel, Mickaël, & Clavien, P.-A. (2014). Platelet-derived serotonin: Translational implications for liver regeneration. *Hepatology*, *60*(1), 30–33. https://doi.org/10.1002/hep.27067

Li, J., Wang, Q., Chai, W., Chen, M.-H., Liu, Z., & Shi, W. (2011). Hyperglycemia in apolipoprotein E-deficient mouse strains with different atherosclerosis susceptibility. *Cardiovascular Diabetology*, *10*(1), 117. https://doi.org/10.1186/1475-2840-10-117

Lievens, D., & Hundelshausen, P. von. (2011). Platelets in atherosclerosis. *Thrombosis and Haemostasis*, *106*(11), 827–838. https://doi.org/10.1160/TH11-08-0592

Liu, Q., Yang, Q., Sun, W., Vogel, P., Heydorn, W., Yu, X.-Q., … Shi, Z.-C. (2008). Discovery and Characterization of Novel Tryptophan Hydroxylase Inhibitors That Selectively Inhibit Serotonin Synthesis in the Gastrointestinal Tract. *The Journal of Pharmacology and Experimental Therapeutics*, *325*(1), 47–55. https://doi.org/10.1124/jpet.107.132670

Liu, Y., Wei, L., Laskin, D. L., & Fanburg, B. L. (2011). Role of Protein Transamidation in Serotonin-Induced Proliferation and Migration of Pulmonary Artery Smooth Muscle Cells. *American Journal of Respiratory Cell and Molecular Biology*, *44*(4), 548–555. https://doi.org/10.1165/rcmb.2010-0078OC

López, M. L., Kieling, C. O., Uribe Cruz, C., Osvaldt, A., Ochs de Muñoz, G., Meurer, L., … Matte, U. (2014). Platelet increases survival in a model of 90% hepatectomy in rats. *Liver International*, *34*(7), 1049–1056. https://doi.org/10.1111/liv.12326

Lovenberg, W., Jequier, E., & Sjoerdsma, A. (1967). Tryptophan Hydroxylation: Measurement in Pineal Gland, Brainstem, and Carcinoid Tumor. *Science*, *155*(3759), 217–219. https://doi.org/10.1126/SCIENCE.155.3759.217

Luo, X., Persico, A. M., & Lauder, J. M. (2003). Serotonergic Regulation of Somatosensory Cortical Development: Lessons from Genetic Mouse Models. *Developmental Neuroscience*, *25*(2–4), 173–183. https://doi.org/10.1159/000072266

Maletzki, C., Bock, S., Fruh, P., Macius, K., Witt, A., Prall, F., & Linnebacher, M. (2019). NSG mice as hosts for oncological precision medicine. *Laboratory Investigation*, *2*. https://doi.org/10.1038/s41374-019-0298-6

Matthes, S., & Bader, M. (2018). Peripheral Serotonin Synthesis as a New Drug Target. *Trends in Pharmacological Sciences*, *39*(6), 560–572. https://doi.org/10.1016/j.tips.2018.03.004

Mayer, B., Lieb, W., Radke, P. W., Götz, A., Fischer, M., Bässler, A., … Schunkert, H. (2007). Association between arterial pressure and coronary artery calcification. *Journal of Hypertension*, *25*(8), 1731–1738. https://doi.org/10.1097/HJH.0b013e328165cbb6

McCall, R. B. (1990). Role of neurotransmitters in the central regulation of the cardiovascular system. *Progress in Drug Research. Fortschritte Der Arzneimittelforschung. Progres Des Recherches Pharmaceutiques*, *35*, 25–84. Retrieved from http://www.ncbi.nlm.nih.gov/pubmed/1981283

Medina-Martel, M., Urbina, M., Fazzino, F., & Lima, L. (2013). Serotonin Transporter in Lymphocytes of Rats Exposed to Physical Restraint Stress. *Neuroimmunomodulation*, *20*(6), 361–367. https://doi.org/10.1159/000353797

Mekontso-Dessap, A., Brouri, F., Pascal, O., Lechat, P., Hanoun, N., Lanfumey, L., … Eddahibi, S. (2006). Deficiency of the 5-hydroxytryptamine transporter gene leads to cardiac fibrosis and valvulopathy in mice. *Circulation*, *113*(1), 81–89. https://doi.org/10.1161/CIRCULATIONAHA.105.554667

Mendis, S., Puska, P., & Norrving, B. (2011). Global Atlas of Cardiovascular Disease 2000-2016: The Path to Prevention and Control. *WHO Press*. https://doi.org/10.1016/j.gheart.2018.09.511

Mennini, T., Mocaer, E., & Garattini, S. (1987). Tianeptine, a selective enhancer of serotonin uptake in rat brain. *Naunyn-Schmiedeberg's Archives of Pharmacology*, *336*(5), 478–482. https://doi.org/10.1007/BF00169302

Mercado, C. P., & Kilic, F. (2010). Molecular mechanisms of SERT in platelets: regulation of plasma serotonin levels. *Molecular Interventions*, *10*(4), 231–241. https://doi.org/10.1124/mi.10.4.6

Millan, M. J., Marin, P., Bockaert, J., & Mannoury la Cour, C. (2008). Signaling at G-protein-coupled serotonin receptors: recent advances and future research directions. *Trends in Pharmacological Sciences*, *29*(9), 454–464. https://doi.org/10.1016/J.TIPS.2008.06.007

Morecroft, I., Dempsie, Y., Bader, M., Walther, D. J., Kotnik, K., Loughlin, L., … MacLean, M. R. (2007). Effect of tryptophan hydroxylase 1 deficiency on the development of hypoxia-induced pulmonary hypertension. *Hypertension (Dallas, Tex. : 1979)*, *49*(1), 232–236. https://doi.org/10.1161/01.HYP.0000252210.58849.78

Nakashima, Y., Plump, A. S., Raines, E. W., Breslow, J. L., & Ross, R. (1994). ApoE-Deficient Mice Develop Lesions of All Phases of Atherosclerosis Throughout the Arterial Tree. *Atherosclerosis, Thrombosis, and Vascular Biology*, 133–140.

Nebigil, C. G., Choi, D.-S., Dierich, A., Hickel, P., Meur, M. Le, Messaddeq, N., … Maroteaux, L. (2000). Serotonin 2B receptor is required for heart development. *Proceedings of the National Academy of Sciences*, *97*(17), 9508–9513. https://doi.org/10.1073/PNAS.97.17.9508

Nebigil, C. G., & Maroteaux, L. (2001). A Novel Role for Serotonin in Heart. *Trends in Cardiovascular Medicine*, *11*(8), 329–335. https://doi.org/10.1016/S1050-1738(01)00135-9

Nemecek, G. M., Coughlin, S. R., Handley, D. A., & Moskowitz, M. A. (1986). Stimulation of aortic smooth muscle cell mitogenesis by serotonin. *Proceedings of the National Academy of Sciences of the United States of America*, *83*(3), 674–678. https://doi.org/10.1073/pnas.83.3.674

Ni, W., Geddes, T. J., Priestley, J. R. C., Szasz, T., Kuhn, D. M., & Watts, S. W. (2008). The existence of a local 5-hydroxytryptaminergic system in peripheral arteries. *British Journal of Pharmacology*, *154*(3), 663–674. https://doi.org/10.1038/bjp.2008.111

Nichols, D. E., & Nichols, C. D. (2008). Serotonin Receptors. *Chemical Reviews*, *108*(5), 1614–1641. https://doi.org/10.1021/cr078224o

Niesler, B., Frank, B., Kapeller, J., & Rappold, G. A. (2003). Cloning, physical mapping and expression analysis of the human 5-HT3 serotonin receptor-like genes HTR3C, HTR3D and HTR3E. *Gene*, *310*, 101–111. https://doi.org/10.1016/S0378-1119(03)00503-1

Nishina, P. M., Verstuyft, J., & Paigen, B. (1990). Synthetic low and high fat diets for the study of atherosclerosis in the mouse. *Journal of Lipid Research*, *31*(5), 859–869. Retrieved from http://www.jlr.org/content/31/5/859.short

Nocito, A., Dahm, F., Jochum, W., Jang, J. H., Georgiev, P., Bader, M., … Clavien, P.-A. (2008). Serotonin Regulates Macrophage-Mediated Angiogenesis in a Mouse Model of Colon Cancer Allografts. *Cancer Research*, *68*(13), 5152–5158. https://doi.org/10.1158/0008-5472.CAN-08-0202

Nocito, Antonio, Dahm, F., Jochum, W., Jang, J. H., Georgiev, P., Bader, M., … Clavien, P. A. (2007). Serotonin Mediates Oxidative Stress and Mitochondrial Toxicity in a Murine Model of Nonalcoholic Steatohepatitis. *Gastroenterology*, *133*(2), 608–618. https://doi.org/10.1053/j.gastro.2007.05.019

O'Kane, R. L., Viña, J. R., Simpson, I., & Hawkins, R. A. (2004). Na^{+} -dependent neutral amino acid transporters A, ASC, and N of the blood-brain barrier: mechanisms for neutral amino acid removal. *American Journal of Physiology-Endocrinology and Metabolism*, *287*(4), E622–E629. https://doi.org/10.1152/ajpendo.00187.2004

Oh, C. M., Namkung, J., Go, Y., Shong, K. E., Kim, K., Kim, H., … Kim, H. (2015). Regulation of systemic energy homeostasis by serotonin in adipose tissues. *Nature Communications*, *6*. https://doi.org/10.1038/ncomms7794

Ohtsuki, S. (2004). *New Aspects of the Blood–Brain Barrier Transporters; Its Physiological*

Roles in the Central Nervous System. *27*(October).
Ormsbee, H. S., & Fondacaro, J. D. (1985). Action of Serotonin on the Gastrointestinal Tract. *Experimental Biology and Medicine*, *178*(3), 333–338. https://doi.org/10.3181/00379727-178-42016
Paigen, B., Holmes, P. A., Mitchell, D., & Albee, D. (1987). Comparison of atherosclerotic lesions and HDL-lipid levels in male, female, and testosterone-treated female mice from strains C57BL/6, BALB/c, and C3H. *Atherosclerosis*, *64*(2–3), 215–221. https://doi.org/10.1016/0021-9150(87)90249-8
Pakala, R., Willerson, J. T., & Benedict, C. R. (1994). Mitogenic effect of serotonin on vascular endothelial cells. *Circulation*, *90*(4), 1919–1926. https://doi.org/10.1161/01.cir.90.4.1919
Pallaghy, P. K., Melnikova, A. ., Jimenez, E. C., Olivera, B. M., & Raymond S. Norton. (1999). *Solution Structure of Contryphan-R, a Naturally Occurring Disulfide-Bridged Octapeptide Containing d-Tryptophan: Comparison with Protein Loops†,‡*. https://doi.org/10.1021/BI990685J
Patel, P. D., Pontrello, C., & Burke, S. (2004). Robust and Tissue-Specific Expression of TPH2 versus TPH1 in Rat Raphe and Pineal Gland. *Biological Psychiatry*, *55*(4), 428–433. https://doi.org/10.1016/j.biopsych.2003.09.002
Paulmann, N., Grohmann, M., Voigt, J.-P., Bert, B., Vowinckel, J., Bader, M., … Walther, D. J. (2009). Intracellular Serotonin Modulates Insulin Secretion from Pancreatic β-Cells by Protein Serotonylation. *PLoS Biology*, *7*(10), e1000229. https://doi.org/10.1371/journal.pbio.1000229
Pavone, L. M., Spina, A., Rea, S., Santoro, D., Mastellone, V., Lombardi, P., & Avallone, L. (2009). Serotonin transporter gene deficiency is associated with sudden death of newborn mice through activation of TGF-β1 signalling. *Journal of Molecular and Cellular Cardiology*, *47*(5), 691–697. https://doi.org/10.1016/j.yjmcc.2009.07.021
Pendse, A. A., Arbones-Mainar, J. M., Johnson, L. A., Altenburg, M. K., & Maeda, N. (2009). Apolipoprotein E knock-out and knock-in mice: atherosclerosis, metabolic syndrome, and beyond. *Journal of Lipid Research*, *50 Suppl*(Suppl), S178-82. https://doi.org/10.1194/jlr.R800070-JLR200
Peng, Y.-Q., Xiong, D., Lin, X., Cui, R.-R., Xu, F., Zhong, J.-Y., … Yuan, L.-Q. (2017). Oestrogen Inhibits Arterial Calcification by Promoting Autophagy. *Scientific Reports*, *7*(1), 3549. https://doi.org/10.1038/s41598-017-03801-x
Plump, A. S., Smith, J. D., Hayek, T., Aalto-Setälä, K., Walsh, A., Verstuyft, J. G., … Breslow, J. L. (1992). Severe hypercholesterolemia and atherosclerosis in apolipoprotein E-deficient mice created by homologous recombination in ES cells. *Cell*, *71*(2), 343–353. https://doi.org/10.1016/0092-8674(92)90362-G
Radwanski, E. R., & Last, R. L. (1995). Tryptophan biosynthesis and metabolism: biochemical and molecular genetics. *The Plant Cell*, *7*(7), 921–934. https://doi.org/10.1105/tpc.7.7.921
Rahman, M. K., Toshiharu, N., & Takeshi, K. (1981). Aromatic l-amino acid decarboxylase activity in central and peripheral tissues and serum of rats with l-dopa and l-5-hydroxytryptophan as substrates. *Biochemical Pharmacology*, *30*(6), 645–649. https://doi.org/10.1016/0006-2952(81)90139-8
Rami, M., Guillamat-Prats, R., Rinne, P., Salvermoser, M., Ring, L., Bianchini, M., … Steffens, S. (2018). Chronic Intake of the Selective Serotonin Reuptake Inhibitor Fluoxetine Enhances Atherosclerosis. *Arteriosclerosis, Thrombosis, and Vascular Biology*, *38*(5), 1007–1019. https://doi.org/10.1161/ATVBAHA.117.310536
Rapport, M M, Green, A. A., & Page, I. H. (1948). Crystalline Serotonin. *Science*, *108*(2804), 329–330. https://doi.org/10.1126/science.108.2804.329
Rapport, Maurice M., Green, A. A., & Page, I. H. (1948a). SERUM VASOCONSTRICTOR

(SEROTONIN): III. CHEMICAL INACTIVATION. *J. Biol. Chem.*, *176*, 1237–1241.

Rapport, Maurice M., Green, A. A., & Page, I. H. (1948b). SERUM VASOCONSTRICTOR (SEROTONIN): IV. ISOLATION AND CHARACTERIZATION. *J. Biol. Chem.*, *176*, 1243–1251.

Raymond, J. R., Kim, J., Beach, R. E., & Tisher, C. C. (1993). Immunohistochemical mapping of cellular and subcellular distribution of 5-HT1A receptors in rat and human kidneys. *The American Journal of Physiology*, *264*(1 Pt 2), F9-19. https://doi.org/10.1152/ajprenal.1993.264.1.F9

Regmi, S. C., Park, S.-Y., Ku, S. K., & Kim, J.-A. (2014). Serotonin regulates innate immune responses of colon epithelial cells through Nox2-derived reactive oxygen species. *Free Radical Biology and Medicine*, *69*, 377–389. https://doi.org/10.1016/J.FREERADBIOMED.2014.02.003

Rekhter, M. (1999). Collagen synthesis in atherosclerosis: too much and not enough. *Cardiovascular Research*, *41*(2), 376–384. https://doi.org/10.1016/S0008-6363(98)00321-6

Ross, R. (1993). The pathogenesis of atherosclerosis: a perspective for the 1990s. *Nature*, *362*(6423), 801–809. https://doi.org/10.1038/362801a0

Ross, R. (1994). Cell biology of atherosclerosis. *Journal of Hypertension*, *12*(SUPPL. 10), 791–804.

Ruddell, R. G., Mann, D. A., & Ramm, G. A. (2008). The function of serotonin within the liver. *Journal of Hepatology*, *48*(4), 666–675. https://doi.org/10.1016/J.JHEP.2008.01.006

Ruddell, R. G., Oakley, F., Hussain, Z., Yeung, I., Bryan-Lluka, L. J., Ramm, G. A., & Mann, D. A. (2006). A Role for Serotonin (5-HT) in Hepatic Stellate Cell Function and Liver Fibrosis. *The American Journal of Pathology*, *169*(3), 861–876. https://doi.org/10.2353/AJPATH.2006.050767

Rudnick, G. (2006). Structure/Function Relationships in Serotonin Transporter: New Insights from the Structure of a Bacterial Transporter. In *Neurotransmitter Transporters* (pp. 59–73). https://doi.org/10.1007/3-540-29784-7_3

Rudnick, Gary. (2006). Serotonin Transporters – Structure and Function. *Journal of Membrane Biology*, *213*(2), 101–110. https://doi.org/10.1007/s00232-006-0878-4

Salter, M., Hazelwood, R., Pogson, C. I., Iyer, R., & Madge, D. J. (1995). The effects of a novel and selective inhibitor of tryptophan 2,3-dioxygenase on tryptophan and serotonin metabolism in the rat. *Biochemical Pharmacology*, *49*(10), 1435–1442. https://doi.org/10.1016/0006-2952(95)00006-L

Sasaki, T., Kuzuya, M., Nakamura, K., Cheng, X. W., Shibata, T., Sato, K., & Iguchi, A. (2006). A simple method of plaque rupture induction in apolipoprotein E-deficient mice. *Arteriosclerosis, Thrombosis, and Vascular Biology*, *26*(6), 1304–1309. https://doi.org/10.1161/01.ATV.0000219687.71607.f7

Sato, Y., Seo, N., & Kobayashi, E. (2006). Genetic background differences between FVB and C57BL/6 mice affect hypnotic susceptibility to pentobarbital, ketamine and nitrous oxide, but not isoflurane. *Acta Anaesthesiologica Scandinavica*, *50*(5), 553–556. https://doi.org/10.1111/j.1399-6576.2006.001002.x

Saxena, P. R., & Villalón, C. M. (1990). Cardiovascular effects of serotonin agonists and antagonists. *Journal of Cardiovascular Pharmacology*, *15 Suppl 7*, S17-34. Retrieved from http://www.ncbi.nlm.nih.gov/pubmed/1702484

Schürmann, F. W., & Klemm, N. (1984). Serotonin-immunoreactive neurons in the brain of the honeybee. *Journal of Comparative Neurology*, *225*(4), 570–580. https://doi.org/10.1002/cne.902250407

Segura-Puimedon, M., Mergia, E., Al-Hasani, J., Aherrahrou, R., Stoelting, S., Kremer, F., … Aherrahrou, Z. (2016). Proatherosclerotic Effect of the α1-Subunit of Soluble Guanylyl

Cyclase by Promoting Smooth Muscle Phenotypic Switching. *American Journal of Pathology*, *186*(8), 2220–2231. https://doi.org/10.1016/j.ajpath.2016.04.010
Sharma, S. K., Zahradka, P., Chapman, D., Kumamoto, H., Takeda, N., & Dhalla, N. S. (1999). Inhibition of serotonin-induced vascular smooth muscle cell proliferation by sarpogrelate. *The Journal of Pharmacology and Experimental Therapeutics*, *290*(3), 1475–1481. Retrieved from http://www.ncbi.nlm.nih.gov/pubmed/10454527
Shaw, L. J., Raggi, P., Schisterman, E., Berman, D. S., & Callister, T. Q. (2003). Prognostic Value of Cardiac Risk Factors and Coronary Artery Calcium Screening for All-Cause Mortality. *Radiology*, *228*(3), 826–833. https://doi.org/10.1148/radiol.2283021006
Sheng, Y., & Zhu, L. (2018). The crosstalk between autonomic nervous system and blood vessels. *International Journal of Physiology, Pathophysiology and Pharmacology*, *10*(1), 17–28. Retrieved from http://www.ncbi.nlm.nih.gov/pubmed/29593847
Shih, J. C., & Chen, K. (2004). Regulation of MAO-A and MAO-B Gene Expression. *Current Medicinal Chemistry*, *11*(15), 1995–2005. https://doi.org/10.2174/0929867043364757
Shively, C. A., Register, T. C., Appt, S. E., & Clarkson, T. B. (2015). Effects of long-term sertraline treatment and depression on coronary artery atherosclerosis in premenopausal female primates. *Psychosomatic Medicine*, *77*(3), 267–278. https://doi.org/10.1097/PSY.0000000000000163
Sirotkin, A. V., & Schaeffer, H. J. (1997). Direct regulation of mammalian reproductive organs by serotonin and melatonin. *Journal of Endocrinology*, *154*(1), 1–5. https://doi.org/10.1677/joe.0.1540001
Smith, C. C. ., & Betteridge, D. . (1997). Reduced platelet serotonin content and release in familial hypercholesterolaemia. *Atherosclerosis*, *130*(1–2), 87–92. https://doi.org/10.1016/S0021-9150(96)06048-0
Smith, E. B. (1965). The influence of age and atherosclerosis on the chemistry of aortic intima: Part 2. Collagen and mucopolysaccharides. *Journal of Atherosclerosis Research*, *5*(2), 241–248. https://doi.org/10.1016/S0368-1319(65)80065-5
Sontag, T. J., Krishack, P. A., Lukens, J. R., Bhanvadia, C. V, Getz, G. S., & Reardon, C. A. (2014). Apolipoprotein A-I protection against atherosclerosis is dependent on genetic background. *Arteriosclerosis, Thrombosis, and Vascular Biology*, *34*(2), 262–269. https://doi.org/10.1161/ATVBAHA.113.302831
Starlinger, P., Assinger, A., Haegele, S., Wanek, D., Zikeli, S., Schauer, D., … Gruenberger, T. (2014). Evidence for serotonin as a relevant inducer of liver regeneration after liver resection in humans. *Hepatology*, *60*(1), 257–266. https://doi.org/10.1002/hep.26950
Sternberg, E. M., Trial, J., & Parker, C. W. (1986). Effect of serotonin on murine macrophages: suppression of Ia expression by serotonin and its reversal by 5-HT2 serotonergic receptor antagonists. *Journal of Immunology (Baltimore, Md. : 1950)*, *137*(1), 276–282. Retrieved from http://www.ncbi.nlm.nih.gov/pubmed/2423604
Stone, T. W., & Darlington, L. G. (2002). Endogenous kynurenines as targets for drug discovery and development. *Nature Reviews Drug Discovery*, *1*(8), 609–620. https://doi.org/10.1038/nrd870
Strong, P. V., Greenwood, B. N., & Fleshner, M. (2009). The effects of the selective 5-HT2C receptor antagonist SB 242084 on learned helplessness in male Fischer 344 rats. *Psychopharmacology*, *203*(4), 665–675. https://doi.org/10.1007/s00213-008-1413-3
Suguro, T., Watanabe, T., Kanome, T., Kodate, S., Hirano, T., Miyazaki, A., & Adachi, M. (2006). Serotonin acts as an up-regulator of acyl-coenzyme A:cholesterol acyltransferase-1 in human monocyte–macrophages. *Atherosclerosis*, *186*(2), 275–281. https://doi.org/10.1016/J.ATHEROSCLEROSIS.2005.08.007
Sun, C., Li, X., Liu, L., Canet, M. J., Guan, Y., Fan, Y., & Zhou, Y. (2016). Effect of fasting time on measuring mouse blood glucose level. *International Journal of Clinical and Experimental Medicine*, *9*(2), 4186–4189.

Sun, J., Sukhova, G. K., Wolters, P. J., Yang, M., Kitamoto, S., Libby, P., … Shi, G.-P. (2007). Mast cells promote atherosclerosis by releasing proinflammatory cytokines. *Nature Medicine*, *13*(6), 719–724. https://doi.org/10.1038/nm1601

The Jackson Laboratory. (2006). The importance of genetic background in mouse-based biomedical research. Retrieved from https://www.jax.org/news-and-insights/2006/june/the-importance-of-genetic-background-in-mouse-based-biomedical-research

Thyberg, J., Blomgren, K., Hedin, U., & Dryjski, M. (1995). Phenotypic modulation of smooth muscle cells during the formation of neointimal thickenings in the rat carotid artery after balloon injury: an electron-microscopic and stereological study. *Cell & Tissue Research*, *281*(3), 421–433. https://doi.org/10.1007/BF00417860

Trapani, L., Segatto, M., & Pallottini, V. (2012). Regulation and deregulation of cholesterol homeostasis: The liver as a metabolic "power station". *World Journal of Hepatology*, *4*(6), 184–190. https://doi.org/10.4254/wjh.v4.i6.184

Tull, S. P., Anderson, S. I., Hughan, S. C., Watson, S. P., Nash, G. B., & Rainger, G. E. (2006). Cellular pathology of atherosclerosis: smooth muscle cells promote adhesion of platelets to cocultured endothelial cells. *Circulation Research*, *98*(1), 98–104. https://doi.org/10.1161/01.RES.0000198386.69355.87

Twarog, B. M., & Page, I. H. (1953). Serotonin Content of Some Mammalian Tissues and Urine and a Method for Its Determination. *The American Journal of Physiology*, *175*(1), 157–161. Retrieved from http://ajplegacy.physiology.org/content/175/1/157.abstract

Vallés, A. M., & White, K. (1988). Serotonin-containing neurons in Drosophila melanogaster: Development and distribution. *Journal of Comparative Neurology*, *268*(3), 414–428. https://doi.org/10.1002/cne.902680310

van Hooft, J. A., & Yakel, J. L. (2003). 5-HT3 receptors in the CNS: 3B or not 3B? *Trends in Pharmacological Sciences*, *24*(4), 157–160. https://doi.org/10.1016/S0165-6147(03)00051-8

van Leeuwen, M., Gijbels, M. J. J., Duijvestijn, A., Smook, M., van de Gaar, M. J., Heeringa, P., … Tervaert, J. W. C. (2008). Accumulation of myeloperoxidase-positive neutrophils in atherosclerotic lesions in LDLR-/- mice. *Arteriosclerosis, Thrombosis, and Vascular Biology*, *28*(1), 84–89. https://doi.org/10.1161/ATVBAHA.107.154807

Vanhoutte, P. M. (1991). Platelet-derived serotonin, the endothelium, and cardiovascular disease. *Journal of Cardiovascular Pharmacology*, *17 Suppl 5*, S6-12. Retrieved from http://www.ncbi.nlm.nih.gov/pubmed/1717775

Vikenes, K., Farstad, M., & Nordrehaug, J. E. (1999). Serotonin Is Associated with Coronary Artery Disease and Cardiac Events. *Circulation*, *100*(5), 483–489. https://doi.org/10.1161/01.CIR.100.5.483

von Hundelshausen, P., Koenen, R. R., & Weber, C. (2009). Platelet-Mediated Enhancement of Leukocyte Adhesion. *Microcirculation*, *16*(1), 84–96. https://doi.org/10.1080/10739680802564787

von Zychlinski, A., Williams, M., McCormick, S., & Kleffmann, T. (2014). Absolute quantification of apolipoproteins and associated proteins on human plasma lipoproteins. *Journal of Proteomics*, *106*, 181–190. https://doi.org/10.1016/J.JPROT.2014.04.030

Walther, D. J., & Bader, M. (2003). A unique central tryptophan hydroxylase isoform. *Biochemical Pharmacology*, *66*(9), 1673–1680. https://doi.org/10.1016/S0006-2952(03)00556-2

Walther, D. J., Peter, J.-U., Winter, S., Höltje, M., Paulmann, N., Grohmann, M., … Bader, M. (2003). Serotonylation of Small GTPases Is a Signal Transduction Pathway that Triggers Platelet α-Granule Release. *Cell*, *115*(7), 851–862. https://doi.org/10.1016/S0092-8674(03)01014-6

Walther, D. J., Peter, J. U., Bashammakh, S., Hörtnagl, H., Voits, M., Fink, H., & Bader, M.

(2003). Synthesis of serotonin by a second tryptophan hydroxylase isoform. *Science*, *299*(5603), 76. https://doi.org/10.1126/science.1078197

Watanabe, H., Nakano, T., Saito, R., Akasaka, D., Saito, K., Ogasawara, H., … Aso, H. (2016). Serotonin Improves High Fat Diet Induced Obesity in Mice. *PloS One*, *11*(1), e0147143. https://doi.org/10.1371/journal.pone.0147143

Watanabe, H., Rose, M. T., & Aso, H. (2011). Role of peripheral serotonin in glucose and lipid metabolism. *Current Opinion in Lipidology*, *22*(3), 186–191. https://doi.org/10.1097/MOL.0b013e3283462273

Watts, S. W., Morrison, S. F., Davis, R. P., & Barman, S. M. (2012). Serotonin and Blood Pressure Regulation. *The American Society for Pharmacology and Experimental Therapeutics*, *64*(2), 359–388.

Watts, S. W., Priestley, J. R. C., & Thompson, J. M. (2009). Serotonylation of Vascular Proteins Important to Contraction. *PLoS ONE*, *4*(5), e5682. https://doi.org/10.1371/journal.pone.0005682

Watts, S. W., & Thompson, J. M. (2004). Characterization of the contractile 5-hydroxytryptamine receptor in the renal artery of the normotensive rat. *The Journal of Pharmacology and Experimental Therapeutics*, *309*(1), 165–172. https://doi.org/10.1124/jpet.103.062562

Weber, C. (2005). Platelets and chemokines in atherosclerosis: partners in crime. *Circulation Research*, *96*(6), 612–616. https://doi.org/10.1161/01.RES.0000160077.17427.57

Weibust, R. S. (1973). Inheritance of plasma cholesterol levels in mice. *Genetics*, *73*(2), 303–312.

Whitman, S. C. (2004). A practical approach to using mice in atherosclerosis research. *The Clinical Biochemist. Reviews*, *25*(1), 81–93. Retrieved from http://www.ncbi.nlm.nih.gov/pubmed/18516202

World Health Organization (WHO). (2017). Cardiovascular diseases (CVDs). Retrieved August 19, 2019, from https://www.who.int/en/news-room/fact-sheets/detail/cardiovascular-diseases-(cvds)

Wozniak, G., Toska, A., Saridi, M., & Mouzas, O. (2011). Serotonin reuptake inhibitor antidepressants (SSRIs) against atherosclerosis. *Medical Science Monitor : International Medical Journal of Experimental and Clinical Research*, *17*(9), RA205-14. https://doi.org/10.12659/msm.881924

Wu, M., Rementer, C., & Giachelli, C. M. (2013). Vascular calcification: an update on mechanisms and challenges in treatment. *Calcified Tissue International*, *93*(4), 365–373. https://doi.org/10.1007/s00223-013-9712-z

Ximenes, V. F., Maghzal, G. J., Turner, R., Kato, Y., Winterbourn, C. C., & Kettle, A. J. (2009). Serotonin as a physiological substrate for myeloperoxidase and its superoxide-dependent oxidation to cytotoxic tryptamine-4,5-dione. *The Biochemical Journal*, *425*(1), 285–293. https://doi.org/10.1042/BJ20090776

Yadav, V. K., Oury, F., Suda, N., Liu, Z. W., Gao, X. B., Confavreux, C., … Karsenty, G. (2009). A Serotonin-Dependent Mechanism Explains the Leptin Regulation of Bone Mass, Appetite, and Energy Expenditure. *Cell*, *138*(5), 976–989. https://doi.org/10.1016/j.cell.2009.06.051

Yu, X.-H., Fu, Y.-C., Zhang, D.-W., Yin, K., & Tang, C.-K. (2013). Foam cells in atherosclerosis. *Clinica Chimica Acta*, *424*, 245–252. https://doi.org/10.1016/J.CCA.2013.06.006

Zhang, J., Song, S., Pang, Q., Zhang, R., Zhou, L., Liu, S., … Liu, C. (2015). Serotonin Deficiency Exacerbates Acetaminophen-Induced Liver Toxicity In Mice. *Scientific Reports*, *5*(1), 8098. https://doi.org/10.1038/srep08098

Zhang, S., Reddick, R., Piedrahita, J., & Maeda, N. (1992). Spontaneous hypercholesterolemia and arterial lesions in mice lacking apolipoprotein E. *Science*,

214(4526), 1239–1241. https://doi.org/10.1126/science.6795720
Zhao, B., Dierichs, R., Harrach-Ruprecht, B., & Winterhorff, H. (1995). Oxidized LDL induces serotonin release from blood platelets. *American Journal of Hematology*, *48*(4), 285–287. https://doi.org/10.1002/ajh.2830480417
Zill, P., Büttner, A., Eisenmenger, W., Möller, H.-J., Ackenheil, M., & Bondy, B. (2007). Analysis of tryptophan hydroxylase I and II mRNA expression in the human brain: A post-mortem study. *Journal of Psychiatric Research*, *41*(1–2), 168–173. https://doi.org/10.1016/J.JPSYCHIRES.2005.05.004
Zucker, M., Weizman, A., & Rehavi, M. (2001). Characterization of high-affinity [3H]TBZOH binding to the human platelet vesicular monoamine transporter. *Life Sciences*, *69*(19), 2311–2317. https://doi.org/10.1016/S0024-3205(01)01301-7

Acknowledgements

Performing and finishing this PhD thesis was one of the greatest professional and personal challenges I've ever went through and it would have never been possible without the endless help, support and patience from colleagues, friends and family, things for which I am deeply grateful.

First, I warmly thank Prof. Dr. **Michael Bader** and Dr. **Natalia Alenina** for giving me the great chance to work in their lab and to extend my horizon to the fields of serotonin and cardiovascular research. They opened many doors for my work and for my personal life and created an inspiring, challenging and fruitful working environment with the freedom to develop own scientific ideas and critical thinking. Without them, this project had never been possible.

The members of our collaborating group at the University of Lübeck, Dr. **Zouhair Aherrahrou**, **Annett Liebers**, Dr. **Jaafar Al-Hasani**, **Maren Behrensen** and their colleagues patiently taught me everything about relevant issues and sophisticated techniques for this project and had always a sympathetic ear for questions and problems. I thank them very much for all their time and ideas.

For their valuable time and support of this project I thank the members of my *Promotionskomitee*, Prof. Dr. **Martina Seifert** and Prof. Dr. **Thomas Sommer** who supervised and reviewed this thesis elaborately and Prof. Dr. **Markus Landthaler** and Prof. Dr. **Ana Pombo** for the nice offer to support the committee with their scientific expertise and perspective.

I further thank Dr. **Sabine Bartosch** and **Bianca Kühn** as well as the BSRT for the valuable support of the study organization, the great network and the access to funding facilitations.

Even the most excellent project performed in the best-equipped laboratory comes only to life and feels satisfying when it is supported by inspiring and motivating colleagues. I was blessed having more than only one of such persons working together with me in the Bader lab and I deeply thank them all: At the very beginning there was my former mentor Dr. **Daniel Beis** who always provided me with innovative ideas and enabled me to think outside the box when it came to experimental design and data interpretation. Further, I was glad to work in such a relaxed and frank office atmosphere with colleagues who where always there to help me with huge and small practical and personal problems and questions; thank you so much Dr. **Anne Järve**, Dr. **Susann Matthes** and Dr. **Franziska Rother**. Dr. **Cornelia Hainer,** Dr. **Katrin Nitz,** Dr. **Frederike Klempin** and (future Dr.) **Markus Petermann** enriched the working environment with nice conversations, excellent technical skills they taught me patiently, and, most importantly, critical questions at all stages of my work. Special thanks go to (soon to be Dr.) **Bernadette Nickl** and **André Felipe Rodriques**, who boosted my thesis writing phase with a lot of motivation and on point comments and valuable hints.

One of the most efficient ways to deeply understand and challenge the own ideas and experiments is the exchange with fresh, motivated minds and the supervision of ambitious young researchers. I had the great honor to become a small part of their scientific career and I learned a lot from them: **Anna Krebs**, **Malosree Maitra**, **Lisa Johann** and **Isabelle Clayton**.

I really mean it when I say: The best laboratory is nothing without its powerful, helpful, patient and well skilled technicians. I was more than blessed to work in close cooperation with **Andrea Rodak** and **Susanne da Costa Goncalves**, who did not just enable me to produce huge amounts of good and reliable scientific data, but were also always on the spot to help me with even the strangest lab requests, but even more important, with all kinds of personal issues.

I further thank **Cathrin Gerhard**, **Madeleine Skorna-Nußbeck** and **Vivien Latuske** for their help and excellent laboratory expertise and **Vivien Rabke** and **Steve Bomberg** for taking good care of all of my animals and prompt reactions on all of my requests.

For the invaluable support of my project and the immediate and accurate performance of physiological and biochemical assays and measurements as well as for scientific advices and ideas I greatly thank **Stefanie Schelenz**, **Martin Taube** and **Patrick Langner** of the MDC Pathophysiology core facility and Dr. **Luiza Rabêlo** and Dr. **Valéria Nunes de Souza**. Further, I greatly thank Dr. **Mihail Todiras** without whom my project couldn’t have been finished.

A last but not least professional but also personal thank goes to Dr. **Fatimunnisa “Sayeeda” Quadri**, who offered me her endless expertise in the fields of anatomy and histology but also inspired me with her calm and assertive aura.

“Ohana means family.

Family means nobody gets left behind or forgotten”

Following the spirit of *Ohana*, I will express my deepest thank in German language to those who carried the flag for me during the past 5 years aside from laboratory and office:

Zunächst danke ich meinen geliebten Großeltern, **Irene Hasenjäger** und **Joachim Blauel**, die mir immer den Rücken freigehalten haben und mir viele Dinge ermöglicht haben, die meinen Werdegang enorm beeinflusst haben. Sie haben mich nicht nur frühestmöglich zum eigenständigen Denken ermutigt und in mir die Neugier zu allen Dingen dieser Welt geweckt, sondern waren auch immer für mich da, wenn ich Sorgen oder Probleme hatte und haben niemals daran gezweifelt, dass ich meinen beruflichen Weg gehen werde. Dankeschön!

Der wohl größte und weitreichendste Einfluss in meinem jungen Leben war und ist meine Mutter, **Kerstin Graf**, die mir das Leben schenkte, um es dann mit Liebe, Freude, Mut, Selbstvertrauen, aber auch mit Kunst, Musik, Beobachtungsgabe und Kreativität zu füllen. Sie steht mir immer zur Seite und ihre Stärke und ihr Durchhaltevermögen, die sie mir als alleinerziehende Mutter jeden Tag vorlebte, formten mich nachhaltig. 1000 Dank!

Auch meine Schwiegereltern, **Helena und Eugen Seibel** haben mich immer gestützt und mich ihren Stolz und ihren Glauben in mich und meine eigene Stärke spüren lassen. Ohne ihre

Hilfe und ihren Zuspruch hätte ich so manche Tage nicht so einfach durchgestanden. Ich danke euch!

Ein ganz besonders großer Dank gilt meinem geliebten Ehemann und besten Freund, **Slava Seibel**. In erster Linie danke ich ihm dafür, dass er diese Zeit, die auch von emotionalen Hochs und Tiefs geprägt war, mit mir durchgestanden hat. Aber ich danke ihm auch für das offene Ohr, den kritischen Mund, die starken Nerven und das große Herz. Du bist mein Fels und meine Brandung: Du gibst mir Halt ohne Stillstand. Ich danke dir von ganzem Herzen!

Und zu guter Letzt danke ich dem kleinen großen Menschen, dem ich diese Arbeit gewidmet habe: Meiner bezaubernden Tochter, **Elly Seibel**. Ohne dich wäre manch ein Tag leichter gewesen, aber das Leben nicht halb so schön. Du bist mein größtes Vorbild und, um dir zu zeigen, dass man mit Ausdauer und Zuversicht alles schaffen kann, habe ich diese Arbeit vollendet und niedergeschrieben. Deine bedingungslose Liebe ist meine größte Motivation, ich danke dir unendlich!

Eidesstattliche Erklärung zur Selbstständigkeit

Hiermit erkläre ich, dass ich die vorliegende Arbeit selbstständig und nur unter der Verwendung der angegebenen Quellen und Hilfsmittel angefertigt habe. Alle Materialien oder Dienstleistungen, die ich von Dritten erhalten habe, sind als solche gekennzeichnet.

Ich versichere, dass ich mich nicht anderweitig um einen Doktorgrad beworben habe oder einen entsprechenden Doktortitel bereits besitze.

Die Promotionsordnung 2012 der Lebenswissenschaftlichen Fakultät der Humboldt-Universität zu Berlin ist mit bekannt.

Yasmine Seibel Berlin, 30. 10. 2019

Additional Documents

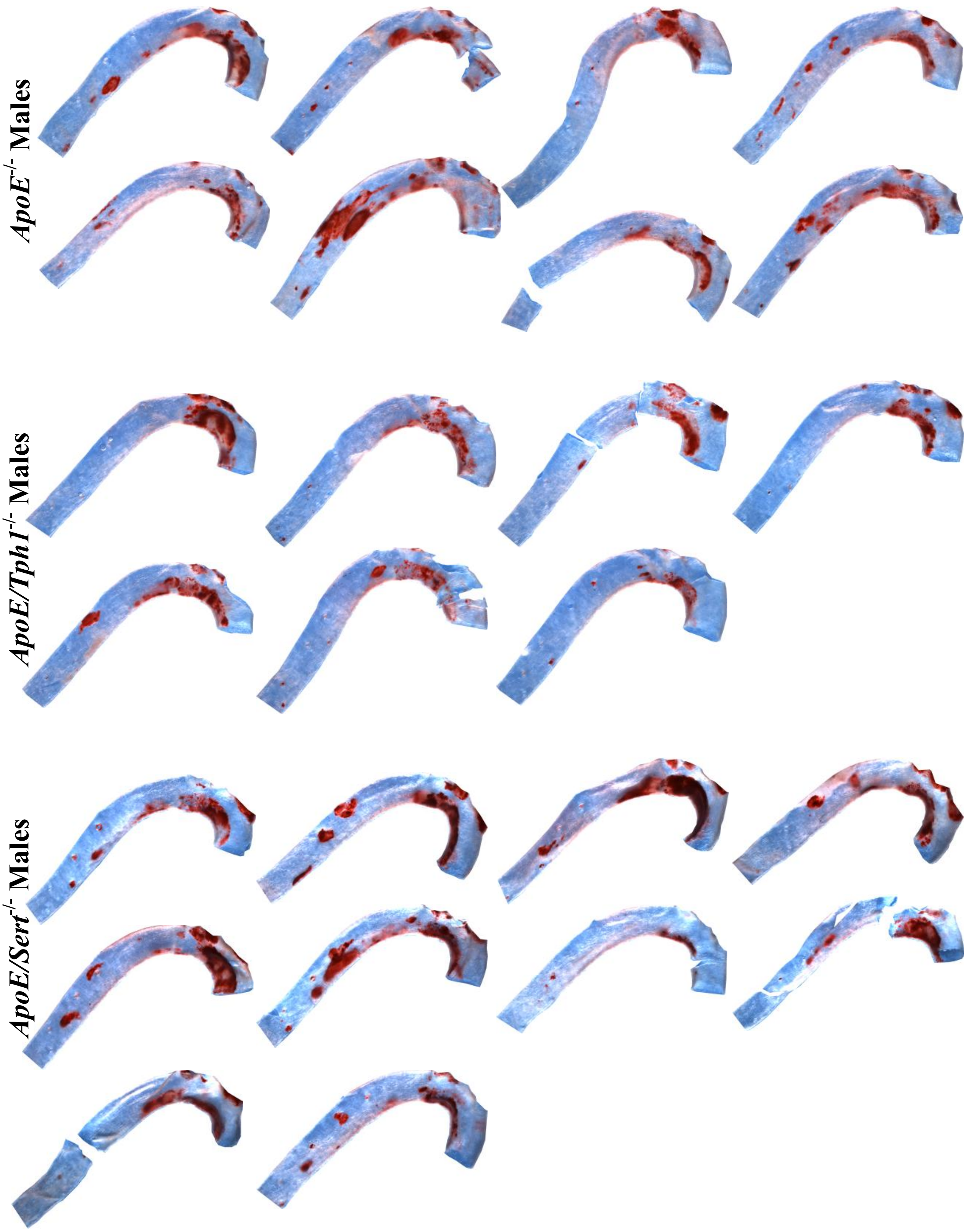

Fig.I – Aortic Arches of 45 Week old Male Mice (ORO stained)

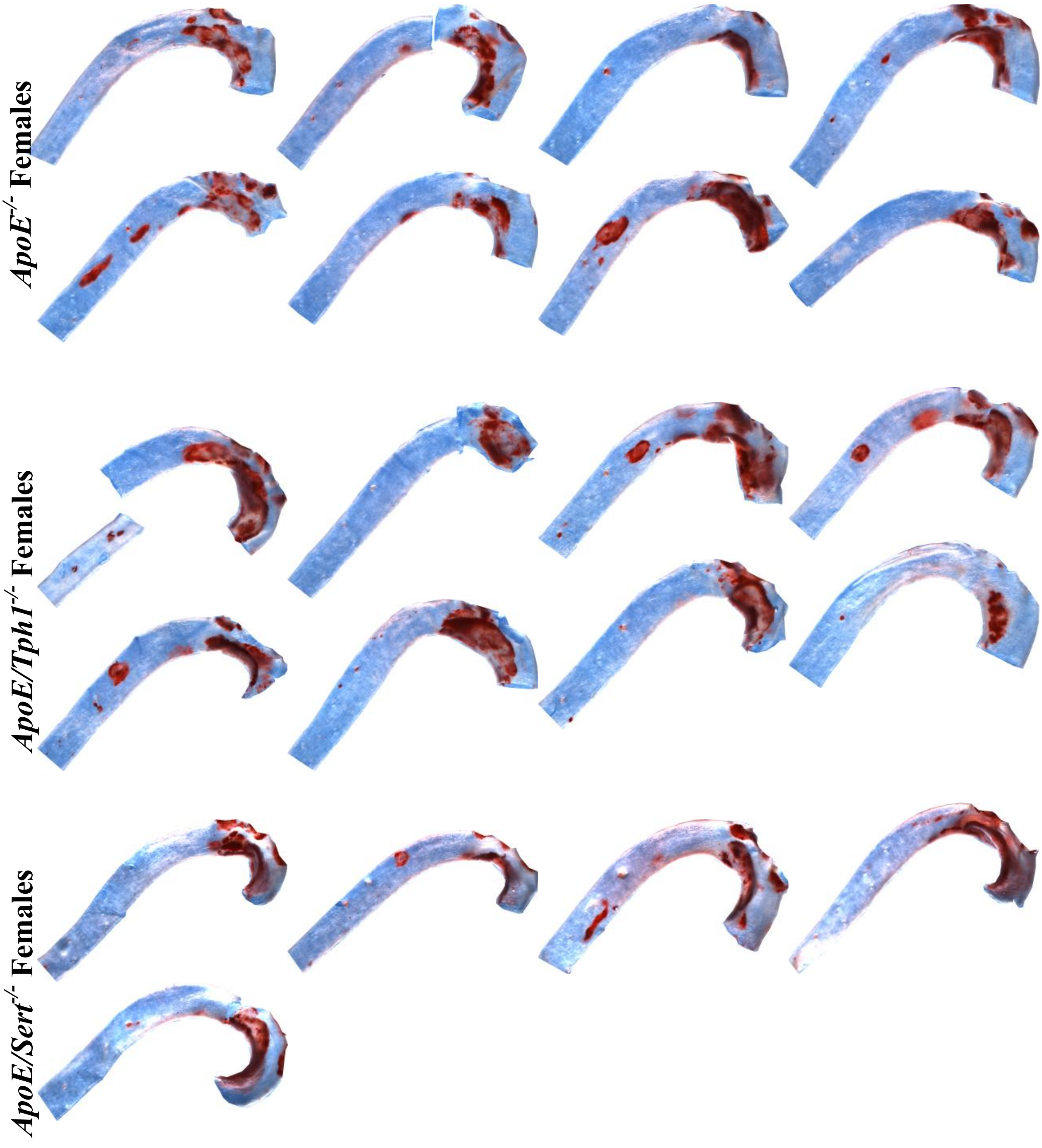

Fig.II – Aortic Arches of 45 Week old Female Mice (ORO stained)